Infrared and optical studies of cool low-mass dwarfs

Hugh Richard Arthur Jones

Presented for the Degree of Doctor of Philosophy
at the University of Edinburgh
1995

This thesis is solely my own composition, except where specifically indicated in the text.

Hugh Jones,
April 1995.

Abstract

Infrared and optical studies of cool low-mass dwarfs are made in order to determine their properties. The goal of distinguishing low-mass stars from brown dwarfs is engaged by studies on a number of different fronts.

(1) The first infrared spectral sequence of cool dwarfs from GL411 (M2V) to GD165B (>M10V) enables derivation of reliable bolometric luminosities down to the hydrogen burning limit. The strength of the deep water absorption bands is used as the basis of a new reliable method to calculate effective temperatures. We find that GD165B is the only star in the sample that is a good brown dwarf candidate.

(2) Expected temperatures, metallicities and gravities of cool dwarfs are compared to inferences from fitting synthetic to observed spectra at the peak of the energy distribution. A good representation of the overall spectral features is found, although the study is limited by (i) the quality of atomic and molecular opacities and (ii) the complex behaviour of atomic lines having strengths which *increase* with decreasing metallicity down to around −1.5 dex. The comparisons suggest a similar spread in metallicities to that anticipated, although for our sample neither kinematic motion nor membership of a particular photometric class are, on their own, reliable indicators of metallicity.

(3) A high resolution study of the strongest water vapour absorption band in cool dwarfs is compared to predictions from a preliminary *ab initio* computation for water vapour incorporated into a stellar atmosphere calculation. The comparisons show that water vapour lines are formed relatively high in the photosphere at pressures about an order of magnitude lower than atomic lines. The overestimated pressure broadening of water vapour, and probably other molecular lines, is likely to explain much of the past discrepancy between observed and theoretical spectral energy distributions.

(4) The discovery is reported of the reddest known brown dwarf candidate. Classification as a star or a brown dwarf depends on the adopted age and the evolutionary model used. Its discovery within an infrared field survey places the first lower limit on the space density for objects fainter than $M_{\rm bol} = 14$ and suggests that the luminosity function does not fall dramatically into the brown dwarf regime.

Acknowledgements

I owe the largest debt for this thesis to Andy Longmore who had the idea of understanding M dwarfs as the stepping stone to the brown dwarf regime. Despite the fact that Andy really wanted me to get excited about globular clusters his calm but firm hand gave me enough freedom to call the research my own but enough direction to ensure that a little of it got done. In addition to Andy I have been fortunate to have a number of people who have taken me under their scientific wings: Mike Hawkins, France Allard, Peter Hauschildt, Richard Jameson and Lance Miller.

Many people at the ROE who have given me valuable insights for this thesis; in particular I thank Phil James, Phil Puxley, Suzie Ramsay, Horst Mayerdicks, Martyn Wells, John Peacock, Andrew Harrison, Matt Mountain, Dave Buckley, David Emerson, Peter Brand and Andy Lawrence. In the field of low-mass stars, I have been impressed by a general willingness to share and discuss results. For sharing their data with me and putting me straight on lots of different things I am indebted to Mike Hawkins, France Allard, Peter Hauschildt, Richard Jameson, Andrew Thackrah, Steve Miller, Jonathan Tennyson, Ian Steele, John Fernley, Davy Kirkpatrick, Sandy Leggett, Nigel Hambly, Chris Tinney and Didier Saumon.

During my time in Edinburgh, I have had the pleasure of working amoungst a great bunch of students. In a traditional order thanks to Rijdat for wise words, Karl for giving me chapter 5, Dave for being a mentor, Suzie for her patience and knowledge of CGS4, Pippa for pompadoms, Ant for his fast mind (and car), Amadeu for being Bob, Ruth for rude words, Kath for teases shared, Isabelle for Pims, Bob for coftea, PC Dodds for Ω, Alan for serenity, Mike and Ramon for understanding of long distance romance, Harry for chuzpah, Johnny for taking over as student rep, Thackers for bomb disposal, Han Ying for helmet-prose, Steve change your T-shirt, Bill we know it is a wig, Henry 4 fluffybunnysquirrelkins, Mike for Rome and an honorary mention for ANT for buying me nearly as many drinks as he ought.

The Edinburgh festivals kept me sane and sometimes sociable. The MadDogs, James and Andy are especially thanked for doing all kinds of jobs that I should have been doing. Thank you Mum, Dad and MadLab for providing money in times of crisis. Thanks to Simon the numero uno friend and flatmate and to Mum, Dad, Suzy, Judy, Lyn, Judge and Angie for their inspiration, encouragement and all the fun times. Last and certainly not least Constanza who carried me through most of this thesis and without whom it probably would not have happened in the first place – the emotional roller coaster does not stop here.

Contents

Chapter 1

Introduction

Cool dwarf stars comprise 88 of the closest 100 stars, although their physical properties are not well understood because of their intrinsic faintness and low temperatures. In this introduction I present why an understanding of their properties and even lower mass objects called brown dwarfs are an essential part of a physical theory of the Universe.

The observable Universe is made of different structures which are primarily bound together by gravity. They come in a number of shapes, sizes and masses ranging from clusters of galaxies with masses of 10^{48} kg to dust grains less than 10^{-9} kg. The principal source of energy and evolution of observable properties in the Universe comes from stars. These form in a range of masses from 10^{26} to 10^{29} kg and all have the same driving energy. The thermonuclear fusion of hydrogen into helium in their cores provides the energy which eventually escapes and can be observed as starlight.

The similar energy source for all stars means they have largely continuous properties which depend on their mass. This relationship is known as the main sequence and can be visualised by plotting colour against intrinsic brightness. Such a plot is known as the Hertzsprung-Russell diagram since it was developed independently by Hertzsprung (1911) and Russell (1913). Its use and interpretation is the foundation of stellar astrophysics.

The main sequence on the Hertzsprung-Russell (HR) diagram is just one stage in an

evolutionary cycle. Stars form from a fragment of a gas cloud undergoing gravitational collapse. Once the newly formed star has collapsed to sufficient density and pressure, thermonuclear fusion converts hydrogen to helium in its core releasing enough energy to stop the star collapsing further. The subsequent evolution of the star is a strong function of its mass. In stars such as the Sun, once the central source of hydrogen has been used up, after about 10 billion years, the core regions collapse over a period of a few thousand years. This leads to a large release of energy and the ejection of most of the outer regions of the star; this is followed by collapse of the remaining core to a very dense object known as a white dwarf. Stars more massive than the Sun have much shorter more spectacular histories. The higher temperatures and pressures in their cores allows higher energy fusion process to take place which enable large scale chemical evolution of the star including the wholesale processing of core regions from hydrogen and helium to heavier elements. Once all the material available for nuclear fusion has been used their core regions also collapse. In massive stars the energy released is enormous (as much as 10^{53} ergs) and can result in a supernova explosion where most of the star is returned to the interstellar medium.

The in-depth understanding of the structure and evolutionary cycle of stars, represented on the HR diagram and briefly outlined above, is one of the major scientific achievements of the 20th century. Its development is recorded in the seminal treatises of Eddington (1926), Chandrasekhar (1938), Schwarzschild (1958) and Clayton (1968). An important well-tested consequence of the evolutionary cycle of stars is that it leads to the chemical evolution of the Universe. This occurs because processed stellar matter is returned to the interstellar medium and eventually to gas clouds which then coalesce and form into future generations of stars. This scenario yields a consistent basis which explains the appearance of different mass stars at different ages and provides for the observed large scale chemical and colour evolution of galaxies.

The main sequence lifetimes of stars with masses less than the Sun are significantly longer than the age of the Universe and so have not contributed to the evolutionary cycle. However the star formation process is expected to produce objects at least down to masses of 0.01 solar masses ($M_{\odot}$) (Boss 1986, 1989). The objects between about 0.65 and 0.08 $M_{\odot}$ undergo hydrogen fusion and are known as M dwarf stars. Below around

0.08 $M_{\odot}$, objects are not expected to undergo hydrogen fusion and so will not reach the main sequence; if they are more massive than Jupiter (0.0095 $M_{\odot}$) they are known as brown dwarfs (for discussion of the nomenclature see Tarter 1986 and Henry 1990).

Over the last 40 years numerous surveys have derived the low-mass stellar mass function. Critical reviews of the various survey techniques and the regions to which they have been applied are presented in Bessell & Stringfellow (1993) and Burrows & Liebert (1993). These surveys have discovered many thousands of new M dwarfs of which more than 50 have been claimed as brown dwarfs. However, improvements in detector technology and in evolutionary modelling have meant that with hindsight many of the claims have turned out to be an optimistic interpretation of the available data (e.g. Table 1.1 in Henry 1990).

Although no brown dwarfs have yet been definitively identified, there is a large body of evidence that only a small fraction of the mass of the Universe is in visible form (e.g. Carr 1994). This has become known as the dark matter problem and there are several reasons why brown dwarfs in particular are a very plausible solution. Firstly, Hawkins (1995) indicates that the stellar mass function is rising into the brown dwarf regime. Secondly, there may be direct evidence from cluster cooling flows that low-mass objects are formed with high efficiency even at the present epoch (reviewed by Fabian 1994). Thirdly, microlensing data from massive compact halo objects (known as MACHOS, e.g. Alcock et al. 1993, Aubourg et al. 1993) and quasar variability (Hawkins 1993) may already indicate that there is dark matter in the form of brown dwarfs.

Despite the identification of brown dwarf candidates the lack of understanding of M dwarfs has meant that it has not been possible to unambiguously distinguish these candidates from cool M dwarfs. Even M dwarfs are so intrinsically cool and faint that despite their dominance in the solar neighbourhood it has always been very difficult to observe them. Furthermore their energy distributions are complex to interpret and understanding of them has been hampered by a lack of model predictions resembling observation (e.g. Persson, Aaronson & Frogel 1977, Reid & Gilmore 1984, Ruan 1991, Tinney, Mould & Reid 1993, Brett 1995). Unlike hotter stars their atmospheres are dominated by a variety of species of molecules, many with billions of line transitions

modulating their energy output. Despite the formidable problems, the evolution of computing power over the last few years has enabled major improvements in low-mass star models, these are critically reviewed for (i) model atmosphere calculations by Ruan (1991) and (ii) evolutionary model calculations by Burrows & Liebert (1993). My thesis uses the new generation of models and the boom in infrared technology (charted by meetings of The Society of Photo-Optical Instrumentation Engineers, e.g. Crawford & Craine 1994) to determine the properties of M dwarfs and brown dwarf candidates.

The M dwarf properties of mass, luminosity, metallicity and temperature are poorly determined (e.g. review by Bessell & Stringfellow 1993). In order to derive an accurate mass functions for low-mass objects and to distinguish M dwarfs from brown dwarfs it is necessary to know the relationships between mass, luminosity, metallicity and temperature. In this thesis, I have primarily considered the latter three parameters since the direct determination of masses requires a long term program to monitor the orbits of dwarfs in close binary systems. Such programs have been carefully carried out over many years principally by Heintz (e.g. 1994) and Henry & McCarthy (e.g. 1993). I frequently make use of the masses which they have derived. The interpretation of the observations made for this thesis has largely been possible due to the work of groups modelling M dwarfs. Principal among these has been the synthetic spectra generated by Allard & Hauschildt (e.g. 1995) with whom I have worked closely. Also of great importance has been the evolutionary models for M dwarfs computed by Burrows et al. (1993), D'Antona & Mazzitelli (1994) and Nelson, Rappaport & Joss (1993). The main source of opacity stopping energy being released from M dwarf atmospheres is water vapour whose opacity at high temperatures is poorly known. I have collaborated with Fernley, Miller & Tennyson (1991) who have made extensive *ab initio* calculations for water vapour transitions to remedy this situation.

Thus over the last three years I have been fortunate to work on a number of exciting projects to understand low-mass stars. The research submitted for this thesis makes up chapters 2–5. Each of these has been prepared with the goal of publishing it as a separate paper. Chapter 2 appeared in MNRAS, 267, 413 with A.J. Longmore, R.F. Jameson and C.M Mountain as co-authors. Chapter 5 appeared in MNRAS, 270, L47 with L. Miller and K. Glazebrook as co-authors. Chapter 4 has been accepted by MNRAS with

A.J. Longmore, F. Allard, P.H. Hauschildt, S. Miller and J. Tennyson as co-authors. I also intend to submit Chapter 3 to MNRAS. Chapter 2 forms the basis for the other research work, where spectra across the peak of their energy output from 1 to 2.5 μm for a broad sample of low-mass objects were obtained and analysed to define accurate effective temperature and luminosities. These observations also enabled the important spectral features to be identified and provided vital feedback for the modelling of M dwarfs. This work suggested a region from 1.16 to 1.22 μm, particularly rich in spectral absorption features sensitive to M dwarf parameters, to be worthy of higher resolution observations and detailed spectral modelling. Chapter 3 presents these comparisons to determine M dwarf properties.

The low-resolution spectra presented in Chapter 2 show M dwarfs to be dominated by water vapour absorption bands but M dwarf models have great difficulty in modelling these bands. The reason for this was suspected to be the poor resolution and quality of the water opacities available for the model atmospheres (e.g. Tinney et al. 1993) and spurred the calculation of *ab initio* water transitions in the regimes of temperature relevant for M dwarfs (Miller et al. 1994). Spectra of a subset of the objects studied in Chapter 2 were taken in a region of strong water absorption in order to test the usefulness of the *ab initio* calculations and to understand the formation of water vapour in M dwarf atmospheres. The results of this analysis are presented in Chapter 4.

Despite their large number density relatively few late-type M dwarfs and brown dwarf candidates have yet been discovered. Their low luminosities and temperatures means that even within 8 pc there is strong evidence that $\sim$ 30 per cent (Henry, Kirkpatrick & Simons 1994) have yet to be discovered. The recent and continuing increase in the sensitivities and the number of pixels of infrared detector arrays means that infrared surveys are the most sensitive method to detect them. Chapter 5 presents the discovery of the reddest brown dwarf candidate in the infrared K-band and uses it to put a constraint on the luminosity function into the brown dwarf regime.

Combining experience and results from all these areas, it is possible to identify the most promising areas for future observation and theoretical research needed to continue the significant progress of the last three years. For example, the interpretation of new

brown dwarf candidates found from digitally stacking photographic plates (Hawkins 1995) within a new generation of the model atmosphere code from Allard & Hauschildt (1995, in preparation) is underway. Although these new objects are very cool and faint (Jones & Hawkins 1995a,b and Chapter 6.1.1) preliminary interpretation indicates that their temperatures are not significantly below 2000 K. The discovery and interpretation of 1000 K objects will probably have to wait a year or so until a significant fraction of the large-area infrared survey projects being carried out by the deep near infrared survey of the southern sky (known as DENIS, Epchtein 1993) and the infrared space observatory (known as ISO, Kessler, Metcalfe & Salama 1992) have been completed. These projects together with other areas for future work and the relevance of this thesis are discussed in Chapter 6.

Chapter 2

An infrared spectral sequence for M dwarfs

The first infrared spectral sequence for M dwarfs is presented.

• This sequence shows the progressive importance of water absorption in the atmospheres of M dwarfs. The strength of the water absorption bands is used as the basis of a new method to derive a temperature from which effective temperatures, masses and radii are calculated. This scale is consistent with recent evolutionary model calculations but not with previous empirical temperature scales which do not account for the importance of water absorption.

• GD165B has an effective temperature of 1860±160 K and it is the only star in the sample which might be classified as a brown dwarf but to decide its true nature a more accurate parallax and a representative model atmosphere will be necessary.

• The most important atomic and molecular features from 1–2.5 μm in M dwarfs are identified and theirs strengths correlated with effective temperature. Molecular absorption bands strengths are found to be the most reliable indicators of effective temperature.

• Together with spectra from Kirkpatrick et al. at shorter wavelengths, bolometric luminosities are found down to the hydrogen burning limit.

2.1 Introduction

M dwarfs are the most common stars in our stellar neighbourhood yet are also amongst the least understood, largely due to their intrinsic faintness. Over the last decade, numerous surveys have been made in an attempt to derive the space density of stars at the bottom of the main sequence. Such studies have been motivated by the desire to find substellar objects (brown dwarfs) and to understand the space density of such objects by extrapolating the mass function for objects above the hydrogen-burning limit to masses below. While the numbers of known faint M dwarfs and candidate brown dwarfs have increased dramatically, our understanding of their fundamental properties has not. In particular, the scales used to convert the optical or infrared colours into bolometric luminosities and effective temperature (and by extension into estimates of mass) are poorly defined. The interpretation has relied on (i) the assumption that the observed colours are monotonic in their effective temperature and (ii) a bolometric luminosity determined from spectrophotometry and from extrapolation of a blackbody curve into unmeasured parts of the star's energy distribution. Between 1 and 5 μm, however, where a 2500 K star emits 80 per cent of its flux, there are four strong water absorption bands, and thus spectra of cool dwarf stars do not resemble the blackbody curves which are shown by hotter stars across the infrared.

This deviation from a blackbody curve has implications for the measurement both of colour and of bolometric luminosity. The early temperature determinations (e.g. Veeder 1974) were achieved by fitting a blackbody to the observed broad-band colours of each star, assuming short wavelengths to have a certain amount of blocking and requiring the total flux under the blackbody curve and the bolometric luminosity to be equal. This technique was extended in later determinations where it was assumed that no significant backwarming occurs at 2.2 μm, and so the flux at that wavelength was adopted as a measure of the continuum emission from a blackbody with a temperature the same as the star's effective temperature (e.g. Berriman & Reid 1987). Hence the temperature for each star was determined from the blackbody curve having (i) flux equal to the observed flux at 2.2 μm, and (ii) the same bolometric luminosity. Such methods (Greenstein, Neugebauer & Becklin 1970; Veeder 1974; Peterson 1980; Reid & Gilmore

1984; Berriman & Reid 1987; Berriman, Reid & Leggett 1992; Tinney, Mould & Reid 1993) indicate a Hertzsprung–Russell (HR) diagram offset by some 400 K from current theoretical predictions. This is accepted to be an offset in temperature rather than in luminosity in that many of the stars in the above studies have parallaxes measured to better than 1 per cent and so the errors associated with the measurement of luminosity tend to be considerably smaller than those of temperature. This is supported by the large scatter in determinations of temperature but not in the determinations of luminosity found by the various investigators.

In order to construct accurate luminosity and mass functions for these stars, it will be necessary to understand how their spectra behave with temperature, metallicity and gravity (see Chapter 3). For this work spectra have been taken from 1 to 2.5 μm for a sample of M dwarfs and brown dwarf candidates with similar metallicity but a range of temperature. The observations and data reduction are presented in Sections 2.2 and 2.3, a derivation of effective temperatures of low-mass stars in Section 2.4, an HR diagram in Section 2.5 and a discussion of trends shown by the strong atomic and molecular features in Section 2.6. The conclusions are highlighted in Section 2.7.

2.2 Observations

The brown dwarf candidate, GD165B and a range of M dwarfs: LHS2924, VB10, GL406, GL699 and GL411 were observed. GD165B, discovered by Becklin & Zuckerman (1988), was chosen because its photometric colours make it the best brown dwarf candidate yet discovered by the numerous surveys for low mass stars conducted over the last 40 years. The others were chosen because they have been the subject of previous studies of M dwarfs (Veeder 1974; Mould 1978; Berriman & Reid 1987; Arnaud, Gilmore & Collier Cameron 1989; Bessell 1991; Berriman, Reid & Leggett 1992; Leggett 1992; Kirkpatrick et al. 1993a; Tinney et al. 1993) and because they form a sample whose space motions and colours indicate approximately the same age and metallicity (Table 2.1).

Observations were made with the Cooled Grating Spectrometer 4 (CGS4, Mountain et al. 1990) on the UK Infrared Telescope on Mauna Kea, Hawaii. The observations

Table 2.1: Photometry and distances of observed objects. The data for GL411, GL699, GL406, VB10 and LHS2924 are taken from Leggett's (1992) compilation of photometry for low-mass stars, for GD165B the data are from Zuckerman & Becklin (1992) and Tinney et al. (1993). The errors are quoted as ~ 0.03, except for GD165B for which the errors are ~ 0.05. U, B and V photometry is on the Johnson system; R and I band photometry is on the Cousins system; J, H and K photometry is on the California Institute of Technology (CIT) system; L and L' photometry is on the Mauna Kea Observatories system (MKO). Distances, d, are derived from the absolute trigonometric parallaxes from the Yale General Catalogue of Trigonometric Stellar Parallaxes (van Altena, Lee & Hoffleit 1992) except for GD165B (from Zuckerman & Becklin 1992) and GL411 (from Gliese & Jahreiss 1979). Population types are taken from Leggett (1992), where KIN signifies kinematic and COL colour, OD means old disc and OD/H means old disc–halo. Old disc represents [Z/H] ~ -0.5 and an old disc–halo type corresponds to [Z/H] ~ -1.0. We adopt the standard spectroscopic notation [Z] $\equiv \log Z_{\rm star} - \log Z_{\odot}$ for any abundance quantity Z.

Object	d (pc)	KIN	COL	$U_{\rm J}$	$B_{\rm J}$	$V_{\rm J}$	$R_{\rm J}$	$I_{\rm C}$	$J_{\rm CIT}$	$H_{\rm CIT}$	$K_{\rm CIT}$	$L_{\rm CIT}$	$L'_{\rm MKO}$	$M_{\rm UKIRT}$	$IRAS_{12}$	$IRAS_{25}$
GL411	2.535	OD	OD/H	10.12	8.98	7.47	6.46	5.32	4.10	3.56	3.36	3.20	3.08	-	2.7	2.4
GL699	1.83	OD/H	OD/H	12.54	11.28	9.55	8.34	6.77	5.27	4.77	4.51	4.20	4.17	4.2	4.0	3.9
GL406	2.83	OD	-	17.03	15.44	13.45	11.57	9.39	7.06	6.44	6.08	5.73	5.69	-	-	-
VB10	5.79	OD	-	-	19.63	17.50	15.10	12.80	9.90	9.24	8.80	8.35	8.15	-	-	-
LHS2924	10.7	OD	-	-	-	19.58	-	15.21	11.84	11.17	10.67	-	10.02	-	-	-
GD165B	36.0	-	-	-	-	-	-	19.25	15.78	14.77	14.13	13.30	-	-	-	-

were made with a 58 x 62 InSb array which was moved in the focal plane in order to over-sample the spectrum. Sky subtraction was performed by nodding the telescope approximately 30 arcsec up and down the slit, ensuring that during alternate 'object' and 'sky' observations the star remained on the detector. There were two observing runs, on 1991 June 20 and 1992 May 6–8.

The 75 line mm^{-1} grating was used in six different configurations in order to cover the wavelength of 1–2.5 μm with some overlap between each spectral segment. The coverage and resolution of the grating positions used are shown in Table 2.2. The combined spectra from 1 to 2.5 μm for all the objects are shown in Fig. 2.1, and their photometric colours in Table 2.1. For the fainter objects, GD165B, LHS2924 and VB10, integration times at each grating position were 20–35 min; for the brighter objects, GL411, GL699 and GL406, they were about 5 min. In this work far-red spectra for all of the stars other than GD165B were also used. These spectra were taken on the Multiple Mirror Telescope (MMT), Kitt Peak, Arizona, and kindly made available to us by Douglas Kelly and Davy Kirkpatrick. The full data set and reduction procedures are described by Kirkpatrick, Henry & McCarthy (1991) and Kirkpatrick et al. (1993a).

2.2.1 Standards

Stars in the spectral type ranges F6–G0 and A0–5 were used to remove from the observations the effects of atmospheric absorption. Except for Paschen and Brackett series hydrogen lines and very weak CO bands in the G dwarfs, these standards are thought to be featureless at the spectral resolution used and to be well described by a Rayleigh-Jeans tail. All observations were made in excellent conditions (typically around 1 arcsec seeing) and the airmass difference between object and standard never exceeded 0.05. Thus the spectra have excellent cancellation of atmospheric features.

2.2.2 Wavelength Calibration

The 1992 May observations were calibrated using a combination of lines from krypton and argon arc lamps. The 1991 June observations (VB10) were taken without arc lines

Table 2.2: Grating positions used to obtain the spectral sequence. The central wavelength positions used was λ_{cen}, all wavelengths are given in μm.

λ_{cen}	λ Range	$\lambda/\Delta\lambda$ at λ_{cen}	Date	Objects
1.04	0.95–1.14	349	920505–7	all
1.22	1.12–1.33	374	"	all except VB10
1.40	1.29–1.51	429	"	"
1.67	1.46–1.88	255	"	"
2.03	1.82–2.24	310	"	"
2.31	2.19–2.61	367	"	"
1.10	1.10–1.20	305	910620	VB10
1.30	1.20–1.40	398	"	"
1.50	1.40–1.60	460	"	"
1.75	1.56–1.95	268	"	"
2.04	1.84–2.24	312	"	"
2.20	2.00–2.40	337	"	"

and so use was made of the OH lines in the J and H windows (as described by Ramsay, Mountain & Geballe 1992) and the hydrogen recombination lines in the standards. VB10 was calibrated using OH lines and is accurate to $0.3\Delta\lambda$ μm, where $\Delta\lambda$ is the instrumental resolution; the other spectra were calibrated with lines from the CGS4 arc lamps and are typically accurate to $0.1\Delta\lambda$ μm.

2.3 Data Reduction

In the reduction of CGS4 data, the off-line CGS4 data reduction system was used (described in detail by Puxley, Ramsay & Beard 1992) together with the library of routines contained in the software packages FIGARO and SPECDRE supplied by STARLINK. Identifiable Paschen and Brackett series absorption lines were interpolated across, before using the spectra of standard stars to correct for the effects of terrestrial absorption in the target objects. The target object spectra were then divided by the standard star

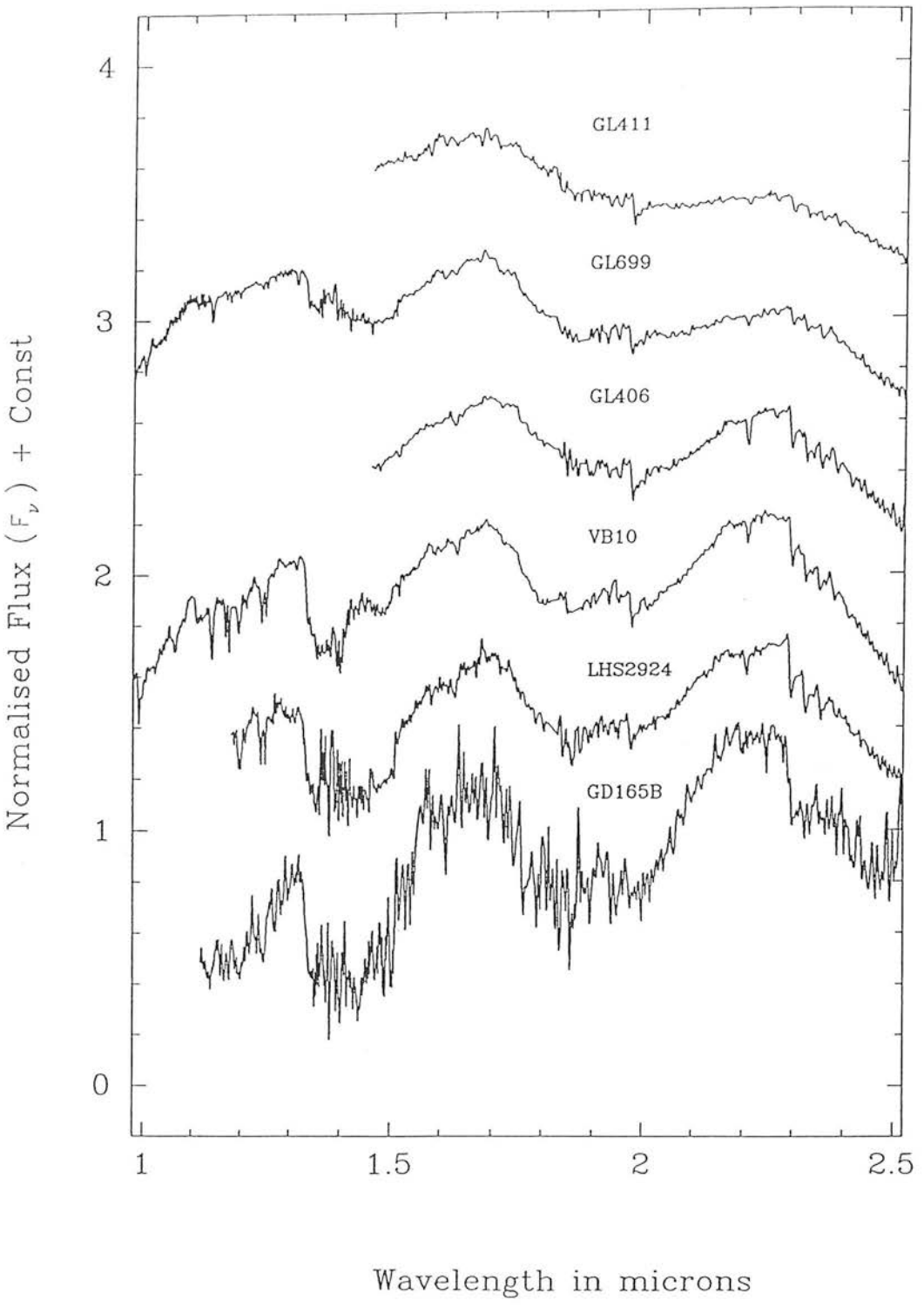

Figure 2.1: A spectral sequence for M dwarfs. The various spectra have been normalized and then shifted vertically in steps of 0.5 for the purpose of display. The increasingly humped appearance of the spectra with decreasing spectral type (down the page) results from the increasing importance of water absorption.

spectra and multiplied by a blackbody spectrum for the temperature (from Popper 1980) appropriate to the spectral type of that standard star. In addition to the deep, broad water absorption bands the resolution of each spectrum is sufficient to show a number of other prominent molecular and atomic features.

Once reduced, the overlapping spectral regions were joined together into J, H and K spectral regions. In the regions of overlap, the spectral features and continuum shape are well reproduced but the flux levels between different spectral regions differ by 5–20 per cent. Such differences probably arise from wind shake which causes the target to move out of the narrow slit (3 arcsec) during an observation. The overlapping spectral regions were combined by adjusting the flux levels of each of the spectral J, H and K bands so that the combined spectra reproduced the observed photometric colours. The California Institute of Technology (CIT) filter profiles and atmospheric transmission profiles (for 1.5 mm of precipitable water vapour at 5000 m) were used to ensure that the photometric $J-H$, $H-K$ colours derived from the spectra agreed with the values given in Table 1.

2.4 A temperature scale for M dwarfs

In order for the methods of temperature determination discussed in Section 2.1 to be successful it is necessary to appeal to a representative model atmosphere, which for M dwarfs has frequently been that of a blackbody.

2.4.1 Use of model atmospheres

Allard (1990) and Ruan (1991) have recently computed model atmospheres for M dwarfs. As yet, however, the models are not in good agreement with infrared observations (e.g. Graham et al. 1992; Kirkpatrick et al. 1993a; Tinney et al. 1993). In particular, there are considerable problems in modelling the 0.65–1.1 μm regions of the spectra and in the treatment of the dominant absorber in the infrared – water vapour. In the 0.65–1.1 μm region, the models used by Kirkpatrick et al. (1993a) did not include FeH which produces a deep band at 0.99 μm, and were unable properly to include bands due to TiO ϵ and VO (C–X) for which laboratory oscillator strengths have not been measured. While there

are gross discrepancies in the 0.6–1.1 μm region, which is near the blackbody peak for many of these spectra, it is problematic to make useful comparisons with the models in the infrared. In their papers, Graham et al. and Tinney et al. illustrated the problems and discussed the drawbacks of the models, in particular the use of the "just overlapping line approximation" (e.g. Tsuji 1994) for water vapour absorption, which gives a mean absorption coefficient for 72 spectral meshes between 0.27 and 30 μm. New derivations of the molecular band strengths (Allard & Hauschildt 1995) together with a detailed *ab initio* treatment of the water band (Miller et al. 1994; Allard et al. 1994) allow models and observations to be more reasonably compared (Chapters 3 and 4). However since the *ab initio* calculations for water vapour are known to be incomplete shortward of 1.8 μm (Allard et al. 1994) and the laboratory data for water absorption coefficient versus wavelength (Fig. 2.2 based on Ludwig 1971) have a very similar shape to the M dwarf spectra, I use these absorption coefficients to derive effective temperatures for the sample.

2.4.2 Derivation of effective temperature

At wavelengths longer than 1.34 μm, water vapour is the dominant opacity. Allard's models confirm that it dominates over its nearest rival, H^-, between 1 and 2.5 μm. The oscillatory nature of the water vapour opacity allows us to choose a number of wavelengths at which the optical depths will be equal at a given temperature, say 2500 K. It can be seen from Fig. 2.2 that at 2000 and 3000 K the opacities at these wavelengths are different from but still close to those at 2500 K. Stellar atmosphere theory tells us that a blackbody can be fit through points of constant optical depth; such a fit generates a temperature T. Having found T we can select slightly better wavelengths that have exactly equal opacities at this temperature. This can be done by interpolation between the water absorption coefficients. This procedure can be iterated until convergence is found. In order to get the most reliable fits, for GD165B and LHS2924 it was necessary to smooth the spectra through the water bands to the same resolution as the laboratory data. In regions where water opacity is clearly not the dominant opacity at a chosen wavelength point, in particular for the CO bands at 2.29–2.51 μm, it was necessary to interpolate across the feature. The final value of T is not the effective temperature, $T_{\rm eff}$.

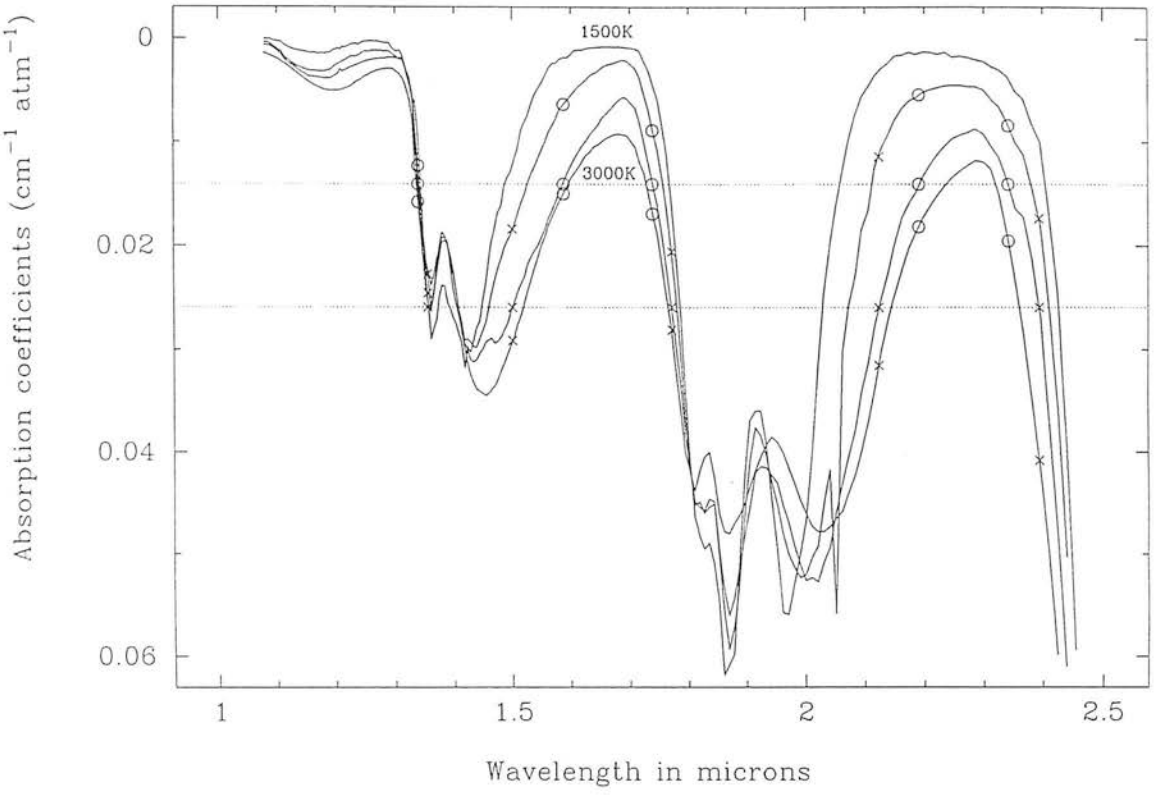

Figure 2.2: Absorption coefficient versus wavelength for water vapour at 1500, 2000, 2500 and 3000 K from Ludwig (1971). Wavelengths that are chosen have exactly equal opacity at 2500 K, but have slightly different values at 2000 and 3000 K. Crosses denote high-opacity points; circles denote low-opacity points.

However, T does allow us to calculate $(R/d)^2$ from the equation

$$f_\lambda = R^2 F_\lambda(T) d^2, \tag{2.1}$$

where f_λ is the measured flux at one of the wavelengths, R the effective radius, d the distance of the object and $F_\lambda(T)$ the Planck function. The effective temperature $T_{\rm eff}$ can now be found from the bolometric flux, $F_{\rm bol}$, using

$$\sigma T_{\rm eff}^4 = (d/R)^2 F_{\rm bol}, \tag{2.2}$$

where σ is the Stefan-Boltzmann constant. The radius can be assumed to be constant as the photospheres of these high gravity dwarf stars are extremely thin (e.g. Allard 1990). No evidence is found for a difference in the radii derived from blackbody fits for levels of different opacity, and so consider this to be a valid assumption.

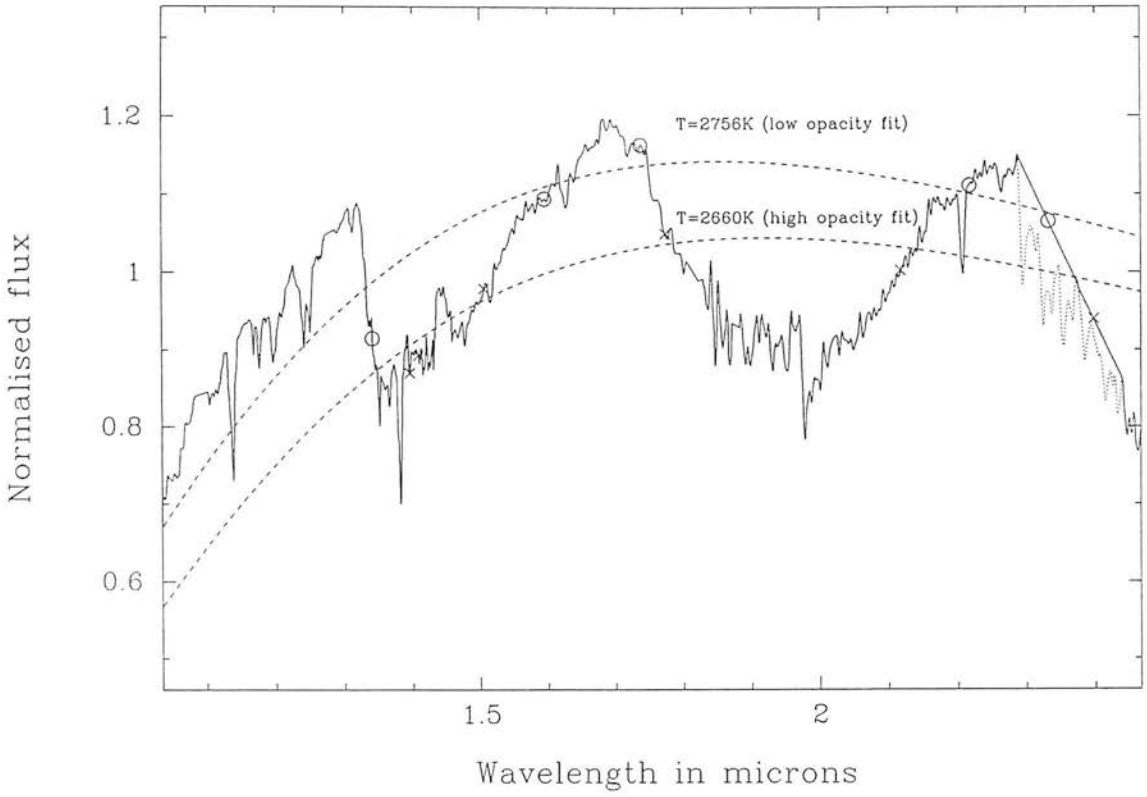

Figure 2.3: GL406 shown with the high-opacity (2660 K) and the low-opacity (2756 K) best-fitting blackbodies. The derived effective temperature would lie virtually on top of the high opacity fit. The worst-fitting point for GL406 and the other objects is the longest wavelength one, which falls in a regime where CO absorption dominates over water vapour absorption. This was corrected for by linear interpolation over the CO absorption bands.

Except for GD165B, the bolometric flux was determined by combining the photometry presented in Table 2.1, the 0.65–1.45 μm spectra from Kirkpatrick et al. (1991, 1993a) and the infrared spectra presented in Fig. 2.1 and beyond 2.5 μm with spectra from Berriman & Reid (1987) and synthetic spectra from Allard (1993, private communication). For GD165B Allard's models were also used for wavelengths shortward of 1.1 μm.

Hence effective temperatures were derived for the sample by determining f_λ, $F_\lambda(T)$ and $F_{\rm bol}$. The validity of the method was checked by repeating the fitting sequence for different levels of opacity. Use of wavelength points corresponding to lower water opacity led to slightly higher values for T and a larger f_λ. For example, for the star GL406 shown in Fig. 2.3, using high-opacity points (0.0262 cm^{-1} atm^{-1}) a constant opacity temperature of 2660 K is found, which gives an effective temperature of 2671 K;

using a set of low-opacity points ($0.01405\ \mathrm{cm}^{-1}\ \mathrm{atm}^{-1}$) the constant opacity temperature is 2756 K and the effective temperature is 2667 K. Higher temperatures for all the objects were derived using the points of lower opacity, because the blackbody is then fitted to a region slightly deeper (and hotter) in the photosphere. The quality of such blackbody fits tended to be poorer than that obtained when using high opacity points. The derived effective temperatures were in all cases within 160 K of one another. Our final adopted values for effective temperature were found by weighting the T_{eff} derived from the high opacity by 2/3 and those derived from the low opacity by 1/3. The high opacity points were favoured because (i) they gave the lower fitting errors, (ii) they are less affected by other sources of opacity and (iii) they allow a longer wavelength baseline.

Our derived values for T_{eff}, M_{bol} and R are given in Table 2.3. In Fig. 2.4 the derived values of effective temperature and bolometric luminosity are compared with those derived by previous authors. The derived bolometric luminosities are similar to those found by other investigators. The effective temperatures, however, are considerably hotter than those derived by Veeder (1974), Berriman & Reid (1987) and Tinney et al. (1993), but cooler than those derived by Kirkpatrick et al. (1993a). In Fig. 2.3 the blackbody corresponding to T_{eff} lies virtually on top of the high opacity curve which passes about mid-way between the spectral peaks and troughs. The method of Berriman & Reid (1987) is to solve the equation

$$C f_{2.2}/f_{\mathrm{bol}} = F_{2.2}(T_{\mathrm{eff}})/\sigma T_{\mathrm{eff}}^4, \tag{2.3}$$

where $f_{2.2}$ and f_{bol} are the measured quantities with the assumption that the constant, $C = 1$. However, in Fig. 2.3, $C < 1$ and so 2.2 μm is not a point of continuum for such cool stars. This possibility was discussed by Berriman & Reid (and by Tinney et al., who chose a reference wavelength of 3.82 μm). The lower values of T_{eff} found by Berriman & Reid can be explained in terms of C as follows. 2.2 μm is close to the wavelength of maximum intensity of the Planck curve at 2000 K, so that $F_\lambda(T_{\mathrm{e}}) \propto T_{\mathrm{eff}}^3$. Therefore, for an observed value of $f_{2.2}/f_{\mathrm{bol}}$, $T_{\mathrm{eff}} \propto C^{-1}$ and so finding that $C < 1$ leads to the derivation of systematically higher temperatures than did these investigators. The stars' rank order in temperature will probably be unaffected by the value of C.

Table 2.3: Fundamental parameters derived for observed stars. In our derivation of bolometric luminosity, effective wavelengths and flux densities are assumed for a zero-magnitude star as given by Berriman et al. (1992) for U, B and R bands, by Tokunga (1987) for V, I, J, H, K, L and L' and by Berriman & Reid (1987) for the M and IRAS bands. The values of g and R are calculated assuming $M_{\rm bol} = 4.75$ and $T_{\rm eff} = 5770$K for the Sun (Allen 1973).

Object	Radius ($R_\odot$)	Mass ($M_\odot$)	Gravity ($g_\odot$)	$M_{\rm bol}$	$T_{\rm eff}$ (K)
GL411	0.430	0.43	2.33	8.79	3471
GL699	0.208	0.17	3.91	10.86	3095
GL406	0.149	0.10	4.50	12.23	2670
VB10	0.103	0.085	7.96	13.30	2506
LHS2924	0.095	0.081	8.97	14.01	2219
GD165B	0.089	0.078	9.68	14.91	1856

Kirkpatrick et al. determined temperatures by comparisons with Allard's (1990) model atmospheres, which show reasonable agreement with observations from 1.1 to 1.35 μm. However, it is difficult to trust these higher temperatures whilst the fit through the 0.65–1.1 μm and 1.35–2.5 μm regions has been shown to be poor. If water vapour is indeed the dominant source of opacity then the method should be reliable. Nevertheless, the major problem with the models has been with the strength of the water vapour bands (e.g., Ruan 1991, ch. 3.4). This is discussed at length in Chapter 4.

2.5 Location on theoretical HR diagram

In Fig. 2.4 the sample luminosities and effective temperatures are plotted against various evolutionary models: (i) the model from D'Antona & Mazzitelli (1985), which has become the benchmark for evolutionary models of low mass stars, (ii) the extremal models by Burrows, Hubbard & Lunine (1989), and (iii) the standard model X adopted by Burrows et al. (1993). Using the Burrows et al. model X masses have been derived for the objects in the sample (Table 2.3).

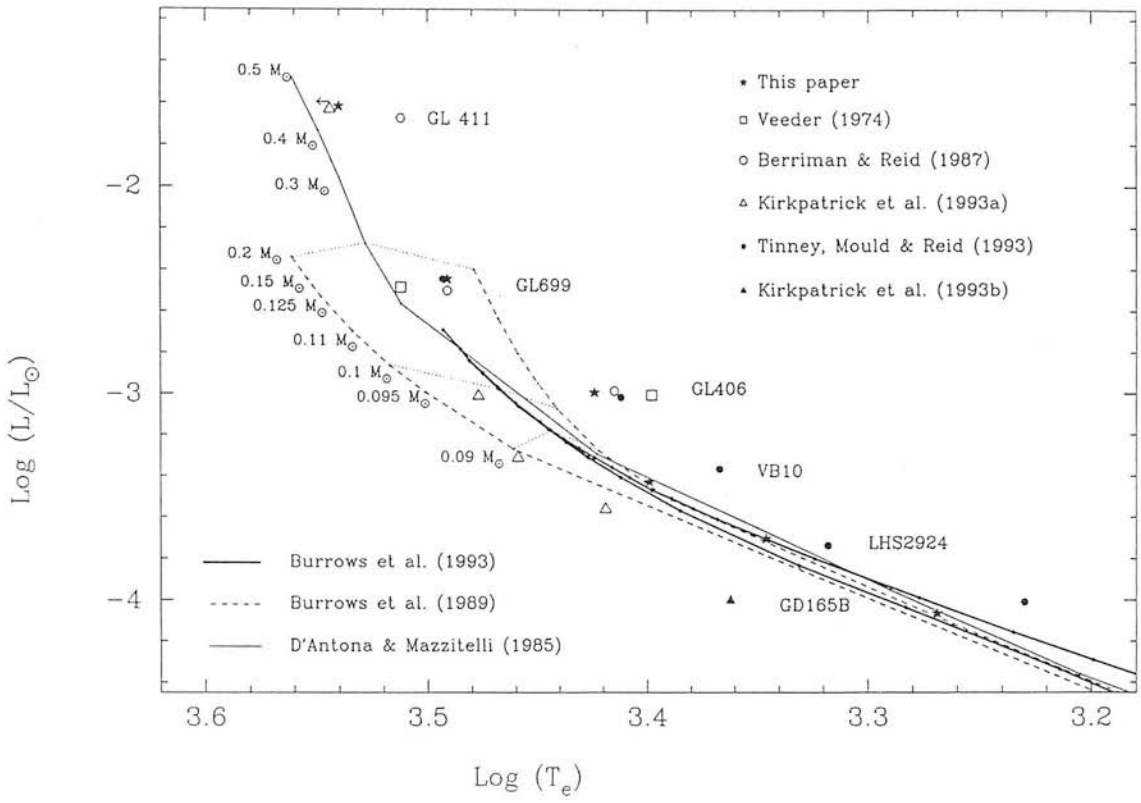

Figure 2.4: Derivation of mass using theoretical temperature versus luminosity for different models. The dashed lines represent the two extremes of the models presented by Burrows et al. (1989) at 10 Gyr. Each of the model points is marked with a small solid dot, and some equal-mass lines are shown as dotted lines connecting the corresponding points from models D (high opacity, low helium abundance) and E (low opacity, high helium abundance). The value of the mass is given to the left of the model E isochrone; below 0.09 $M_{\odot}$ these models are incremented in steps of 0.02 $M_{\odot}$. The thick solid lines are the standard models at 0.6 and 10 Gyr (the younger one is the slightly higher of the two) due to Burrows et al. (1993). The thin solid line is due to D'Antona & Mazzitelli (1985), and is for 1 Gyr. All models are for solar abundances. Previous determinations of the effective temperature and bolometric luminosity for this sample of low mass stars are plotted as open squares (Veeder 1974) open circles (Berriman & Reid 1987), open triangles (Kirkpatrick et al. 1993a), filled circles (Tinney et al. 1993), filled triangles (Kirkpatrick et al. 1993b) and stars (this work).

Leggett (1992) classifies all the stars in the sample, apart from GD165B, as old disc stars. In Fig. 2.4 it can be seen that for masses above 0.09 $M_\odot$ the evolutionary tracks for stars between 0.6 and 10 Gyr are almost indistinguishable. This means that for all of the sample, apart from LHS2924 and GD165B, masses can be assigned with some confidence. Below 0.09 $M_\odot$, however, the mass of an object with a given effective temperature and luminosity cannot be determined reliably without first assigning an age. For example, the standard model by Burrows et al. (1993) predicts that an object at about 2090 K and $L/L_\odot = 1.5 \times 10^{-4}$ will have a mass of 0.065 $M_\odot$ if it is 0.6 Gyr old whereas if it is 10 Gyr old then its mass will be 0.080 $M_\odot$. Since LHS2924 is classified as an old disc star the 10 Gyr model track was adopted to derive its mass. For GD165B the situation is more ambiguous. Leggett's (1992) assignments of age/metallicity were based on space motions which have not yet been measured for GD165B. However, it does have a well studied companion, the cool ZZ Ceti white dwarf GD165A which had a progenitor in the mass range 1.5–6 $M_\odot$. This places only a loose constraint on evolution, plus cooling time-scales of greater than 0.5 Gyr. Conservative limits on the mass of GD165B can be placed by using models at 0.6 and 10 Gyr, that is, between 0.067 and 0.078 $M_\odot$. Burrows et al. (1993) find that the main sequence ends at 0.0767 $M_\odot$ for solar metallicity objects and at 0.094 $M_\odot$ for zero-metallicity objects, so GD165B is a good brown dwarf candidate. To decide its true nature, a more accurate parallax (better than the current 12 per cent) and an accurate model atmosphere will probably be necessary.

2.6 Spectral Features

The spectra are dominated by deep broad absorption bands of H_2O, but have many other strong features, both molecular and atomic. The spectral identifications shown for VB10 in Fig. 2.5 come from M giants (Chauville et al. 1970), α Orionis (Vieira 1985) and an infrared solar line list by Hall (1980). Other important sources were Kirkpatrick et al. (1993a), Allard (1990), Ruan (1991), Davidge & Boeshaar (1991, 1993), Allen (1973), Spinrad & Wing (1969), Merrill & Ridgway (1979) and Kleinmann & Hall (1986). In Table 2.4, the absorption lines for which there are firm identifications and which are observable in all the objects are given with the equivalent widths measured

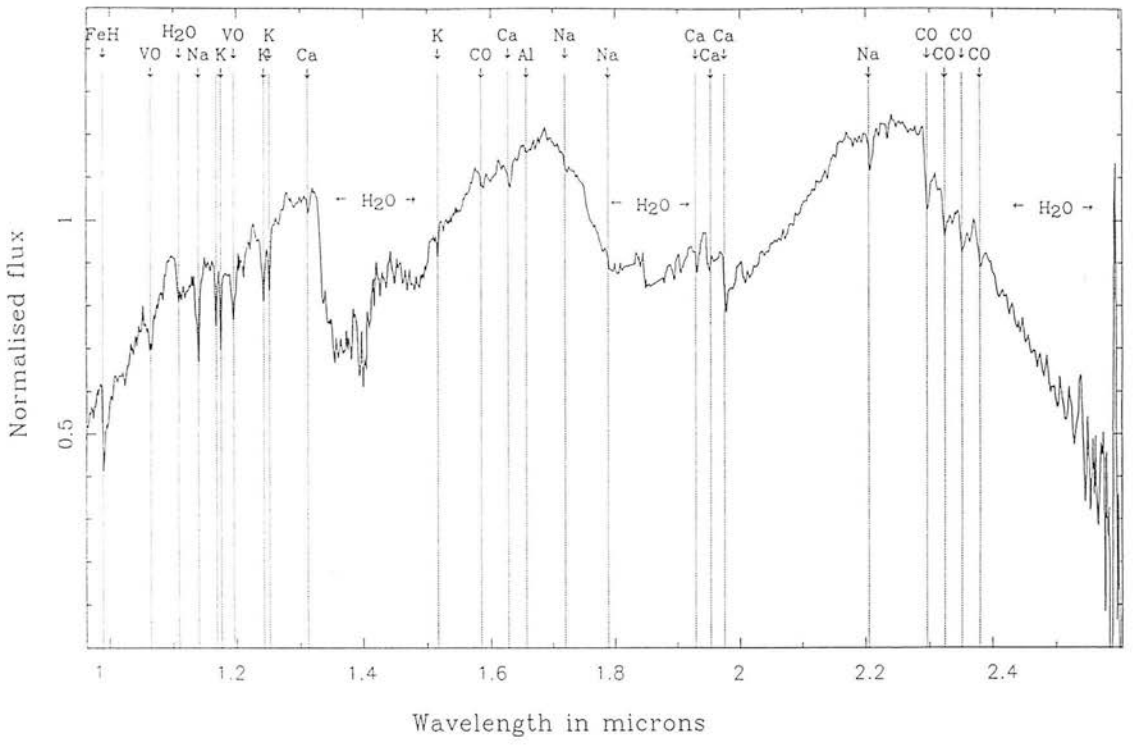

Figure 2.5: Spectral identifications for VB10.

using ABLINE (Robertson 1986). For each feature a quality index is assigned to indicate the estimated measurement errors: x (~5 per cent), y (~25 per cent) and z (~50 per cent) for the brighter stars in the sample, and 40 per cent, 60 per cent and 80 per cent respectively for GD165B because of its considerably poorer signal-to-noise ratio. It should be noted that in absolute terms these widths are very tricky to determine, since all of the features measured are superposed at some level on molecular bands and in many cases also blended with other atomic lines. By using the same procedure for each line in different objects, we trust that these widths should at least be internally consistent. All continuum fits were based on fitting a low- order polynomial to the level immediately adjacent to the feature rather than trying to measure the equivalent widths of features by estimating an overall continuum level. Overlapping atomic doublets and triplets were in a number of cases measured as single equivalent widths, rather than attempting to measure a number of blended lines. In Fig. 2.5 the equivalent widths are plotted against the values for effective temperature. A number of prominent spectral features have equivalent widths that are apparently very strongly correlated with effective temperature.

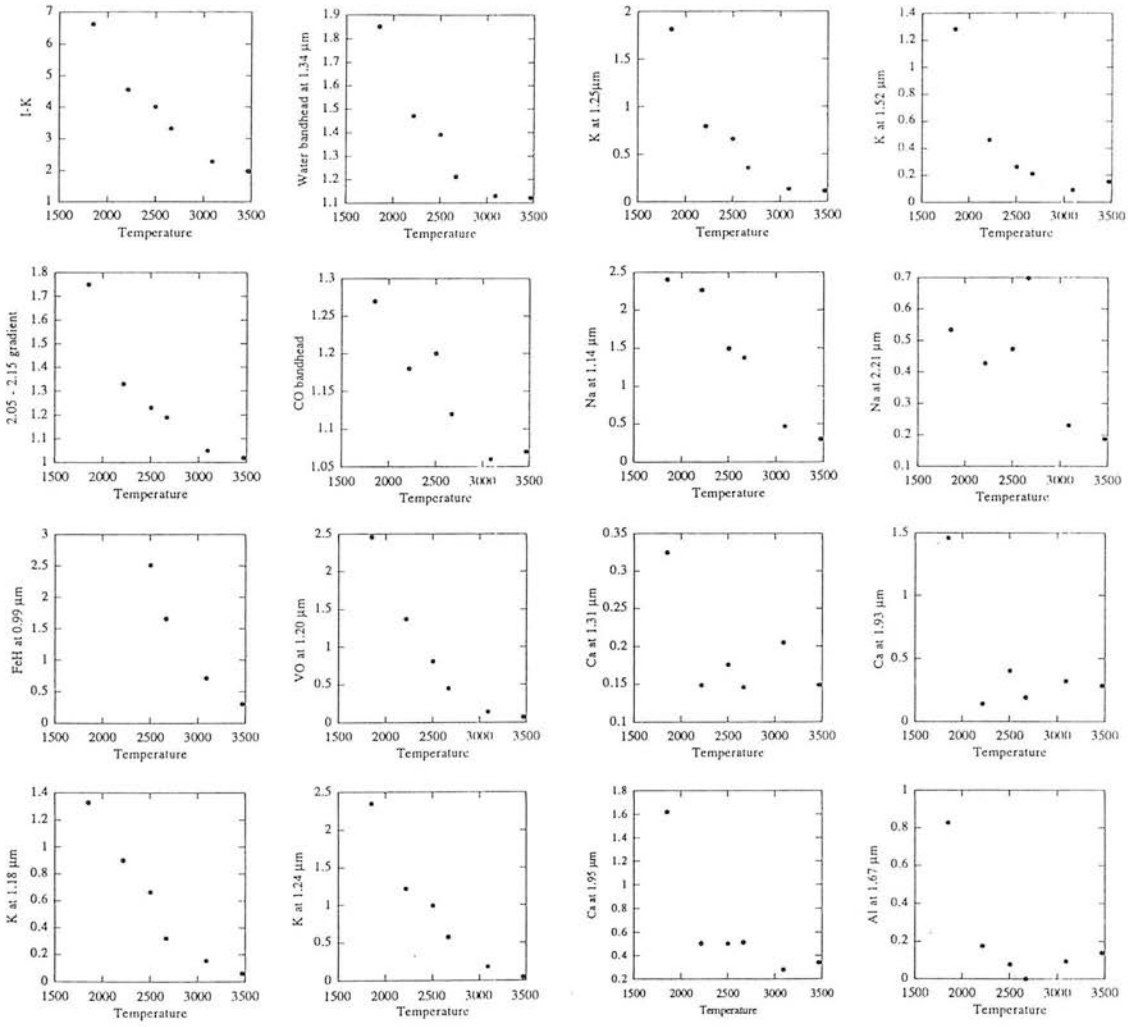

Figure 2.6: Equivalent width (in nm) versus effective temperature (in K) for infrared features that appear in each of the sample.

Table 2.4: Equivalent widths for the major infrared absorption features observed in M stars.

Species	λ (μm)	Equivalent widths in nm						Quality
		GL411*	GL699	GL406*	VB10	LHS2924	GD165B	
FeH	0.99	*0.305*	0.714	*1.66*	2.51	-	-	x
NaI	1.1404,1.1381	*0.299*	0.468	*1.37*	1.49	2.26	2.40	y
KI	1.1690	*0.0299*	0.102	*0.153*	0.575	0.556	1.36	x
KI	1.1777, 1.1773	*0.0559*	0.157	*0.321*	0.664	0.902	1.33	x
VO	1.20	*0.0714*	0.139	*0.449*	0.808	1.37	2.46	y
KI	1.2432	*0.0468*	0.179	*0.574*	0.995	1.22	2.35	x
KI	1.2522	*0.111*	0.133	*0.353*	0.656	0.790	1.81	x
CaI	1.3135	*0.149*	0.205	*0.146*	0.176	0.149	0.325	y
KI	1.5167, 1.5172	0.151	0.0896	0.211	0.261	0.459	1.28	z
Al	1.6755, 1.6768	0.139	0.0932	0.00153	0.0784	0.176	0.829	z
CaI	1.9272	0.284	0.320	0.192	0.403	0.141	1.46	y
CaI	1.95	0.340	0.281	0.514	0.504	0.505	1.62	y
CaI	1.987,1.992	0.741	0.771	1.01	0.919	0.850	0.992	z
NaI	2.2062, 2.2090	0.187	0.229	0.697	0.471	0.427	0.910	x
Spectral indices								
H_2O bandhead at 1.34 (1.286–1.303)/(1.338–1.356)		*1.12*	1.13	*1.21*	1.39	1.47	1.85	x
CO bandhead at 2.294 (2.22–2.28)/(2.30–2.36)		1.07	1.06	1.12	1.20	1.18	1.27	x
2.05-2.15 gradient		1.02	1.05	1.19	1.23	1.33	1.75	x

*Data in italics are equivalent widths measured from Kirkpatrick et al. (1993) dataset.
The Quality measure in the final column assigns an error bar to the measurement of each feature, x < 20%, y < 40% and z < 50%.

Within the uncertainties of poorly defined metallicity, the $I - K$ colour is a reliable indicator of effective temperature. This result should be useful, as it allows good estimates of effective temperatures to be made from $I - K$ colour alone without the need for higher spectral resolution. Within the same caveat for metallicity, a number of features at higher resolution scale with temperature: at low spectral resolution, the H_2O bandhead at 1.34 μm, the 2.05–2.15 μm gradient and the CO bandhead at 2.29 μm; at higher spectral resolution, K with two strong doublets in the J window, FeH at 0.99 μm and VO at 1.2 μm. Particular care is needed when using features that occur in between the atmospheric windows. For example there are a number of strong Ca lines around 1.95

μm for which it is especially difficult to deduce a reliable continuum. In addition, there are a number of features that are strongly blended with other species – in particular, the FeH band at 1.20 μm is probably blended with VO, Fe and Ti.

The interpretation of atomic equivalent widths in cool stars is considerably more complex than in hotter stars because below 4000 K, hydrogen is neutral and easily ionized metal elements, such as Na, Ca and K, are the major contributors of free electrons. Because the metallic elements are partly ionized, the number densities of the atomic metallic species are determined not only by the elemental abundance but also by the ionization state of the stellar atmosphere, so that, even for an accurate [Z/H], the uncertainty in ionic abundances will be significant. Moreover, some metallic elements are involved in the formation of molecules, and the number densities of the atomic species are not therefore directly proportional to the abundances of the elements. Whereas in hotter stars the equivalent widths of "weak" (<0.6 nm) metallic lines are insensitive to small changes in number density, in cooler stars such changes will affect the atmospheric structure and with it the measured equivalent width. Ruan (1991) shows that the separation between curves of growth calculated with slightly different values of [Z/H] dramatically increases as the temperature falls. Furthermore, it can be seen from Table 2.4 that our sample of stars covers a range of $g/g_{\odot}$, where g is surface gravity, which increases with decreasing temperature. It is to be expected that many of the spectral features will also have some gravity dependence. Until the detailed dependences of temperature, elemental abundance and gravity on the derived equivalent width using accurate synthetic spectra have been examined the interpretation of the trends apparent from Fig. 2.5 in terms of temperature only must be treated with caution. In Chapter 3 these issues are investigated for the 1.16–1.23 μm region.

2.7 Conclusions

A new set of effective temperatures for M dwarf stars has been derived by using the dominance of water opacity. These temperatures correlate well with $I - K$ colour and agree with the theoretical main sequence predictions for the coolest M stars, but not with those found by previous investigators. We show that most atomic and molecular infrared

spectral features in M dwarf stars are sensitive to temperature, and find the depth of the H_2O bandhead at 1.34 μm, the strongest spectral feature, to be a good indicator of temperature. It does, however, have the disadvantage that it is measurable in faint objects only from a high, dry site. On the other hand, the 2.05–2.15 μm gradient and the CO bandhead at 2.29 μm, although not quite as prominent, are also good indicators of temperature and somewhat easier to measure.

Chapter 3

Spectral analysis of M dwarfs

Spectra of M dwarfs, close to the peak of their energy output (1.16–1.22 μm) are compared with synthetic spectra calculated with a stellar atmosphere code. The synthetic spectra give a representation of the overall spectral features which has not been possible in previous comparisons with cool low-mass dwarf spectra, although the interpretation of the observed spectra is hampered by the quality of atomic and molecular input data.

- The comparisons suggest a similar spread in metallicities to that anticipated, although for our sample neither kinematic motion nor membership of a particular photometric class are, on their own, reliable indicators of metallicity.

- Comparison between observed and synthetic spectra for GD165B indicate that [K/H] > -1. This together with a improved distance measurement for GD165B leaves only a small parameter space for it not being a brown dwarf.

- In the spectral region 1.16–1.22 μm all atomic and molecular features show a strong sensitivity to temperature, especially the K lines. Metallicity and gravity effects are relatively much smaller.

- Atomic lines in cooler M dwarfs (< 3300 K) do not show the intuitive behaviour of atomic lines decreasing in strength with decreasing metallicity. In cool M dwarfs the sensitivity of atomic line profiles to increases in pressure resulting from lower metallicities are more important than decreases in atomic number density.

3.1 Introduction

Comparison of synthetic and observed spectra of low-mass stars can yield directly the properties of effective temperature, surface gravity and metallicity which can be used to infer mass and age. Since all low-mass objects, even hydrogen burning ones, take at least 0.5 Gyr to contract to a stable configuration age is vital for their interpretation on an Hertzsprung-Russell (HR) diagram. Metallicity can be related to the age of formation (e.g. reviews by Sandage 1986, Gilmore, Wyse & Kuijken 1989, Wheeler, Sneeden & Truran 1989). Surface gravity is also sensitive to age and to a lesser extent mass. In principle the measurement of accurate surface gravities enables young cooling brown dwarfs and older late-type M dwarfs with similar colours and luminosities to be distinguished (e.g. Burrows, Hubbard & Lunine 1993). Effective temperatures are sensitive to both mass and age. Compared to the spectral analysis required to determine metallicity and gravity, effective temperatures can be estimated relatively easily using photometric colours. The ability to measure and to model these properties is vital to disentangle M dwarfs from brown dwarfs and to derive an accurate mass function below 0.2 $M_{\odot}$.

Although the theory of low-mass stars (< 0.7 $M_{\odot}$) has a long pedigree (e.g. review by Ruan 1991) models have had little success in matching observed spectral energy distributions. The effective temperatures ($T_{\rm eff} < 4000$ K) and pressures (> 10 atmospheres at an optical depth of 1) prevalent in M dwarfs atmospheres allows for the widespread formation of molecules. This means that a realistic model atmosphere for a low-mass star, in addition to the many difficulties encountered in construction of model atmospheres for a hotter stars, must account for the formation of a variety of little studied molecules, with large opacities, each affecting the abundance of the parent atomic populations.

A number of researchers has compared synthetic spectra from model atmospheres with observed spectra for M dwarfs to derive stellar parameters. Kirkpatrick et al. (1993) and Chapter 4 found effective temperatures for assumed metallicity and surface gravity using a range of M dwarfs. Mould (1978) and Naftilan, Sandmann & Pettersen (1992) inferred effective temperatures and metallicities with assumed gravities for samples of early-type M dwarfs. With large errors they indicated that their samples were slightly metal-poor relative to solar abundance. Despite the relative ease of measuring

M dwarf colours, uncertainty in translation to temperature and the inadequacy of model atmosphere calculations for late-type M dwarfs seems to have stalled further investigations.

Since the computations of Mould (1976) on which the Mould and Naftilan et al. analyses were based significant improvements to molecular and atomic data bases have been achieved. Using these new databases, Allard (1990) and Ruan (1991) constructed models able to reproduce many of the features observed at optical and near infrared wavelengths. The Allard model code has since been included in the model atmosphere code PHOENIX (Hauschildt 1991; Hauschildt et al. 1994; Hauschildt et al. 1995) and substantially upgraded by Allard & Hauschildt (1995) and Allard, Hauschildt & Jorgensen (1995, in preparation) and these are the models used for this study. The model improvements combined with the opportunity provided by a new generation of sensitive infrared spectrometers has encouraged us to investigate how observed and synthetic M dwarf spectra behave with effective temperature, metallicity and gravity. We have selected a spectral region based on the work of Chapter 2 from 1.16 to 1.22 μm shown to be particularly sensitive to changes in the properties of M dwarfs. The observations and data reduction are presented in Section 3.2. The model atmospheres are discussed in Section 3.3. Spectral identifications are made in Section 3.4. The expected M dwarf parameter space is examined in Section 3.5. Section 3.6 compares the observed and synthetic spectra; Sections 3.7 and 3.8 discuss and summarise the results.

3.2 Observations

We observed the brown dwarf candidate, GD165B and a range of M dwarfs: LHS2924, GL569B, VB10, GL406, GJ1111, GL699, GL388, GJ1062, GL411, GL569A and GL123. GD165B, discovered by Becklin & Zuckerman (1987), was chosen because its photometric colours make it one of the best brown dwarf candidates yet discovered by the numerous surveys for low-mass stars conducted over the last 40 years. The others were chosen because they have been the subject of many previous studies of M dwarfs and because they form a sample whose space motions and colours indicate they cover a wide range of temperature, metallicity and gravity. The diversity of the sample can be seen in

Table 3.1. The sample do not form a monotonic sequence in spectral type, in absolute K magnitude or in photometric colour. Thus we consider this an intriguing sample to examine the properties of M dwarfs.

Observations were made with the Cooled Grating Spectrometer 4 (CGS4, Mountain et al. 1990) on the UK Infrared Telescope (UKIRT) on Mauna Kea, Hawaii. The instrument then had a 58 x 62 InSb array which was moved in the focal plane in order to three times over-sample the spectrum. Sky subtraction was performed by nodding the telescope approximately 30 arcsec up and down the slit, ensuring that during alternate 'object' and 'sky' observations the star remained on the detector. The observations presented in this paper were made during four nights, 1993 April 23 and 24, 1994 Jan 21 and April 24 in a wide variety of conditions of optical seeing (0.75–2 arcsec) and of atmospheric humidity (10–75 per cent). The airmass difference between object and standard never exceeded 0.05 and so we are confident that the spectra have good cancellation of atmospheric features.

Although the observations required several hours on a number of nights the actual time spent integrating was relatively short because of the large overhead of making frequent observations of standards. For GD165B an on-chip integration time of 1 hour was used; for LHS2924, GJ1111 and VB10 on-chip integration times were 20–35 min; for GL569A, GL569B, GJ1062, GL388, GL123, GL411, GL699 and GL406, on-chip integration times were 5–10 min.

The 150 lines mm^{-1} grating was used in third order with the 150 mm focal length camera at a central grating wavelength of 1.19 μm. This grating position was chosen as it is close to the peak of the energy distribution for M dwarfs, at a maximum in the grating efficiency, has high atmospheric transmission (>95 per cent) and gives a relatively high resolution, $\lambda/\Delta\lambda$, where $\Delta\lambda$ is the detector resolution at wavelength λ, of 1085 (equivalent to 276 km/s).

Table 3.1: A selection of important properties of the stars used in the analysis. They are based on the compilation of Leggett (1992) except where specific references are given. The V_C–K_{CIT} colour has an error of ± 0.03. The I_{CCD}–L'_{MKO} colour has an error of ± 0.05 except for GD165B and GL569B for which the error is ± 0.1. GD165B has I_{CCD}-band photometry from Tinney, Mould & Reid (1993) and L'_{MKO} from Jones et al. (1995, in preparation and). The V-band and I-band photometry is on the Cousins system (I_{CCD}); the K-band photometry is on the California Institute of Technology (K_{CIT}) system and the L'-band photometry is on the Mauna Kea Observatories system (L'_{MKO}). Distances, d, are derived from Gliese & Jahreiss (1991) except for GD165B, from Dahn et al. (1995, in preparation) and for GL569AB, from van Altena, Lee & Hoffleit (1994). Spectral types (Sp Type) are taken from Kirkpatrick et al. (1991) and Kirkpatrick et al. (1995). Population types are inferred from the objects kinematics (KIN) and photometric colours (COL). The symbols YD, OD and H refer to the young disc, old disc and halo populations and imply ages of 0.3–1.5 Gyr (Eggen & Iben 1988), 1.5–6 Gyr (Eggen 1989) and older than 6 Gyr. A backslash (/) symbol indicates that the object is intermediate in type between the two noted populations. The population types also correlate with metallicity, [Z/H]: young disc have [Z/H] $\sim$ 0.0, old disc have [Z/H] $\sim$ –0.5 and halo have [Z/H] $<$ –1.0. We adopt the standard spectroscopic notation [Z] $\equiv \log Z_{star} - \log Z_{\odot}$ for any abundance quantity Z.

Object	d (pc)	KIN	COL	Sp Type	M_K(CIT)	V_C–K_{CIT}	I_{CCD}–L'_{MKO}
GL123	16.13	OD	OD	-	4.59	3.44	-
GL411	2.5	OD	OD/H	dM2e	6.34	4.11	2.24
GJ1062	15.43	H	H	-	7.86	4.21	-
GL569A	9.94	YD	YD	dM2.5e	5.80	4.42	-
GL388	4.89	YD	YD	dM3e	6.16	4.71	-
GL699	2.39	OD/H	OD/H	dM3.5	8.20	5.04	2.59
GL299	6.76	H	H	sdM3	8.49	5.19	2.68
GL406	1.83	OD	-	dM6e	9.19	7.37	3.70
GJ1111	3.626	YD	-	dM6.5e	9.46	7.53	-
VB10	5.79	OD	-	dM8e	9.99	8.70	4.65
GL569B	9.94	YD	YD	dM8.5	9.61	-	4.95
LHS2924	10.72	OD	-	dM9e	10.52	8.91	5.19
GD165B	36.0	-	-	>dM10	11.62	-	6.3

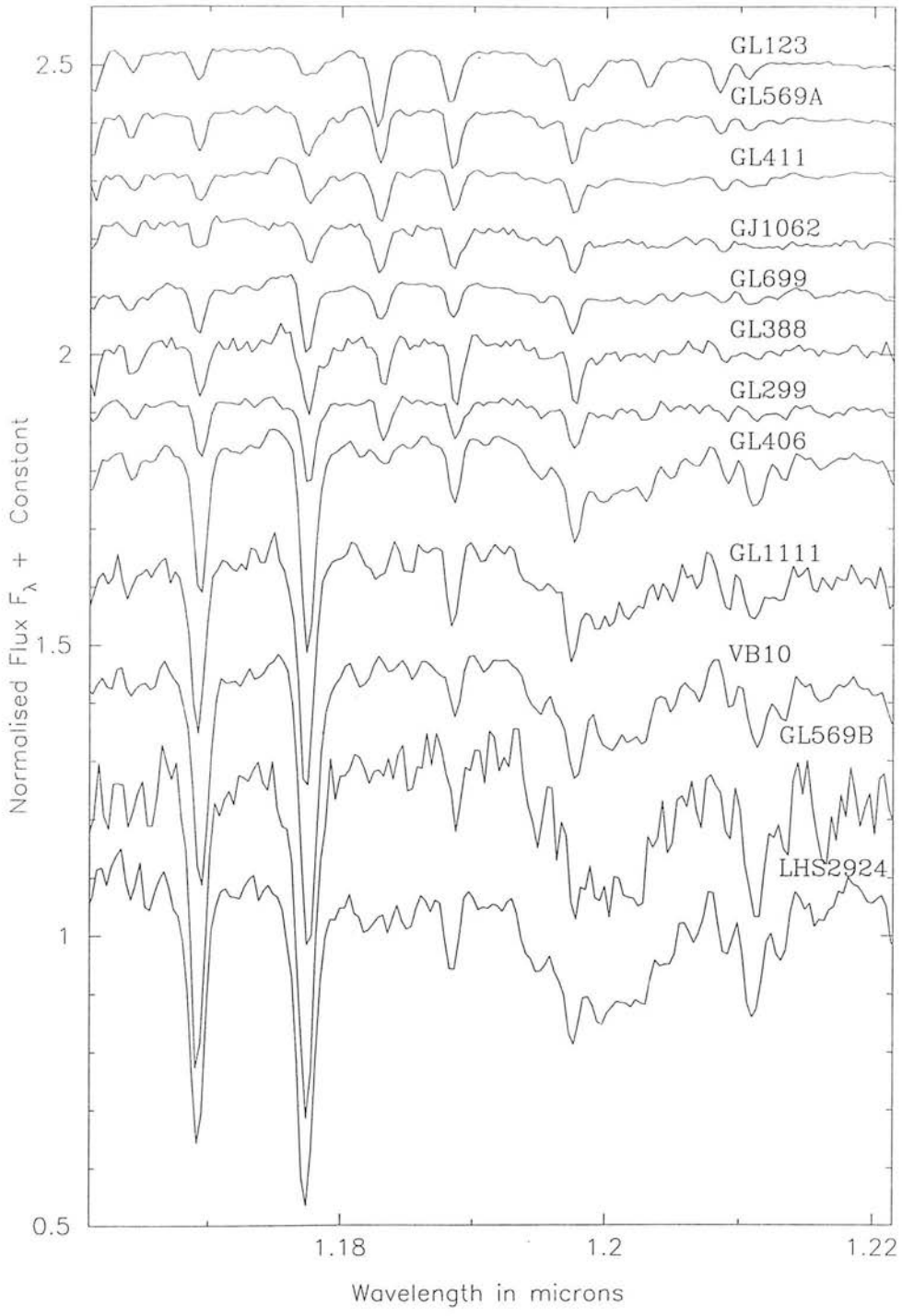

Figure 3.1: Spectral sequence for M dwarfs from 1.16–1.22 μm ranked in order of increasing strength of absorption features. The various spectra have been normalised at 1.191 μm (see Section 3.6.1) and an offset has been added to separate the spectra. The spectrum for GD165B has a much lower signal-to-noise ratio and is presented in Fig. 3.3.

3.2.1 Standards

Stars in the spectral type ranges B5–A5 and F6–G0 were used to remove the effects of atmospheric absorption. These standards were expected to be featureless at the spectral resolution used and to be well described by a Rayleigh-Jeans tail. However the F6–G0 standards were not very useful as they show weak metal lines and should not be used as standards for spectroscopic investigations of cool stars. Although the lines tended to be weaker and different from the M dwarf features we avoided using them where possible.

3.2.2 Data reduction

In the reduction of spectra, we have followed the same procedures as in Chapter 2 except for GL569B. Observations of GL569AB were made in conditions estimated to be sub-arcsec optical seeing using 3 arcsec pixels. The 3 arcsec slit was orientated to a position angle of 90 deg in order to maximise the separation between A and B on the detector to $\sim$ 5 arcsec. Each component was observed in turn, but because A is $\sim$50 times brighter than B, the observations of B had a large peak due to A and a small peak separated by two pixels due to B. Based on the profile of A in the two measurements we estimated the component due to A in the spectrum of B to be 43 per cent (assuming that the relative fluxes of A and B do not change over this small wavelength baseline). This component was removed from B in the reduction procedure.

All observations were wavelength calibrated using lines from observations of an argon lamp in the CGS4 calibration unit. This procedure is typically accurate to 0.1 $\Delta\lambda$. The reduced data from the observations are presented in the spectral sequence shown in Fig. 3.1. The scale of flux density is arbitrary, and an offset has been added to separate the spectra.

3.3 Model atmospheres

Version 5.3 of the model atmosphere code PHOENIX was used to compute synthetic spectra for this study. It is described in detail by Allard & Hauschildt (1995). Here we

draw attention to the important assumptions made in modelling M dwarf atmospheres with PHOENIX.

• Due to the high densities prevailing in dwarf atmospheres, the mean free path of the photons is small enough compared to the thickness of the layers that curvature effects may be neglected. This implies that dwarf atmospheres can be well approximated using a plane-parallel approximation in the solution of the radiation transfer equation.

• The velocities of the convection cells are too small to be detected in low-resolution spectra and will have a negligible influence on the transfer of radiation and so the effects of convective motion on line formation are neglected (Allard & Hauschildt 1995).

• Non-Local Thermodynamic Equilibrium (NLTE) effects are neglected, which may not be a good treatment for individual metal lines. The lack of free electrons, provided principally by relatively easily ionised neutral Mg, Na and Ca, means that collisional rates may be too low to bring species into chemical and thermal equilibrium. The number of free electrons from any particular atomic species is dependent on the ionization potential and the number density. Both of these effects, through the Boltzmann factor and atomic species forming molecules, will lead to a rapid decrease in the number of free electrons towards lower temperatures. For example, Fig. 5a in Allard (1990) shows a decrease of 16 dex in the ratio of ion pressure to gas pressure for Mg I between 3250 and 2000 K. In addition to a lack of free electrons available to give rise to LTE conditions, most M dwarfs radiate strongly in the x-ray range (Fleming et al. 1993). This means that a high x-ray flux impinges on the photospheric material, altering its thermodynamical state.

The major difference between the models presented here and those in Allard & Hauschildt (1995) is the inclusion of new data for TiO which has allowed it to be treated using the opacity sampling technique rather than the less reliable JOLA technique (Tsuji 1994). Jorgensen (1994) has calculated a line list for TiO comprising 12 million lines. The new treatment of TiO has the effect of reducing the derived effective temperatures by around 150 K in comparison with a previous spectral comparison of these model atmospheres (Kirkpatrick et al. 1993) across this region. The inclusion of a line list for TiO represents a vital improvement but nevertheless there are a number of other molecular line lists which are vital for M dwarf models. The most important are H_2O,

VO, FeH and CH_4. A preliminary H_2O calculation is promising (Chapter 4).

For this study a large grid of spectra was synthesized from 1.14–1.24 μm. They encompass

- effective temperature, $1500 \leq T_{\rm eff} \leq 4000$ K in steps of $\Delta T_{\rm eff} = 100$–300 K,
- surface gravity, $3.5 \leq \log g \leq 5.5$ cm/s^2 in steps of $\Delta \log g = 0.5$,
- metallicity, $-4.0 \leq$ [Z/H] $\leq +0.5$ in steps of Δ[Z/H] $= 0.5$.

The different models' parameters are denoted by lteTT–G.G–Z.Z.I.D, where lte indicates local thermodynamic equilibrium, TT = $T_{\rm eff}/100$, G.G = log g (in cm/s^2), Z.Z = [Z/H] and I.D = PHOENIX batch number (ir.7 for the models presented here).

3.4 Spectral features

The spectral sequence in Fig. 3.1 shows the 1.16–1.22 μm region is rich in strong absorption features whose strengths change dramatically across the M dwarf regime. In Fig. 3.2 we label the spectral features in GL406. The identifications were made using the line-identification feature in PHOENIX which outputs the strongest, defined by reaching its own $\tau = 1$ first, atomic and molecular transition for each wavelength point.

In Table 3.2 we tabulate the properties of the principal observed atomic lines from database of Kurucz (1993). We include "astrophysical" log gf 's (where g is the statistical weight and f is the oscillator strength) from Vieira (1985) as an illustration of the possible errors in the basic line data. For some of the lines, particularly the Fe lines, the discrepancies are large enough to seriously affect the interpretation of the observed line strengths. The Vieira values are derived by comparison with high signal-to-noise and resolution spectra of the red giant α Orionis. However, α Orionis's mass loss and spot and chromospheric activity may compromise the reliability of the log gf's derived. We prefer to use the 42 million line Kurucz dataset because (1) the Kurucz dataset are normalised to produce the correct total absorption for each species and (2) they are used in a variety of astrophysical applications.

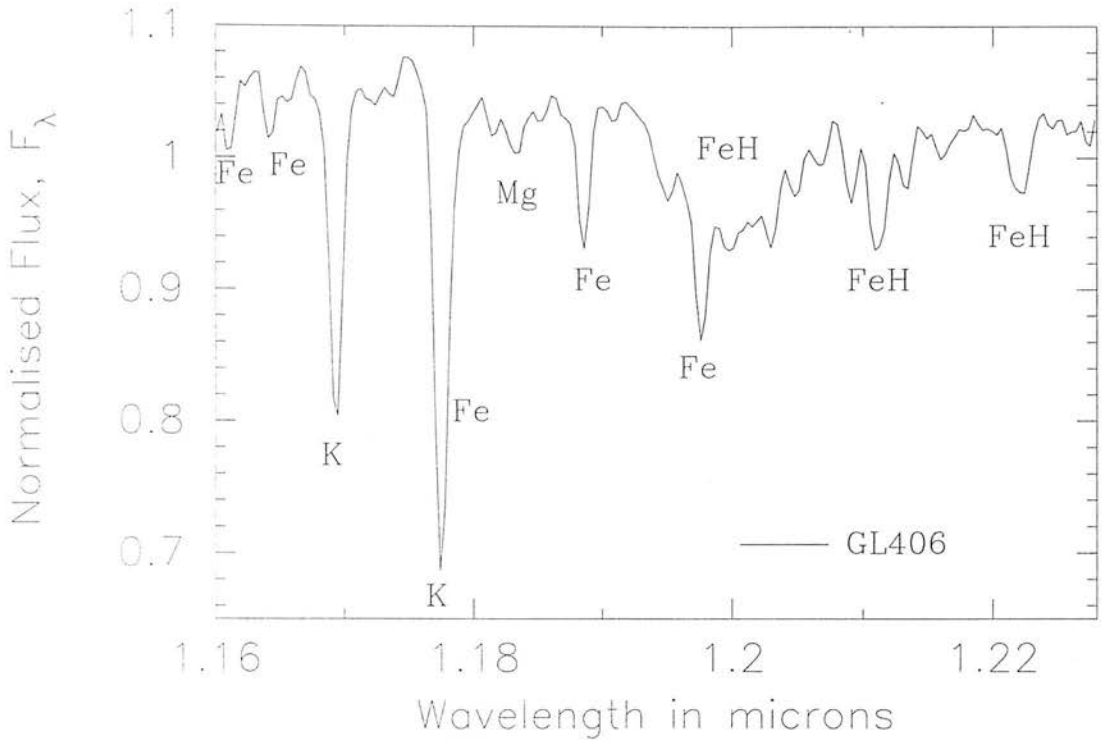

Figure 3.2: Spectral identification of strong spectral absorption features in a 1.16–1.22 μm spectrum of GL406.

Table 3.2: Strong atomic transitions observed in the spectra are given: element, wavelength in vacuo, transition, log gf from Kurucz (1994), log gf from Vieira (1985) and excitation potential.

Atom	λ (μm)	$(\log gf)_{\text{Kurucz}}$	$(\log gf)_{\text{Vieira}}$	χ (eV)
Fe I	1.16414	−2.25	−2.41	2.18
K I	1.16902	0.25	-	1.61
Fe I	1.1693	−2.05	−2.58	2.23
K I	1.17697	−0.45	−0.31	1.62
K I	1.17728	0.51	-	1.62
Fe I	1.1786	−1.48	−1.88	2.23
Mg I	1.1828	−0.29	−0.14	4.34
Fe I	1.1886	−1.7	−2.53	2.20
Fe I	1.1976	−1.5	−1.72	2.18

3.5 M dwarf parameter space

Model atmosphere calculations contain a vast array of physics but they are as yet only a crude representation of a real star. The fundamental parameters of hotter stars, often observed at high signal-to-noise ratio at a variety of different wavelengths and with the benefit of large scale determinations of opacities by the opacity projects (OPAL, Rogers & Iglesias 1992 and OP, Seaton et al. 1994) are still debated (e.g. see discussion of the solar iron abundance Blackwell, Smith & Lynas-Gray 1995). However cool star atmospheres (< 4000 K) are far more complex to model due to the sheer number and variety of molecular transitions. With the lack of basic molecular data we can not expect the model structure to be correct in detail and so it is important to be aware of the observational constraints on M dwarf properties.

The parameter space covered by M dwarfs is large: a factor of $\sim$5 in mass, $\sim$1000 in luminosity and a factor of $\sim$2 in effective temperature. This range is broadly equivalent to the range encompassed by the F, G, K spectral types. When comparisons are made with model atmospheres it is necessary to specify temperature, gravity and metallicity although the observational parameters are luminosity at different wavelengths, distance, space motion, rotation and for objects in binaries systems also mass. The following subsections discuss previous inferences of effective temperature, metallicity and surface gravity for M dwarfs and then combine this work to define the expected parameters of the sample. This allows us to gauge the accuracy of the model spectra and their usefulness in predictions of M dwarf parameters.

3.5.1 Effective temperature

M dwarf effective temperatures have been investigated many times though there is not yet a consensus on a particular scale. Recent work by Bessell (1991), Kirkpatrick et al. (1993), Tinney, Mould & Reid (1993), Chapters 2 and 4 show broad agreement for objects above 3300 K but significant differences for cooler objects. The studies all yield effective temperature sequences which are continuous with the sample properties but offset relative to one another by as much as 500 K. This is significantly more than their

internal errors of 100 to 200 K. Each method is prone to serious systematic uncertainties.

The work of Bessell is an extension of the temperature calibrations of Wing (1979) and Veeder (1974) which were based on blackbody fits to broadband photometry. The problem with this technique was demonstrated by Berriman & Reid (1987) to be, that the presence of deep water vapour absorption bands in the infrared means that blackbody fits measure the peak of the flux distribution and so over estimate luminosities and temperatures. Berriman & Reid devised an alternative method assuming that the flux at 2.2 μm (K-band) measures the continuum emission from a blackbody with a temperature the same as the star's effective temperature. Tinney et al. (1993) have followed this technique with infrared spectra using 3.8 μm (effective wavelength of the L'-band) as their reference wavelength. For stars with $T_{\rm eff} > 3000$ K this technique is accurate but for stars with $T_{\rm eff} < 3000$ K deep water absorption bands, throughout the infrared spectra, mean that a reference wavelength centered on any infrared photometric bands, at relatively transparent wavelengths for the star's atmosphere, is measuring considerably above a blackbody continuum appropriate to an adopted effective temperature. This causes effective temperatures derived using this method to be systematically too low. The concept is discussed in Chapter 2.

Chapter 2 uses the dominance of water vapour absorption in M dwarfs across the near infrared to fit blackbody curves to points in the spectra which are affected by the same amount of water absorption. Although this method is potentially reliable to around 100 K, they used the water vapour absorption coefficients from Ludwig (1971) which from 1–2 μm may be too high by as much as an order of magnitude (Schryber, Miller & Tennyson 1995).

The temperature scale of Kirkpatrick et al. (1993) is based on an earlier generation of the model atmospheres used in this paper at a time when the models showed large discrepancies with observed spectra photometric colours. Nevertheless their study illustrated the complexity of M dwarf spectra and the need to make comparisons with a sophisticated model atmosphere.

Although much effort has been invested to derive a secure effective temperature scale for M dwarfs the scale is still uncertain. With the limited wavelength coverage of this

study it is *not* appropriate to derive a new temperature scale; we defer that to Allard et al. (1995, in preparation). We infer $T_{\rm eff}$'s from photometric colours by combining the work of Berriman, Reid & Leggett (1992), Tinney et al. (1993) and Chapter 2 for $T_{\rm eff} > 3000$ K, and the work of Chapter 2 for $T_{\rm eff} < 3000$ K. From these we derive the relations $T_{\rm eff} = -12.7(V_{\rm C}-K_{\rm CIT})^3 + 245(V_{\rm C}-K_{\rm CIT})^2 - 1730(V_{\rm C}-K_{\rm CIT}) + 7280$ and $T_{\rm eff} = -32.6(I_{\rm CCD}-L'_{\rm MKO})^3 + 441(I_{\rm CCD}-L'_{\rm MKO})^2 - 2240(I_{\rm CCD}-L'_{\rm MKO}) + 6590$ which we use to find the expected values for $T_{\rm eff}$ given in Table 3.3. The long wavelength baseline of the photometric colours used means that the relative effective temperatures of the objects should be reliable; except in cases of extreme metallicity where the relative importance of different opacities becomes dramatically different (e.g. see Saumon et al. 1994 for the extreme case of zero metallicity).

3.5.2 Metallicity

Since the local space distribution for earlier type M dwarfs is in broad agreement with that of well studied classes of hotter stars (Mihalas & Binney 1981), we can use the kinematic populations given in Table 3.1 (from Leggett 1992) to assign approximate metallicities and ages. It is necessary to be wary of their use for the later type dwarfs as there is evidence that the latest type M dwarfs have a low scale height (Hawkins 1988; Hawkins & Bessell 1988; Reid, Tinney & Mould 1994; Kirkpatrick et al. 1994; Kirkpatrick, Henry & Simons 1995) and so may represent a young metal rich population containing a number of brown dwarfs.

3.5.3 Surface gravity

There are two M dwarf eclipsing binary systems from which gravities have been directly determined. YY Gem from the young disk population has log g = 4.59±0.05 (0.62±0.03 $M_\odot$) and 4.66±0.05 (0.57±0.03 $M_\odot$) (Leung & Schneider 1978). CM Dra from the halo population has log g = 5.01±0.05 (0.237±0.011 $M_\odot$) and 5.01±0.05 (0.207±0.008 $M_\odot$) (Lacy 1977).

Observational relations for surface gravity

As described above, M dwarf effective temperatures and their population types, presumed to be indicative of metallicity, have been the subject of some scrutiny. On the other hand surface gravities are usually assumed as a fixed value in previous investigations. Burrows et al. (1994) highlighted, in their fig. 5, the large range of surface gravity which field M dwarfs are likely to have, log g = 4.0–5.5 for ages 0.1–10 Gyr. To find the most appropriate value for log g the Stefan-Boltzmann relation $L = 4\pi R^2 \sigma T_{\rm eff}^4$, where L is luminosity, can be substituted for $R^2 = GM/g$ where R is the radius, G is the gravitational constant, M is the mass and g the surface gravity to give

$$\log T_{\rm eff} = 0.25(\log g + \log L - \log M - \log 4\pi G\sigma). \tag{3.1}$$

This is written in a more instructive form by substituting in standard solar values, $M_{bol\odot}$ = 4.75, $L_\odot$ = 3.826 x 10^{26} W and $M_\odot$ = 1.99 x 10^{30} kg and rearranged to give

$$\log g = 4(\log T_{\rm eff} + 0.1 M_{\rm bol} + 0.25 \log M/M_\odot - 3.624). \tag{3.2}$$

This form is more useful but there is only a small number of objects for which bolometric magnitude, $M_{\rm bol}$ and log $M/M_\odot$ have been determined. In order to derive more widely applicable relationships we can replace these terms by the absolute K-band luminosity, M_K. $M/M_\odot$ can be substituted from the work of Henry & McCarthy (1993) who derive binary $M/M_\odot$ versus M_K relationships valid over the range 0.080 to 1.000 $M/M_\odot$ ($M_{K_{CTIO}}$ = 3.07–9.81). The Henry & McCarthy relations apply to K-band magnitude based on the Kitt Peak filter system which uses the same filter set as CTIO; Elias et al. (1982) find that $K_{CTIO} = K_{CIT}$. We can substitute for $M_{\rm bol}$ by using Tinney et al. (1993) and Chapter 2 to derive $M_{\rm bol} = 1.10\ M_K + 2.06$, for $M_K < 9.81$. Including these relations and transforming for log g from m/s^2 to the standard units for log g of cm/s^2 gives

$$\log g = 4(\log T_{\rm eff} + 0.0680 M_K - 3.283) + 2 \tag{3.3}$$

for M_K = 7.70–9.81 and

$$\log g = 4(\log T_{\rm eff} + 0.0473 M_K - 3.119) + 2 \tag{3.4}$$

for M_K = 5.94–7.70 and

$$\log g = 4(\log T_{\rm eff} + 0.0838 M_K - 3.336) + 2 \tag{3.5}$$

for M_K = 3.07–5.94. The error in determination of log g for (3.3) to (3.5) can be expressed from (3.2) as

$$\Delta \log g = [(4\Delta \log T_{\rm eff})^2 + (0.4\Delta M_{\rm bol})^2 + (\Delta \log M/{\rm M}_\odot)^2]^{0.5}. \tag{3.6}$$

The errors can be taken from the relationships used to derive (3.3) to (3.5): Henry & McCarthy find $\Delta\ M/{\rm M}_\odot = 0.067$ rms error for the relationship used to derive (3.5) and $\Delta\ (M_{\rm bol}) = 0.14$ rms error for the $M_{\rm bol}$ versus M_K relationship using data in Chapter 2 and Tinney et al. (1993). At 3000 K, the error on log g can be written as

$$\Delta \log g = [(0.06(\Delta T_{\rm eff}/100))^2 + 8.09{\rm x}10^{-3}]^{0.5}. \tag{3.7}$$

The random errors in the determination of temperature scales are typically 150 K which indicates that Δ log $g \sim 0.15$.

These relations are based on the Henry & McCarthy results for a sample of nearby M dwarfs with intermediate disc characteristics – the relationship specifically avoids overtly young or old objects. They represent intermediate age objects (OD objects, see Table 3.1) but for the oldest and youngest objects they can not be expected to be valid without consideration of the effects of metallicity and age. We now examine their usefulness by testing them against the two M dwarf eclipsing binary systems for which fundamental parameters are known accurately.

Comparison with eclipsing binaries

The separations of the components of the M dwarf eclipsing binary systems are too small to be resolvable with speckle techniques and so are not included in the Henry & McCarthy results used in Section 3.5.3. These eclipsing systems therefore offer an independent test of (3.3) to (3.5). For the YY Gem components using $M_K = 4.34$ (from Gliese & Jahreiss 1991 and Leggett & Hawkins 1988), the luminosity-ratio and effective temperatures from (Leung & Schneider 1978) substituted into (3.5) gives log g = 4.63±0.12 and log g = 4.72±0.13. For CM Dra adopting component parameters from Lacy (1977) and M_K = 7.79 (Leggett 1992; Gliese & Jahreiss 1991) and substituting in (3.4) gives log g = 4.94±0.11 and log g = 4.99±0.11.

Although the eclipsing binaries are from the extremes of the kinematic populations, the equations (3.3)–(3.5), primarily based on old disk objects, give surface gravities for both which compare well with the "observed" values (Section 3.5.3). This is expected from models of M dwarfs which find almost no dependence of surface gravity on metallicity: for a fixed-mass low (and zero) metallicity M dwarfs will have nearly the same radius but a higher $T_{\rm eff}$ and luminosity (D'Antona 1987; Burrows et al. 1993). The above comparisons indicate that, within the luminosity range over which they are applicable, it is reasonable to use (3.3) to (3.5) to determine expected log g's for the sample. These are given in Table 3.3. In the following sections we examine the expected $T_{\rm eff}$'s, [Z/H]'s and log g's for the sample of observed spectra. We divide the sample into hotter objects, defined as $T_{\rm eff} > 3000$ K, and cooler objects, defined as $T_{\rm eff} < 3000$ K.

3.5.4 Expected Parameters

Hotter objects ($T_{\rm eff} > 3000$ K)

In our sample there are objects which can be expected to have a wide range of sub-solar [Z/H]'s. GJ1062 and GL299, lie within the subdwarf sequence on fig. 10 of Monet et al. and have undisputed halo-type space motions. Linear interpolation within the Monet et al. scale indicates GL299 has [Z/H] $\sim$ –1.5, GJ1062 has [Z/H] $\sim$ –1.0. For GL699 and

GL411 the situation is less clear. GL699 is classified as OD (Monet et al.) or OD/H (Leggett 1992) and GL411 is classified as H (Monet et al.) or OD/H (Leggett 1992). On the other hand fig. 10 of Monet et al. suggests that GL699 is more metal poor. GL699 lies approximately 1.6 mag below the mean main sequence for disk stars and in the subdwarf regime, whereas GL411 lies only a few tenths of a magnitude below the mean main sequence for disk stars. Given the conflicting evidence for these objects we tentatively assign them as [Z/H] $\sim$ –0.5.

The Monet et al. scale is uncertain as it is based on a number of indirect pieces of evidence and has recently been examined using the predictions of evolutionary models. Saumon et al. (1994) compare the offset between their solar and zero metallicity evolutionary model calculations with that between the observed M dwarf and M subdwarf main sequences from Monet et al. Since many of the observed subdwarfs lie very close to the locus for zero metallicity objects, Saumon et al. consider that they may have [Z/H] considerably lower than the average subdwarf metallicity of [Z/H] = –1.7 suggested by Monet et al. If we apply the suggestion of Saumon et al. then GL299 would have [Z/H] $\leq$ –2.0. If this is the case its $T_{\rm eff}$ is expected to be markedly different from other similar $V_{\rm C}$–$K_{\rm CIT}$ colour objects. Allard & Hauschildt (1995) indicate a rapid divergence from the solar-metallicity $V_{\rm C}$–$K_{\rm CIT}$ versus $T_{\rm eff}$ relationship below a value of [Z/H] between –1.0 and –1.5. The relationship shows a difference of 400 K, in $T_{\rm eff}$ at $V_{\rm C}$–$K_{\rm CIT}$ = 5.19 (GL299), between [Z/H] = 0.0 and –1.5. $V_{\rm C}$–$K_{\rm CIT}$ = 5.19, [Z/H] = –2 would correspond to an $T_{\rm eff}$ well below 2500 K and for such a low [Z/H] would imply a definite brown dwarf (Burrows et al. 1993); since it is not possible to fit GL299's luminosity or spectral features with such a low $T_{\rm eff}$ we prefer to use the [Z/H] scale of Monet et al.

In Section 3.5.1 we discussed the $T_{\rm eff}$ scales derived for typical disc-type dwarfs but not for halo-type subdwarfs. For [Z/H] > –1.0 Allard & Hauschildt find $T_{\rm eff}$'s not significantly different from the more metal rich stars. Using the Monet al. [Z/H] scale GL299 is the only object in the sample for which a significant correction is likely and is mentioned above. The YD objects GL123 (OD), GL569A (YD) and GL388 (YD) lie close to the main sequence of Monet et al. and so we expect them to have solar-type [Z/H] and $T_{\rm eff}$'s close to the relations given in Section 3.5.1.

Cooler objects ($T_{\rm eff}$ < 3000 K)

The combination of (1) a slow gravitational contraction leading to a wide spread in parameters at different ages, (2) the lack of eclipsing binaries and (3) the general lack of known objects in this regime means that the parameters of objects with $T_{\rm eff} < 3000$ K are not well determined. Nevertheless the hotter members may be interpreted in the same fashion as for $T_{\rm eff} > 3000$ K.

GJ1111 is a classified as a YD object and lies $\sim$ 0.25 mag above the sequence of Monet et al. This suggests that it is still contracting onto the main sequence and is therefore likely to have a low value of log g and a metallicity which is greater than the solar value. GL406 is classified as an OD object and lies $\sim$ 0.5 mag below the Monet et al. sequence. This suggests [Z/H] $\sim$ –0.5. VB10 is classified as an OD object and lies close to the main sequence of Monet et al. suggesting a solar metallicity. GL569B is classified as a YD object which given its very red colours and close companion means further discussion is useful. LHS2924 and GD165B lie well outside the range of validity of equation (3.3) and so theoretical evolutionary models will be used to estimate their gravities.

GL569AB It has been realised since the discovery of the faint red object GL569B (Forrest, Skrutskie & Shure 1988) that its YD companion means that it may be a cooling brown dwarf. The parallax of GL569A gives a distance (to $\pm$ 5 per cent) which indicates that GL569B's $M_{\rm K}$ is overluminous relative to objects with similar colours by some 0.65 magnitudes. This is in accord with its youth. The slow cooling of objects below 0.1 $M_{\odot}$ has long been expected (Kumar 1963) to lead to a spread in luminosities for a given colour. However an overluminosity of $\sim$ 1.9 is relatively small. For example, a model 0.080 $M_{\odot}$ star decreases in luminosity by a factor of 2.1 between 1 and 5 Gyr (Burrows et al. 1993). To estimate an age for the system Henry & Kirkpatrick (1990) compare GL 569A's Hα line (from Young et al. 1989) with studies of the Hyades and Pleiades. Although there is a large scatter in Hα equivalent widths, they infer that GL569A is consistent with a Hyades age, 0.6 Gyr, rather than a Pleiades age, 0.08 Gyr. Henry & Kirkpatrick hypothesize GL569B's overluminosity as being due to a parallax error,

however, the improved parallax used here (van Altena et al. 1994) bears out its relative brightness for its spectral type and colours. Furthermore, GL569A is not overluminous for its colour on fig. 10 of Monet et al. as would be expected for an overestimated parallax. In conclusion the system's youth ($\sim$ 1 Gyr) and its overluminosity suggests that a low value of log g and a solar-type metallicity but there is not strong evidence for it to be a young brown dwarf.

LHS2924 and GD165B Objects fainter than the cut-off of the observational mass-luminosity relation, $M_{\rm K}$ = 9.81 (0.080 $M_\odot$), are brown dwarf candidates. Although 0.080 $M_\odot$ is the often-quoted transition mass between star and brown dwarf, it is merely a canonical value. The most sophisticated examination of the transition is by Burrows et al. (1993). They find that the transition is sensitive to a number of parameters particularly metallicity and helium fraction and find a range of values from 0.095 $M_\odot$ (for a composition consisting of no 'metals' and helium fraction, Y_α = 0.22) to 0.074 $M_\odot$ (for [Z/H] = 0.0 and Y_α = 0.28). For solar metallicities their 'best' value is 0.0767 $M_\odot$ (Y_α = 0.25). Other investigators find considerably higher 'best' values, 0.084 $M_\odot$ (Nelson, Rappaport & Joss 1993) and $\sim$ 0.085 $M_\odot$ (D'Antona & Mazzitelli 1994). All models with [Z/H] = 0.0 predict a rapid fall in luminosity and effective temperature with mass but only small changes in log g. We choose to use the Burrows et al. models as they predict the lowest masses (and so are the most conservative at identifying objects as brown dwarfs) and agree well with the observational results of Henry & McCarthy (1993). Burrows et al. predict that for solar metallicities at 5 Gyr there is a maximum surface gravity at log g = 5.48 (for a $\sim$ 0.072 $M_\odot$ object); at 0.6 Gyr the maximum log g = 5.32 (for a $\sim$ 0.072 $M_\odot$ object). For either age, $<$ 0.072 $M_\odot$, surface gravity slowly falling into the brown dwarf regime. This turnaround in log g arises from a slight increase in radius as the electron degeneracy pressure exceeds the thermal pressure at the high densities and low entropies prevalent in brown dwarfs.

As mass is reduced by a few hundredths of a solar mass from M dwarfs to brown dwarfs, object properties become very dependent on age. A point on the two-dimensional HR diagram is useful but without age or another third quantity such as mass or gravity, low-mass objects can not easily be classified. Attempts to identify definite brown dwarfs

Table 3.3: Expected parameters for the sample based on Table 3.1 and Section 3.5. The errors are $\Delta(\log g) = 0.15$, $\Delta T_{\rm eff} = 150$ K and Δ [Z/H] = 0.5.

Object	Temperature (K)	Metallicity [Z/H]	log g (cm/s^2)
GL123	3710	0.0	4.47
GL411	3420	–0.5	4.86
GJ1062	3380	–1.0	5.12
GL569A	3320	0.0	4.68
GL699	3170	–0.5	5.10
GL388	3230	0.0	4.73
GL299	3120	–1.5	5.15
GJ1111	2700	0.0	5.17
GL406	2670	0.0	5.07
GL569B	2360	0.0	4.97
VB10	2510	0.0	5.18
LHS2924	2220	–0.5	5.4
GD165B	1860	0.0	5.4

from a small number of candidates in a three-dimensional parameter space have so far given inconclusive results. There is evidence, mentioned in Section 3.5, that the brown dwarf candidates discovered have a low scale-height and represent a population of young cooling brown dwarfs. Although this hypothesis has yet to be fully tested, it is well observed that the best studied brown dwarf candidate LHS2924 has peculiarly blue optical colours relative to other objects with $M_{\rm K} > 10$. This together with its weaker than expected spectral features indicate that it is metal poor (Probst & Liebert 1983; Liebert, Boroson & Giampapa 1984; Monet et al. 1993; Chapter 2). If other objects in the range $M_{\rm K} = 10$–11 are assumed to have solar-type abundances, LHS2924 is likely to have [Z/H] < –0.5. Such a metallicity means that it is likely to be relatively old, at least 5 Gyr. Interpolation within the solar metallicity models of Burrows et al. indicates log

$g \sim 5.4$ (~ 0.081 $M_\odot$).

GD165B has not been as well observed as LHS2924. It does have a white dwarf companion whose likely minimum cooling time means that its age is at least 0.5 Gyr (e.g. Chapter 2). It is separated from the white dwarf by $\sim$ 100 AU and so it is possible (though not likely) that GD165B's surface composition was influenced by the AGB evolution of the primary. In the meantime we assume solar metallicity as GD165B's 1.1–2.5 μm spectrum (Chapter 2) displays molecular and atomic absorption features broadly as predicted for a solar abundance object with its luminosity and temperature. Interpolation within the Burrows et al. models indicates log g between 5.25 (0.6 Gyr, 0.055 $M_\odot$ model) and 5.45 (10 Gyr, 0.077 $M_\odot$ model).

3.6 Spectral Analysis

The models were matched to the instrumental resolution by smoothing with a block function to mimic the effect of being detected by the square pixels used by the infrared detector of CGS4 and resampling to three times oversampling as used for the observations. This was performed using routines within KAPPA (Currie 1992) and SPECDRE (Meyerdierks 1993). The blending of absorption features from this process gives a good indication of the blending problems caused by working at the relatively low resolutions used here. Higher resolution data would allow detection of weak lines and could show the importance of any chromospheric effects on the line cores, however, the high pressures prevalent in M dwarf atmospheres lead to broad line profiles and mean that blending would still be a problem.

3.6.1 Best fit models

To determine the most appropriate model parameters for each object, the observed and synthetic spectra were run through a least-squares minimization program kindly provided by Steele & Jameson (1995). Each spectrum was first resampled to a common resolution of $1\text{x}10^{-4}$ μm, then normalised to 1.191 μm where there is little absorption present in any of the spectra. However because there is some level of noise in each of

Table 3.4: Best least-squares-minimization fit for each object in the region 1.16–1.22 μm. Values are given to half the spacing of the model grid: effectives temperatures to 50 K, metallicities to 0.25 dex, surface gravities to 0.25 dex.

Object	$T_{\rm eff}$ (K)	[Z/H]	log g (cm/s^2)
GL123	4000	–1.25	4.75
GL569A	3650	–1.25	4.25
GL411	4000	–2.5	5.0
GJ1062	3900	–2.25	4.5
GL388	3350	–0.75	4.5
GL699	3200	–0.75	4.0
GL299	3150	–0.75	4.0
GJ1111	2850	+0.5	5.25
GL406	2900	0.0	5.0
VB10	2750	–0.25	5.0
GL569B	2400	–0.5	4.75
LHS2924	2350	+0.5	4.75
GD165B	2050	–0.5	4.5

the spectra, the relative normalization for any pair may not be optimal. The program compares each observed spectrum with all the synthetic spectra in the grid by taking the difference between the flux values of the two spectra at each wavelength point. The sum of the squares of these differences is output for each comparison and they are sorted on this basis to produce a best model fit for each object. Some observed spectra yield very similar least squared values for a number of models and so the best fit model was taken to be the average model parameters of all models with values within 5 per cent of the minimum least-squared-minimisation value. This procedure leads to averaging over typically five models and allows less well sampled regions of the model grid to be interpolated across. The best fit model parameters are given in Table 3.4.

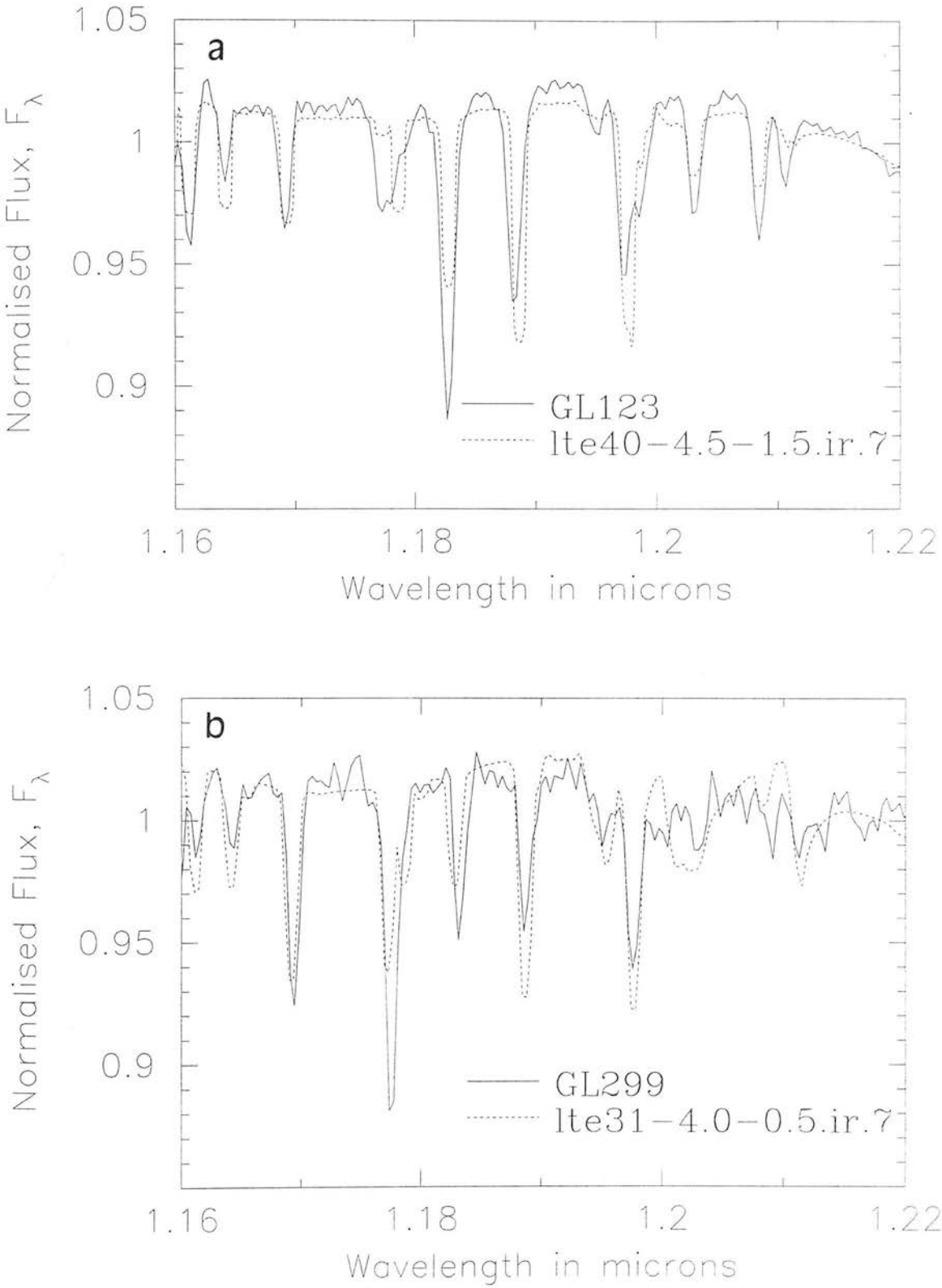

Figure 3.3: Comparisons of synthetic with observed spectra for (a) GL123, (b) GL299, (c) VB10 and (d) GD165B.

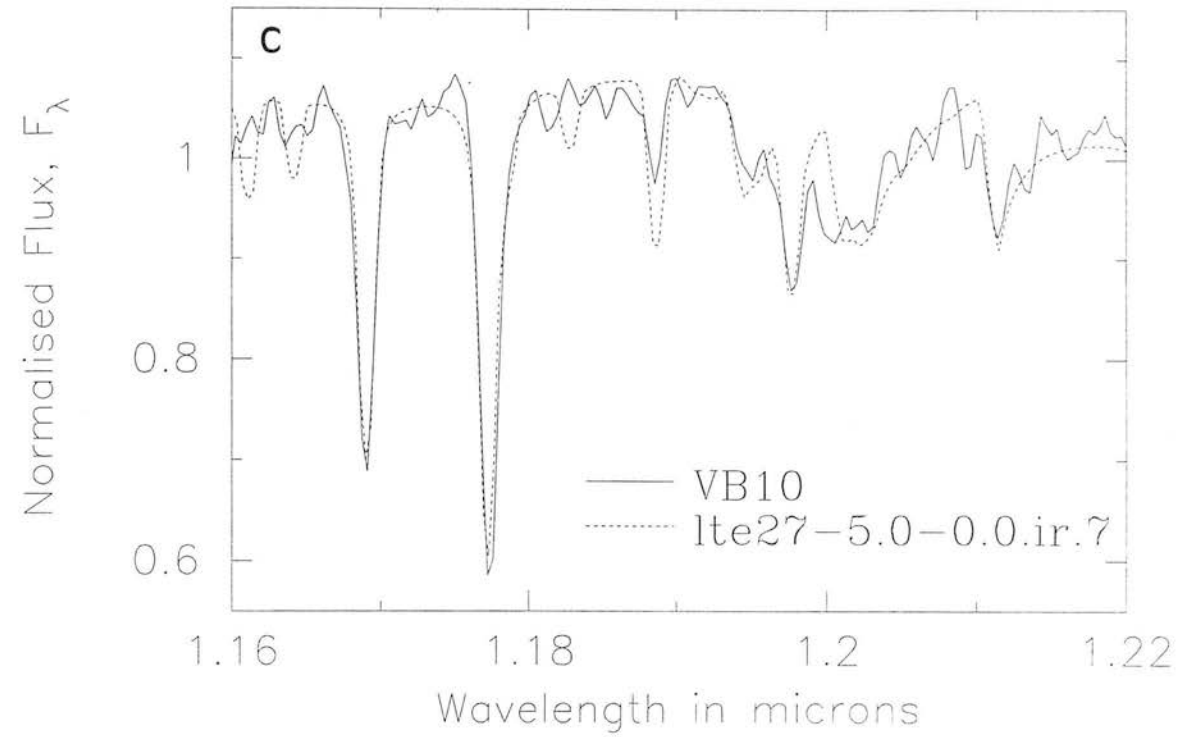
c
Normalised Flux, F_λ
1
0.8
0.6
VB10
lte27−5.0−0.0.ir.7
1.16
1.18
1.2
1.22
Wavelength in microns

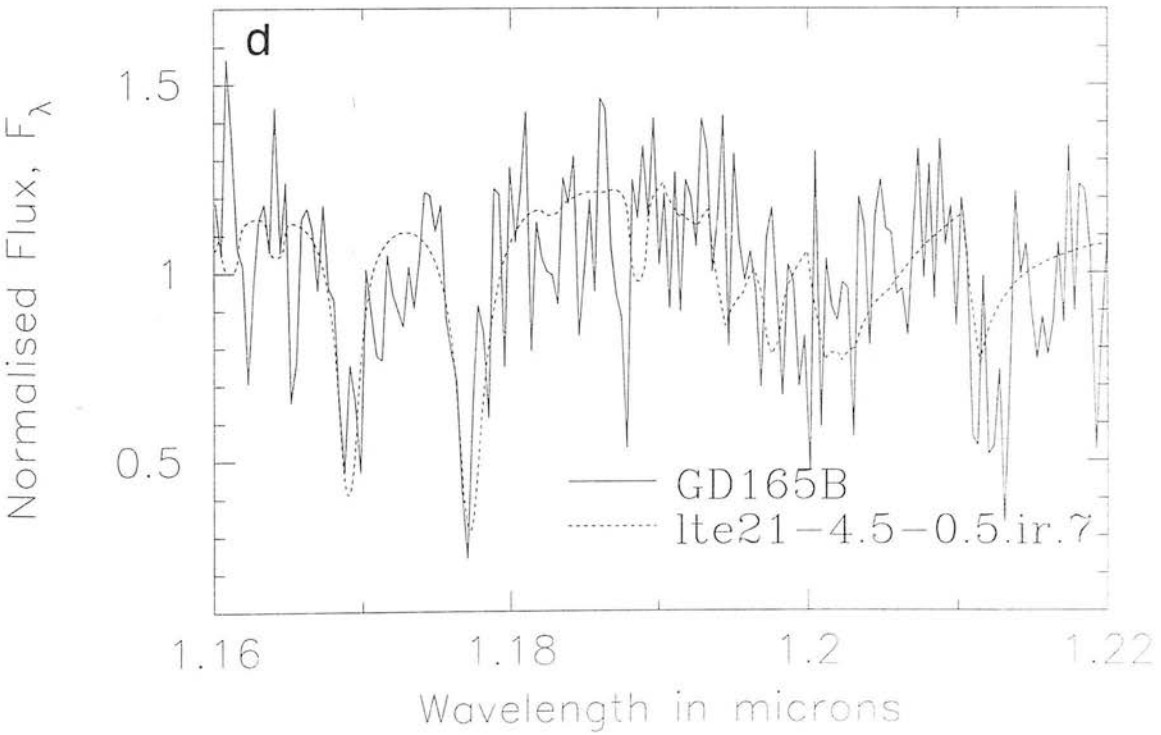
d
Normalised Flux, F_λ
1.5
1
0.5
GD165B
lte21−4.5−0.5.ir.7
1.16
1.18
1.2
1.22
Wavelength in microns

Fig. 3.3 shows comparisons between observed and best fit synthetic spectra for a few of the most interesting objects. The synthetic spectra are a reasonably good match for the cooler objects, e.g. VB10 and GD165B but less good for the hotter objects, e.g. GL123 and GL299. The "best fit" model for GL299 is not convincing. In general the match of the synthetic spectra and the correspondence between model fits given in Table 3.4 and expectations based on Table 3.3 are much better for the cooler objects than for the hotter objects. To examine the reasons for this the plots for GL123 and GL299 are instructive. They illustrate that for the hotter objects the "best fit" models cannot simultaneously predict observed Fe and K line strengths. In the plot for GL123 (Fig. 3.3a) the region from 1.176–1.180 μm shows that the K line blend is predicted to be relatively weak and the Fe line relatively strong, however, the reverse is seen in the observed spectra. This is caused by the Fe line strengths being overpredicted and leads to unphysical "best fit" models, e.g. $\log g = 4.0$ for GL299, rather than $\log g > 5$ based on Table 3.3. The possibility, suggested in Section 3.4, that the Fe oscillator strengths are too large seems a likely cause for the over-predicted Fe lines and the discrepant "best fit" models for the hotter objects. For the cooler objects Fe lines become relatively weak and less important in determining the best fit model parameters. The reasonable match between the observed and synthetic spectra for the cooler objects means that it is more reasonable to view their least-squared-minimisation model parameters as the "best fit model".

To circumvent the problem of placing undue weight on differences between observed and synthetic spectra which are likely to be due to inaccurate atomic parameters and/or missing molecular opacity, equivalent widths of observed and synthetic spectra for individual lines are compared. The measurement of equivalent widths is described in Section 3.6.2. The inferences from the individual atomic absorption lines are given in Section 3.6.3 and discussion of the application of these to the most interesting objects is made in Section 3.7.

Table 3.5: Equivalent widths in μm derived for each of the most prominent atomic lines in the observed spectra. The wavelengths given in brackets are those over which the equivalent widths are measured.

Object	K I (1.168–1.1704 μm)	K I (1.176–1.178 μm)	Mg I (1.182–1.184 μm)	Fe I (1.188–1.189 μm)	Fe I (1.197–1.198 μm)
GL123	5.68e-05	7.46e-05	1.67e-04	9.96e-05	7.30e-05
GL411	5.53e-05	7.45e-05	1.06e-04	7.43e-05	5.50e-05
GL1062	6.21e-05	7.77e-05	9.86e-05	8.20e-05	5.76e-05
GL569A	6.71e-05	9.68e-05	1.04e-04	1.06e-04	6.59e-05
GL388	1.06e-04	1.69e-04	9.59e-05	1.23e-04	7.96e-05
GL699	8.76e-05	1.34e-04	8.20e-05	5.94e-05	5.90e-05
GL299	1.09e-04	1.56e-04	7.47e-05	5.89e-05	6.56e-05
GL406	3.07e-04	4.46e-04	4.96e-05	1.10e-04	1.07e-04
GJ1111	3.54e-04	5.17e-04	8.84e-05	1.34e-04	1.05e-04
VB10	4.67e-04	6.92e-04	3.37e-05	9.75e-05	1.34e-04
GL569B	6.44e-04	7.48e-04	7.16e-05	1.15e-04	1.43e-04
LHS2924	5.52e-04	7.41e-04	6.41e-05	1.28e-04	1.21e-04
GD165B	8.15e-04	1.06e-03	4.06e-04	2.97e-04	6.37e-05

3.6.2 Equivalent widths

Equivalent widths of the strongest observed atomic absorption features are tabulated in Table 3.5 and plotted in Fig. 3.4 together with modelled equivalent widths from the grid of synthetic spectra. They were measured by modifying ABLINE (Robertson 1986) to run non-interactively. All continuum fits were based on fitting a straight line to the spectrum immediately adjacent to the feature rather than trying to measure equivalent widths based on an overall continuum. It can be seen from Fig. 3.3b that the observed K I line at 1.177 μm is contaminated by the prescence of a nearby weak Fe lines. The Fe I line at 1.198 suffers the worst from being blended especially in the cooler objects. In this case it is with FeH. Similar blending is present albeit to a lesser extent in each spectral feature. Such uncertainties in the measurement of equivalent width are generally a small effect and are well modelled. The biggest uncertainty is in setting an accurate continuum. Based on the measurement of equivalent width, whilst testing a number of different wavelength regions to define the "best" continua, we find standard deviations close to 10 per cent. Although this procedure does not give an absolute equivalent width, it gives us confidence that our comparisons are internally consistent because the same problems exist with the determination of equivalent widths from the synthetic spectra. We have not included FeH in the measurements of equivalent width as the intensities of its bands are set empirically (based on the VB10 data of Kirkpatrick et al. 1993) and do not include a number of strong observed transitions.

3.6.3 Atomic absorption lines

Fig. 3.4(a–e) compares the equivalent widths of observed and synthetic spectra. We have chosen to plot equivalent width against effective temperature, rather than metallicity or gravity because in general the synthetic spectra are firstly sensitive to temperature and secondly sensitive to metallicity and gravity. The effective temperatures are from Table 3.3. Synthetic equivalent widths are shown for models of $\log g = 5.0$, close to the expected gravity for many of the sample. Dotted lines show solar metallicity equivalent widths for other gravities: $\log g = 4.5$ to represent an extreme of low gravity for the hotter members of sample, and $\log g = 5.5$ to represent an extreme of high gravity for

the coolest members of the sample. Equivalent widths for log g = 4.5 and 5.5 models at other metallicities are found to scale in a similar way to those of solar abundance and so in order not to overcomplicate Fig. 3.4 are not included.

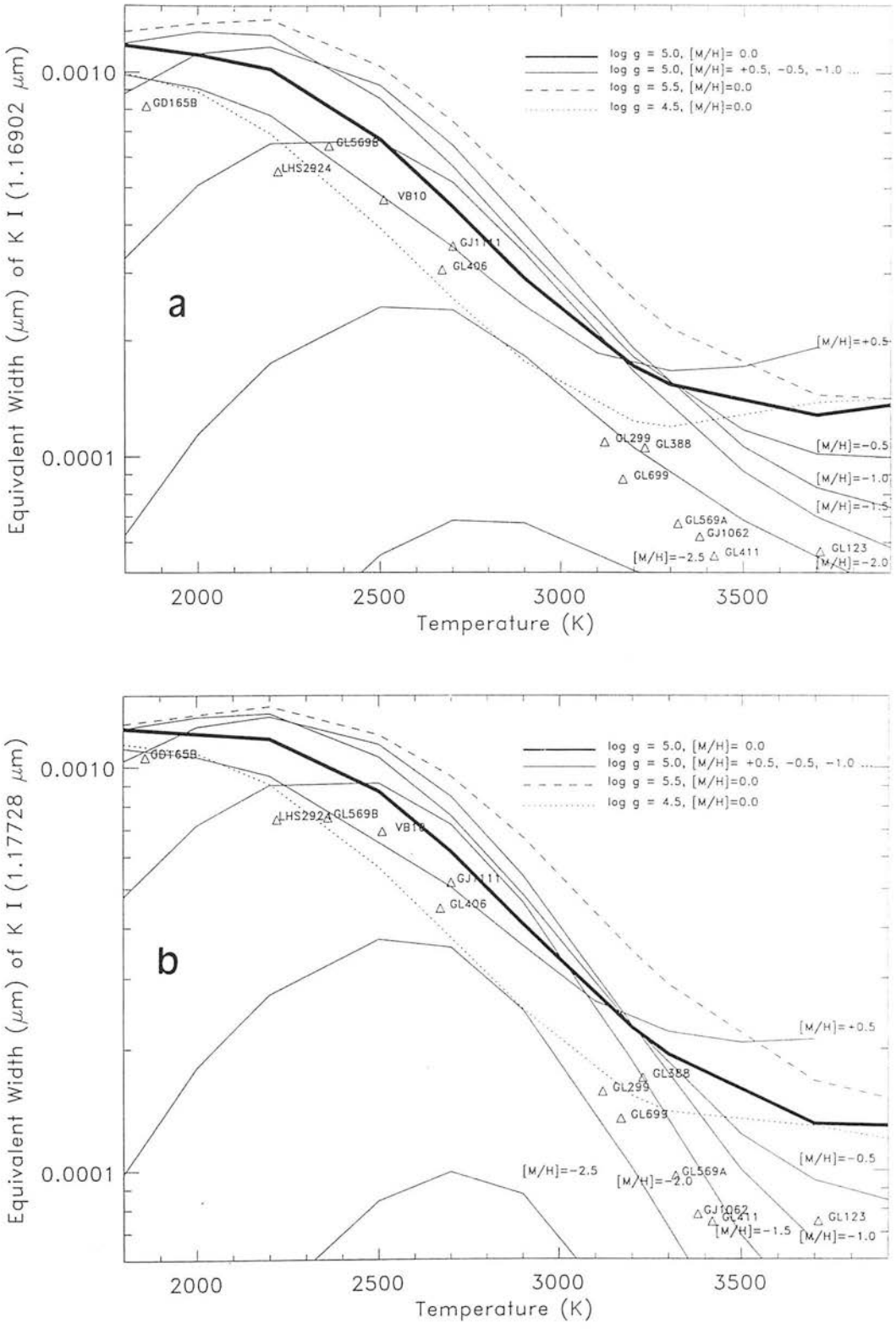

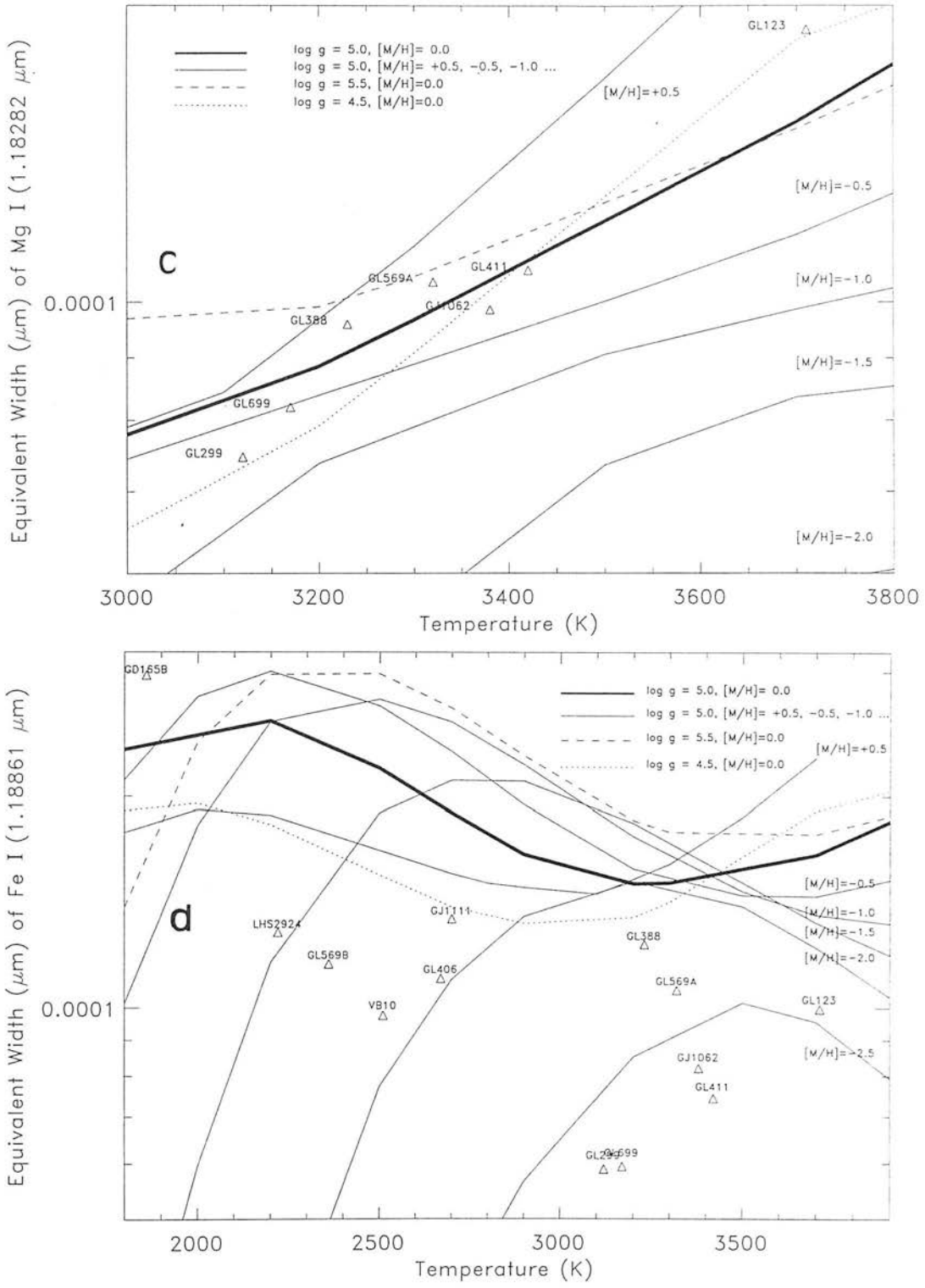

Figure 3.4: Equivalent widths measured from observed spectra are shown by open triangles: (a) for K I (1.169 μm); (b) for K I (1.177 μm); (c) for Mg I (1.183 μm); (d) for Fe I (1.189 μm); (e) for Fe I (1.198 μm). Plots for the equivalent widths of the model grid at log $g = 5.0$ for different metallicities are shown as solid lines (solar composition models in bold). Dotted lines show solar composition models for log $g = 4.5$ and 5.5. Mg is too weak to detect reliably in the cooler objects and so is only plotted for $T_{\rm eff} > 3000$ K.

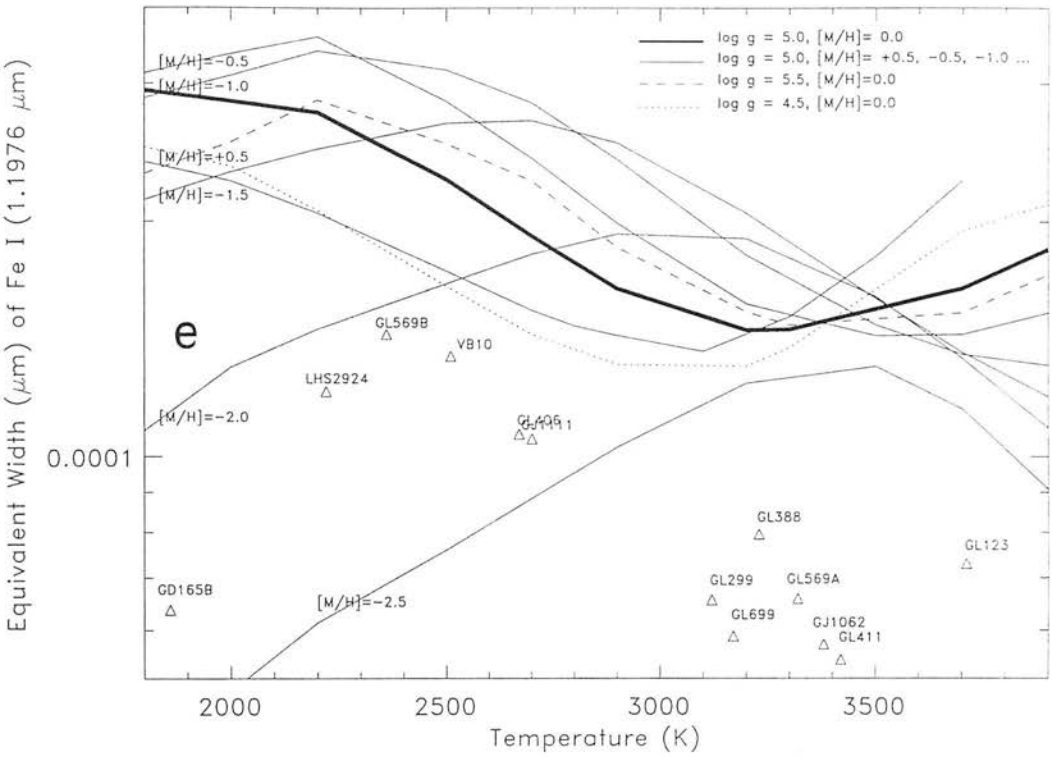

One of the most striking feature of the plots is that for [Z/H] > −1.5 and $T_{\rm eff}$ < 3300 K, modelled equivalent widths often increase in strength with decreasing metallicity, unlike those in hotter stars. In cool dwarfs the strength of metal absorption lines is principally due to pressure broadening. For the regime [Z/H] > −2, increases in gas pressure are more important, for atomic line strengths, than decreases in number density resulting from reduced metallicity. This result is a conclusion by Allard (1990) where the complex behaviour of atomic and molecular absorption lines in cool atmospheres are discussed in detail.

The plots show that the effect of surface gravity on equivalent widths is significant. Increases in surface gravity lead to an increase in the total gas pressure and from the increased efficiency of convective energy transport lead to a decrease in the temperature gradient. All the modelled equivalent widths increase for increasing log g for $T_{\rm eff}$ < 3500 K. At higher temperatures the modelled equivalent widths appear not to increase with log g. However this is a result of blending becoming important rather than a change in the underlying trend with log g.

Although Fig. 3.4(a–e) indicates that the atomic absorption lines all show some sensitivity to each of the model parameters there are distinctive differences in this sensitivity. These form the basis of the following discussion, where line strengths are used to estimate metallicities and gravities for the sample.

Iron

The Fe line strengths in Fig. 3.4 suggest that the entire sample of objects has [Fe/H] < -1.5 and/or gravities significantly less than $\log g = 5$. Although there is evidence that GL411, GL388 and GL699 and other early-type M dwarfs are metal poor (Mould 1978; Naftilan et al. 1992) there is no evidence for such extreme values of [Fe/H]. Such a result contradicts Section 3.5 and inferences from the other spectral features and so as mentioned in Section 3.6.1 it is much more likely that there are problems with the atomic data for Fe. It is possible that part of the discrepancy arises from an underprediction of the number density of FeH molecules though this would lead to the largest discrepancies in the cooler objects - this is not evident. We consider the Kurucz (1993) $\log gf$ values as the most likely source of error, although, it is not clear that those of Vieira (1985) would be more appropriate. Overall the Fe I 1.1886 μm model line strengths are somewhat closer to the observations than those of the Fe I 1.1976 μm line. Although the Vieira values suggest a reduction of 0.83 in $\log gf$ for the 1.1886 μm and a reduction of only 0.22 for the 1.1976 μm line. We thus prefer to use the Kurucz values until improved Fe line data becomes available.

The two measured Fe lines are of similar strength although interpretation of the longer wavelength Fe line (1.1976 μm) is compromised for the cooler objects by its blend with a strong FeH absorption band. Of the hotter objects in the sample GL699, GL299, GJ1062 and GL411 have relatively weak Fe whereas GL388 and GL123 have relatively strong Fe. For the cooler objects GJ1111 has strong Fe and VB10 has weak Fe. To interpret these relative strengths in terms of variations in metallicity and gravity is difficult given the overprediction in Fe line strengths. For the hotter objects a linear scaling indicates a spread of at least [Fe/H] = –2.0 among the sample. The cooler objects exhibit a similar spread in observed equivalent widths. However, the much greater sensitivity

of the synthetic equivalent widths to gravity and metallicity below 3000 K makes any conclusion very uncertain.

Magnesium

Unlike Fe and K lines, the Mg I line at 1.1828 μm can only be unambiguously observed in the hotter objects ($T_{\rm eff} > 3000$ K). For $T_{\rm eff} = 3000$–3500 K, Mg absorption is relatively strong and not seriously blended with other features. The models show a relatively large sensitivity to metallicity with relatively smaller sensitivity to temperature and gravity. The modelled Mg line equivalent widths accord much better with the observations than the Fe lines and suggest a much smaller spread in metallicity than derived from the K and Fe lines. For the expected gravities based on Table 3.3, the equivalent widths of GL123, GL569A and GL388 indicate that they have [Mg/H] $\sim +0.0$, and [Mg/H] ~ -0.25 for GJ1062 and GL411. GL299 and GL699 are significantly metal poor with [Mg/H] ~ -0.5.

Potassium

The K features are the strongest absorption lines for all the cooler members of the sample. The observed trend of increasing K absorption with decreasing temperature is well represented by the models. The modelled K lines are relatively sensitive to temperature and gravity and less sensitive to metallicity above [K/H] = –1.5. If it is assumed that several of the sample will have metallicities close to solar then the predicted strengths of both K absorption lines are too strong by at least 50 per cent for the hotter objects and by at least 20 per cent for the hotter objects. Of the hotter objects GL123 and GL388 have relatively stronger K absorption and so we infer that they are metal rich. Although the models predict significant differences in K absorption strength with varying metallicity and gravity only relatively small star-to-star differences are observed. This also holds for the cooler objects which apart from LHS2924 and GL406 show a smooth increase in equivalent width with temperature. The position of GL406 and LHS2924 could either be interpreted as arising from [K/H] < -1.0 or from them having relatively high metallicity and low gravity compared to GL569B, VB10 and GJ1111.

3.7 Discussion

Although the large discrepancies between synthetic and observed spectra mean that it is not appropriate to assign absolute values for log g and [Z/H] based on the above line-by-line comparison, differential comparison of objects with similar effective temperatures show interesting results. We proceed by assuming the [Z/H] and log g for one or two of the sample at their particular $T_{\rm eff}$ and use these as a starting point to evaluate the parameters of other objects with similar $T_{\rm eff}$'s.

GL123 is the hottest member of the sample and together with GL406, VB10 and LHS2924 provides a long baseline of objects kinematically determined to be from the old disk. GL123's K-line equivalent widths appear significantly low suggesting [K/H] $<$ -1.0 although [Mg/H] $\sim$ 0.0. Given that molecular opacities are relatively unimportant for GL123 we might expect to model its atomic equivalent widths relatively well. The fact that we do not means that for future modelling of this kind, it will be important to test a wider variety of atomic data. To do this it will probably be necessary to digress from the method of Kurucz (1993) which is to re-normalise the strengths of individual lines so that the total absorption coefficient for a species is correct. It should be possible to select the best atomic data to match the strength of individual strong lines without seriously affecting the overall energy distribution.

3.7.1 GL411, GJ1062 and GL569A ($T_{\rm eff} \sim$ 3500 K)

Of these GL569A shows strongest equivalent widths for all spectral features. Since GL569A is expected to have a slightly lower gravity which would tend to reduce its equivalent widths, we infer it has the largest [Z/H] by between $\sim$ 0.5 dex (based on the Mg line), $\sim$ 2.0 dex (based on the Fe lines) and $\approx$ 1.0 dex (based on the K lines). GL411 and GJ1062 have similar equivalent widths despite GJ1062 having an absolute K magnitude 1.5 magnitudes below that of GL411. The small modelled dependence of gravity on equivalent widths around $T_{\rm eff} \sim$ 3500 K suggests that GL411 and GJ1062 have metallicities within 0.25 dex of one another. If we assume (i) that GL569A has a solar-type abundance (based on its probable young age of $\sim$ 1 Gyr, Section 3.5.4),

(ii) that [Mg/H] is enhanced by $\sim$ 0.45 relative to [Fe/H] (Magain 1987, 1989) and (iii) taking account of the problems with the Fe atomic data, then we estimate that GL411 and GJ1062 have [Z/H] $\sim$ –1.0.

Although G411 and GJ1062 have similar space motions, such a low value of [Z/H] for GL411, close to GJ1062, is surprising given that GL411 lies on the disk main sequence, and GJ1062 on the subdwarf sequence, of Monet et al. (1991). The Monet et al. work is based on high quality photometric colours and trigonometric parallaxes for both objects. To verify this peculiar result it is important to repeat this abundance analysis for a larger number of lines and to investigate the differences between the M dwarf photometric classes, indicated by subdwarf and disk sequences, for a range of photometric colours plotted against $M_{\rm bol}$. However, it must be noted that although space motion can be expected be a fair representation of dynamical encounters (history), the correlation of space motion with age is not necesarily reliable when only a few objects are being intercompared.

3.7.2 GL388, GL699 and GL299 ($T_{\rm eff} \sim$ 3200 K)

GL299 and GL699 are expected to have higher gravities by around 0.3 dex relative to GL388. However, GL299 and GL699's relatively weak K and Fe line equivalent widths compared to the slightly hotter GL388 indicates that the increase in equivalent width from their larger gravities is more than offset by the decrease from reduced metallicity. If GL388 is assumed to have [Z/H] = –0.4$\pm$0.3 (Naftilan et al. 1992), GL299 and GL699 have [Z/H] < –1.5 (based on K and Fe lines) and [Mg/H] $\sim$ –1.0 (based on the Mg line) in order to match the theoretical equivalent widths of all the lines considered.

It was discussed in Section 3.5.4 that between [Z/H] = –1.0 and –1.5 the colour for a given $T_{\rm eff}$ becomes increasingly blue leading to effective temperatures, based on presumably solar-type [Z/H] disk stars (Section 3.5.1), being overestimated by around 400 K at [Z/H] = –1.5. Such a correction on the equivalent width plots for GL699 and GL299 would suggest even lower [K/H] and [Fe/H], but [Mg/H] > 0.0. Although there is a well observed precedent for high [Mg/H] values in metal poor stars based on Wheeler et al. (1989, and references therein) it seems improbable that their Mg abundance's

are overabundant by more than $\sim$ 0.75 relative to a scaling of the solar values. If we accept that there will be a large change in the relationship between photometric colour and temperature for [Z/H] < –1.5 we infer that GL299 and GL699 have –1.0 > [Z/H] > –1.5, probably closer to –1.5. Although the space motion of GL388 is not indicative of such a low metallicity (Section 3.5.4), both GL299 and GL699 are associated with the subdwarf sequence of Monet et al. As discussed in Section 3.7.1 further investigation of the M subdwarf sequence is necessary.

3.7.3 GL406, GJ1111, VB10, LHS2924 and GL569B ($T_{\rm eff}$ < 3000 K)

All the objects with $T_{\rm eff}$ < 3000 K (referred to as cooler objects) are in the regime where equivalent widths have a complex dependence on metallicity (Section 3.6.3). For example, synthetic spectra for K and Fe lines with [Z/H] = –1.5 may have larger equivalent widths than models with [Z/H] = +0.5. However the relatively small observed scatter in equivalent widths compared to the hotter objects means it is unlikely that any of them have very different properties. This is because in the hotter objects metallicity and gravity effects would have a tendency to partially cancel out (e.g. Section 3.7.2), however, in the cooler objects log g and [Z/H] effects would conspire to differentiate smaller equivalent widths due to younger objects (high [Z/H], low log g) and larger equivalent widths due to older objects (low [Z/H], high log g). The generally small observed equivalent widths (and small scatter), compared to the models, could be taken as evidence of youth (high [Z/H], low log g), however, the lack of good absolute correspondance between synthetic and observed equivalent widths makes such a conclusion inappropriate.

Significant differences in relative line strengths can be seen between the individual K and Fe lines. This is difficult to explain as the models indicate similar sensitivities to model parameters and we expect [K/H] $\sim$ [Fe/H] for solar-type [Z/H] (Wheeler et al. 1989). Combining the relative line strengths together, LHS2924 and GL406 have somewhat small equivalent widths for their effective temperatures. For GL406 this is reasonable because its gravity is lower by $\sim$ 0.1 in comparison to GJ1111, the other object with $T_{\rm eff}$ $\sim$ 2700 K. On the other hand LHS2924 would be expected to have a high log g ($\sim$ 5.40), considerably boosting its expected equivalent width, and so its

low equivalent width must result from a [Z/H] for which equivalent width declines with metallicity at $T_{\rm eff} \sim 2200$ K, ie., [Z/H] < -1.0.

3.7.4 GD165B

GD165B is one of the best brown dwarf candidates. Based on observations of its white dwarf companion, Dahn (1994, private communication) has improved its distance determination and has found it to be even less intrinsically luminous than previously determined. Its luminosity is now determined to lie at the bottom of the luminosity error bar ($\log L/L_{\odot} = -4.15$) in fig. 5.2 of Chapter 5. This implies that it is likely to be a brown dwarf if it is younger than 5 Gyr. This analysis is based on the Burrows et al. models which predict the lowest luminosities for low-mass stars. Interpreted within the models of Nelson et al. (1993) or D'Antona & Mazzitelli (1994), GD165B lies in the brown dwarf regime, no matter what its age.

The spectrum of GD165B presented in Fig. 3.3 is not of high enough signal-to-noise ratio to be properly inter-compared with the other spectra. Nevertheless it is instructive to see that the equivalent widths of the strong K features are very much in line with those expected based on the synthetic spectra or extrapolations of the observed spectra. This implies that its [K/H] > -1 and thus it is unlikely to be especially old. It thus seems that based on the current data there is only a small parameter space where GD165B can be a low-mass M dwarf rather than a brown dwarf.

Spectra taken in the far-red region by Kirkpatrick et al. (1993) showed GD165B not to be an obvious progression in spectral type from late-type M dwarfs. Spectra over a similar spectral region by Jones & Miller (1995, in preparation and Chapter 6.1.1) confirm this. Kirkpatrick et al. suggested that the cause was an absorption band due to an unknown molecular opacity. However the infrared spectra observed for this paper and those from 1 to 2.5 μm at lower resolution by Chapter 2, show no evidence for unidentified bands. It is likely that the unidentified far-red band arises from absorption by VO bands, expected in this region but not as yet well modelled. It is also possible that it arises from dust formation in the outer layers of the atmosphere, although preliminary models using dust opacities from Alexander & Ferguson (1995) indicate that when dust

forms its very high opacity means that very small quantities will dominate the opacity veiling the spectra in the far-red as well as the near-infrared.

3.7.5 NLTE effects?

In Section 3.3 we cautioned that NLTE effects are not included in the models. Based on the studies of NLTE effects for Li I for $T_{\rm eff}$ = 4500–7500 K, log g = 0.0–4.0, [Z/H] = 0.0 to –3.0, Carlsson et al. (1995) showed NLTE effects to be largest ($\sim$ 0.05 dex) at the highest gravities and the lowest temperatures (and at the extremes of metallicities), ie. the realm of this study. From Carlsson et al. and preliminary NLTE study of cool dwarfs by Hauschildt & Allard (1995, in preparation), we expect that weak chromospheric emission would flatten the cores of spectral lines, thus producing smaller observed equivalent widths than calculated in the modelled absorption features. This effect can be seen in fig. 28 of Allard (1990) which demonstrates core reversal in the Na I doublet at 0.589 μm of GL866, although no sign of core reversal is seen for the 2.21 μm Na I doublet by Jones, Longmore, Allard & Hauschildt (1995, in preparation and Chapter 6.1.1). The lack of NLTE effects in the infrared data is probably due to the chromosphere being much hotter than the photosphere. The fact that observed lines in Fig. 3.4 do seem weaker than the models might be taken as evidence for NLTE effects. Although it is likely they are present, there seems scant supporting evidence that NLTE effects are responsible for the full difference. If chromospheric emission is playing an important role we would expect it to have largest effect in the strongest lines where unit optical depth is reached at the highest regions of the photosphere. However, the observations show that it is the weaker Fe lines which appear to have equivalent widths most discrepant from the model predictions. We consider that any NLTE effects are smaller than uncertainties in the atomic and molecular data used for calculating the model grid. The inclusion of light elements in NLTE to PHOENIX has recently been completed and will be presented in a study of NLTE effects in M dwarfs (Hauschildt, Allard, Baron & Schweitzer 1995, in preparation).

3.8 Summary

The preceding analysis has showed that the PHOENIX synthetic spectra for M dwarfs can be used to infer parameters for M dwarfs from comparisons with observed spectra. Although the interpretation of the observed spectra is hampered by the lack of basic atomic and molecular input data rather than observational signal-to-noise ratios we can draw the following conclusions.

- All the stronger lines and some of the weaker lines in the synthetic spectra appear in the observations. The synthetic spectra give a representation of the overall spectral features which has not been possible in previous comparisons with M dwarf spectra.

- Although the absolute strength of the modelled atomic lines is in many cases discordant with model predictions, the observed and synthetic lines show a similar change in strength across the M dwarf regime which enables a differential comparison between the temperatures, metallicities and gravities for the observed spectra.

- The analysis of the hotter objects in the sample (> 3000 K) indicate a wide range of metallicities. Assuming that GL123 and GL388 have [Z/H] $\sim$ –0.5 and GL569A has [Z/H] $\sim$ 0.0 we find [Z/H] $\sim$ –1.0 for GL411 and GJ1062 and [Z/H] $\sim$ –1.5 for GL699 and GL299.

- The analysis of the cooler objects in the sample (< 3000 K) indicate them to have similar metallicities, presumably solar, except for LHS2924 which is likely to be metal poor by around –1.0 dex.

- The comparisons suggest a similar spread in metallicities to that anticipated, although for our sample neither kinematic motion nor membership of a particular photometric class are, on their own, reliable indicators of metallicity. This means it is important to repeat this abundance analysis for a larger number of lines and to investigate the differences between the subdwarf and disk sequences for a range of photometric colours using longer wavelength baselines plotted against $M_{\rm bol}$.

- There is a much greater spread in observed line strengths between the hotter M dwarfs than between the cooler ones, although for a similar spread in metallicities and

gravities the models predict the reverse. Members of both subsets were broadly chosen to represent the extremes of their spectral type. Although this is only a small sample of cool objects, the results are consistent with the hypothesis that the latest M dwarfs are subject to different selection effects and are relatively young. However, we find no strong evidence that any of the sample have sufficiently low-gravities to clearly distinguish them as young and thus compelling candidates to be young cooling brown dwarfs.

- The models highlight an effect first shown by Allard (1990) that atomic lines in cooler M dwarfs (< 3300 K) do not show the intuitive behaviour of atomic lines decreasing in strength with decreasing metallicity. In cool M dwarfs the sensitivity of atomic line profiles to increases in pressure indirectly resulting from lower metallicities are more important than decreases in atomic number density. This effect is prevalent down to [Z/H] ~ -1.5 and complicates the interpretation of line strengths in cool stars.

- In the spectral region 1.16–1.22 μm all atomic and molecular features show a strong sensitivity to temperature, especially the K lines. Metallicity and gravity effects are relatively much smaller. For the hotter stars, Mg and Fe absorption lines are the most useful discriminators between gravity and metallicity. For the cooler objects the complicated dependence of metallicity on line strengths makes quantitative interpretation of the most sensitive lines, K and Fe, more difficult.

- We find strong evidence that [Mg/H] does not scale with [K/H] or [Fe/H] for low-mass stars, in agreement with results for higher mass stars.

- Comparison between observed and synthetic spectra for GD165B indicate that [K/H] > -1. This together with a improved distance measurement for GD165B leaves only a small parameter space for it not being a brown dwarf.

- Kirkpatrick et al. (1993) suggest that their 0.7–0.9 μm spectrum of GD165B shows evidence for missing opacities. Our analysis shows no evidence for missing opacities from 1.16 to 1.22 μm. We suggest that the "missing opacity" maybe VO and FeH transitions which have yet to be characterised.

- These comparisons emphasize the need for an FeH line list.

- We find no strong evidence for NLTE effects being important in the analysis of spectra from 1.16–1.22 μm.

- Although this analysis was hampered by uncertainties in atomic and molecular input data, the large sensitivity of equivalent widths in M dwarfs means that with new line lists and improvements in the treatment of line lists determination of absolute M dwarf parameters from infrared data such as that presented here should soon be possible.

Chapter 4

Water vapour in cool dwarf stars

Comparisons are presented between observed and synthetic spectra for water vapour transitions in a range of M dwarfs. The observations are from 2.85 to 3.40 μm, where water vapour transitions are strong in cool stars but relatively weak in the Earth's atmosphere. The synthetic spectra include pioneering *ab initio* calculations for ro-vibrational lines arising from water vapour transitions.

• These results strongly suggest that water vapour transitions are not pressure broadened sufficiently to overlap as previously assumed when modelling molecular transitions in cool dwarfs using the Just Overlapping Line Approximation. We demonstrate that this result is likely to explain much of the past discrepancy between observed and theoretical spectral energy distributions for M dwarfs.

• Within the uncertainty of the calculation the predicted strengths and positions of the water transitions accord with observation. Both the observed and synthetic spectra are strongly sensitive to temperature but not to metallicity or surface gravity.

• Formally, we find a similar effective temperature scale to that proposed by Kirkpatrick et al. and Bessell. However, since the molecular opacity at the peak of the flux distribution is not well determined, uncertainties in the model atmosphere structure and the effective temperature scale remain.

4.1 Introduction

Molecular absorption bands have been used as a diagnostic of spectral type since the 1860's. TiO was first identified as the dominant feature in optical spectra of cool giants (Fowler 1904). Over the last 30 years, diatomic molecules have been included in detailed calculations of stellar opacity. The success of these studies and a desire to understand cooler objects means that attention is starting to focus on the incorporation of accurate data for triatomic molecules. The most important is water.

M dwarfs are the dominant stellar population in the Galaxy. They emit the bulk of their radiation at near-infrared wavelengths where water vapour is the principal source of opacity in their atmospheres. The shape of the water absorption bands means that their energy distributions do not resemble the blackbody curves which are shown by hotter stars across the near-infrared. The lack of accurate water vapour data available for inclusion in model atmosphere codes has meant that synthetic and observed spectra do not match well enough for the derived parameters to be trusted (e.g. Tinney, Mould & Reid 1993). This has led to a number of different empirical techniques to determine the effective temperatures of M dwarfs. These have yielded a wide range of effective temperature scales. A model atmosphere calculation which properly accounts for water vapour will yield an unambiguous effective temperature scale for M dwarfs. Over the last ten years many papers have discussed the discovery of candidate brown dwarfs. Yet without an accurate effective temperature scale for M dwarfs it has not been possible to distinguish whether they are brown dwarfs or late-type M dwarfs.

For effective temperatures applicable to cool star atmospheres (<4000 K) it is necessary to cover the band origins of water up to 30,000 cm^{-1} and angular momentum states up to $J = 55$ (30,000 cm^{-1}) above the ground state. Such a calculation requires a significant investment of time on the most powerful computers currently available. Before undertaking such a large investment of computer time a preliminary calculation of 8.4 x 10^6 transitions including states up to $J = 30$ was made (Schryber, Miller & Tennyson 1995) and band origins up to 10,000 cm^{-1}. This preliminary water line list has been incorporated in the PHOENIX model atmosphere code (Hauschildt 1991; Allard et al. 1994; Hauschildt et al. 1994; Hauschildt et al. 1995). The following work compares

the latest version of PHOENIX including the preliminary water line list with high quality observations of stellar water vapour.

The preponderance of water vapour in the Earth's atmosphere makes it very difficult to observe its spectral signature in stars. At near-infrared wavelengths, where cool stars emit most of their flux, the strongest water vapour absorption band for cool stars is centered around 2.65 μm where the atmosphere is opaque. However, all molecular bands become narrower towards lower effective temperatures as less of the higher ro-vibrational states are occupied. Because M dwarfs are an order of magnitude hotter than the atmosphere, ground-based observations can be made in the wings of this band. Transitions of a weaker band at 3.17 μm are also observable. We considered that the 2.65 and 3.17 μm bands were more appropriate for this part of our study than the bands at 1.4 and 1.7 μm because they are affected less by the low energy cut-off of the calculations.

The observations and data reduction procedures are reported in Section 4.2. The *ab initio* calculations are discussed in Section 4.3. Comparisons with other water vapour opacity datasets are made in Section 4.4. The model atmospheres are presented in Section 4.5. Section 4.6 compares the observed and synthetic spectra.

4.2 Observations

We observed a range of M dwarfs – VB10 (M8V), GL406 (M6V), GL699 (M3.5V) and GL411 (M2V). They were chosen because they have been the subject of many previous studies of M dwarfs (e.g. Chapter 2) and because they form a sample whose space motions and colours indicate they cover a wide range of effective temperature, but probably a narrow range in metallicity.

The observations were made on the nights of 21–23 April 1993 with the Cooled Grating Spectrometer 4 (CGS4, Mountain et al. 1990) on the UK Infrared Telescope on Mauna Kea, Hawaii. CGS4 used a 58 x 62 InSb array which was moved in the focal plane in order to over-sample the spectrum. Comparison sky spectra were obtained by nodding the telescope so that the object was measured successively in two rows of the array, separated by 30 arcsec (10 rows on the array).

Table 4.1: The target objects were corrected for atmospheric transmission and flux calibrated using the standards listed above. The spectral types are from Hoffleit & Jaschek (1982), their effective temperatures were obtained from the $T_{\rm eff}$ – spectral type and colour relations of Johnson (1966) and Schlosser, Schmidt-Kaler & Milone (1991).

Object	Standards	Types	$T_{\rm eff}$ (K)
GL411	BS4345, BS4294	G0V, A5III	6030, 8100
GL699	BS6797, BS5304	F5V, F9IV	6440, 6060
GL406	BS4294, BS4386, BS4345	A5II, B9.5V, G0V	8100, 10000, 6030
VB10	BS7235	A0V	9400

The 150 line mm^{-1} grating was used with central grating wavelengths of 2.94, 3.12 and 3.30 μm. These grating positions enable complete coverage from 2.86 to 3.40 μm at a resolution of around 1000. Observations were also made with the 75 line mm^{-1} grating at a central wavelength positions of 3.12 μm giving a resolution of around 500 and covering 2.94–3.34 μm. This was done to check the reproducability of features in a little used spectral region and to ensure that accurate spectral overlaps were made when joining different spectral regions together. The high thermal background in the 2.86–3.40 μm region meant that a number of short integrations (0.5–2.0 s) were made and coadded together. For the faintest object VB10, total on-chip integration times at each grating position were around 1 hour; for the brighter objects, GL411, GL699 and GL406, they were around 30 mins.

4.2.1 Data Reduction

In the reduction of spectra, the same procedures as in Chapter 2 have been followed. All observations were calibrated by taking short exposures of an argon lamp in the CGS4 calibration unit. This procedure is typically accurate to $0.1\Delta\lambda$ (Puxley, Ramsay & Beard 1992), where $\Delta\lambda$ is the instrumental resolution. The observed spectra were taken in a region where there are about a half as many arc lines as normally available and so a

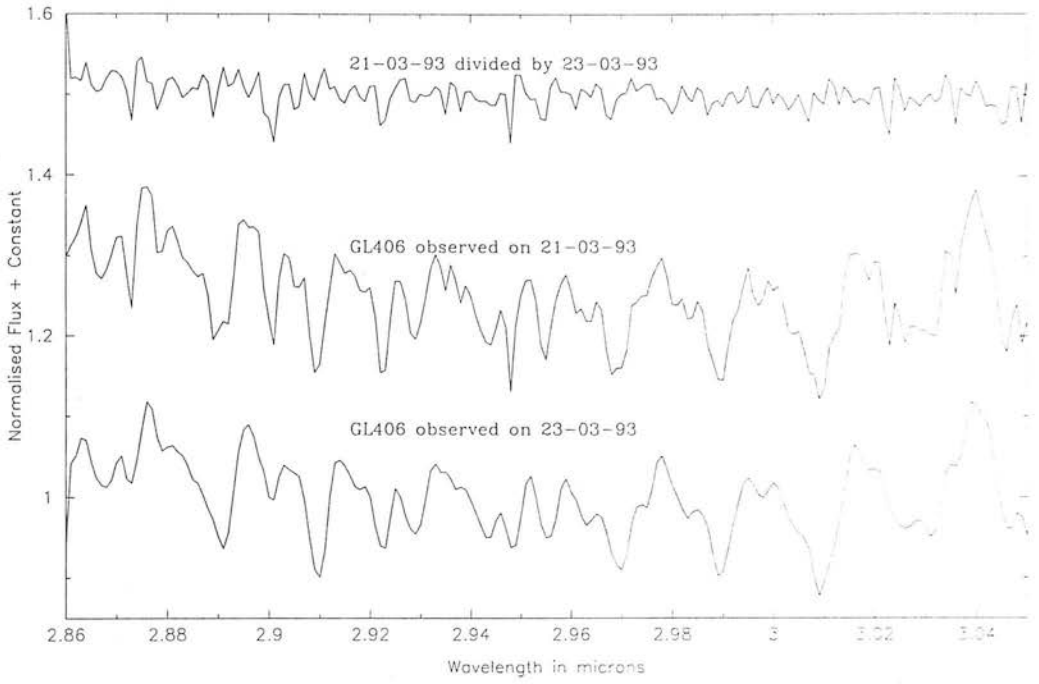

Figure 4.1: To check the reproducability of the spectra in this little used spectral region a number of the observations were repeated. Observations of GL406 at the same grating position taken on 21 April and 23 April 1993 are shown.

wavelength calibration error of $0.2\Delta\lambda$ is more realistic. The wavelength calibration was checked by comparing the wavelength scale from the 75 line mm^{-1} grating with that from the 150 line mm^{-1} grating. They were found to agree to within 0.0006 μm (0.1 $\Delta\lambda$ of those from the 75 line mm^{-1} grating).

Stars from The Bright Star Catalogue (Hoffleit & Jaschek 1982) were used as standards to remove the effects of atmospheric absorption; these are given in Table 4.1. We found them to be featureless and to be well described by a Rayleigh-Jeans energy distribution appropriate to their effective temperature. All observations were made in good conditions (better than 1 arcsec optical seeing) and the airmass difference between object and standard never exceeded 0.05. Thus we believe the spectra have excellent cancellation of atmospheric features. The observations were repeated on subsequent nights to check the cancellation of atmospheric features and the reproducability was found to be good. An example is shown in Fig. 4.1 of GL406 (fully reduced) taken on different nights. Fig. 4.2 (a,b,c) shows a spectral sequence ranking the M dwarfs based on the strength of water absorption features from 2.85 to 3.4 μm for each of the 150 lines mm^{-1} grating positions.

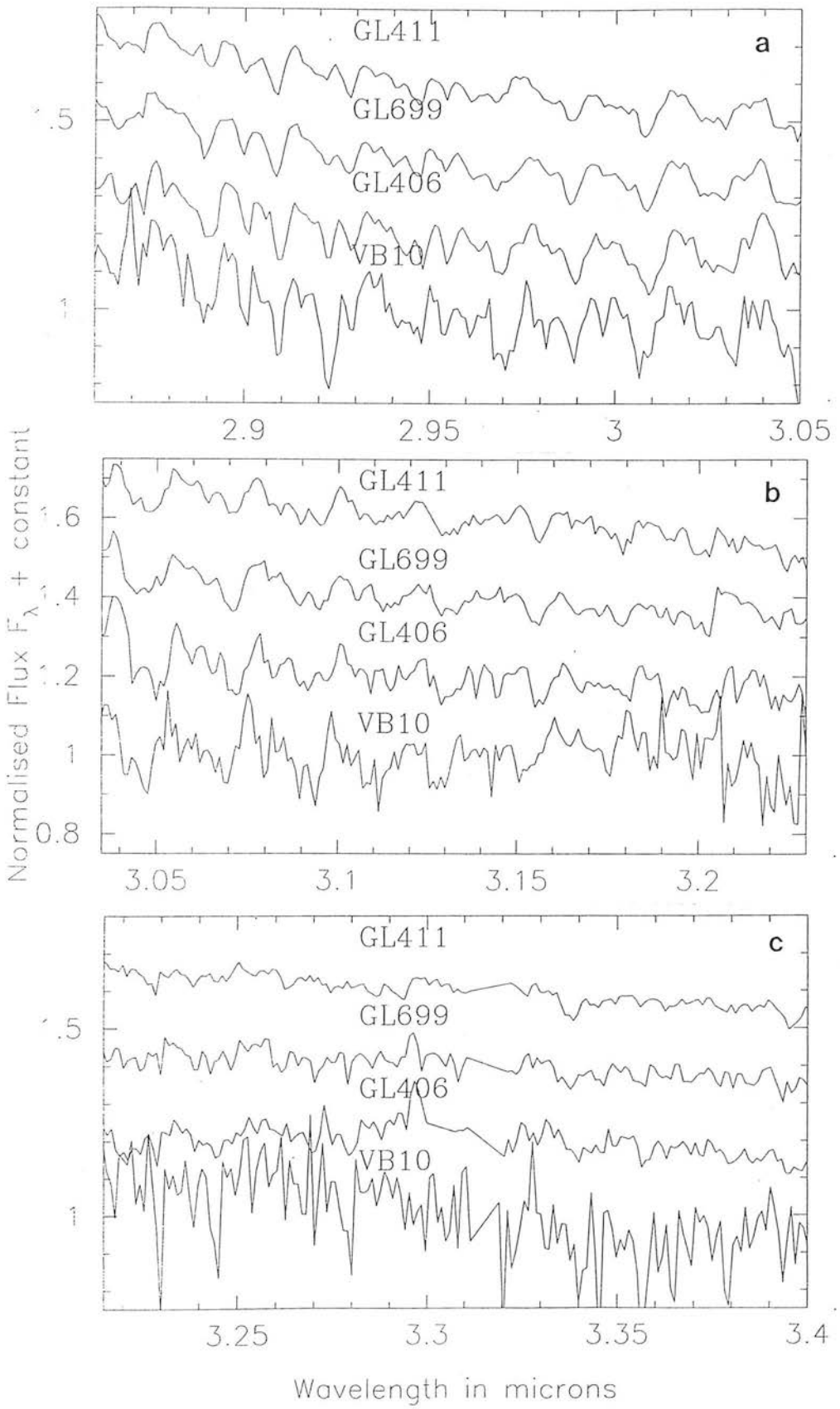

Figure 4.2: Spectral sequence for each 150 lines/mm grating position (a) at 2.94 μm, (b) at 3.12 μm and (c) at 3.30 μm. In plot (c) the region around 3.32 μm has been interpolated over in the region where the atmosphere is opaque due to a strong methane band.

4.3 Calculations of *ab initio* water vapour transitions

At low temperatures water vapour absorption is very thoroughly studied. However little reliable data on hot water (above 1000 K) is available. Over the last decade a number of groups (e.g. Tennyson 1986; Spirko et al. 1985; Carter & Handy 1986) have developed techniques for calculating triatomic energy levels based on variational techniques. In particular, Sutcliffe & Tennyson (1986) have produced a ro-vibrational Hamiltonian which is exact within the constraints of the Born-Oppenheimer approximation (which decouples electronic from nuclear motion in a molecule) and the limitations of the electronic potential energy surface.

The Sutcliffe-Tennyson kinetic energy operator directly relates the Cartesian positions of the nuclei of a triatomic molecule to a set of internal coordinates comprising two radial coordinates and the included angle. Rotation of the molecule-fixed internal coordinates in the laboratory frame is carried by the usual standard rotational matrices. The kinetic energy operator makes no *a priori* assumptions about ro-vibrational separation or equilibrium geometry. The method is described in Tennyson, Miller & Henderson (1993).

The ro-vibrational wavefunctions were calculated by using a suite of programs known as TRIATOM (Tennyson, Miller & Le Seur 1993). The suite contains modules to calculate ro-vibrational transition frequencies and line strengths from dipole moment surfaces. Wavefunctions and energies were generated using the best then available water potential Jensen (1989). Transition intensities were obtained using the program DIPOLE3 (Lynas Gray, Miller & Tennyson 1995; Tennyson, Henderson & Fulton 1995) and the dipole surfaces of Wattson & Rothman (1992).

The calculation includes angular momentum states up to $J = 30$. All band origins up to 11000 cm^{-1} above the ground state are included as well as many, but not all, higher ones. This energy cut off is too low to include all the transitions expected at cool star temperatures and shortward of around 2 μm the calculation does not give a good representation of stellar energy output (Allard et al. 1994). For longer wavelengths where higher energy transitions are relatively less important the calculation is expected to be

much more reliable. This gives us confidence that the spectra observed for this study from 2.86 to 3.4 μm should be well represented by the calculation. The comparisons presented here extend Miller et al. (1994) where the observed spectra were compared, without the use of a model atmosphere, to an earlier, less complete, generation of the calculation.

4.4 Comparison with other water opacity datasets

Water was the first triatomic molecule to be included in a stellar atmosphere calculation (Tsuji 1967) and for 15 years remained the only one. The most frequently used source for water opacity is Ludwig (1971), whose data were obtained to assess the heating effect of radiation by hot water vapour in exhaust fumes from large rockets. Ludwig and co-workers measured the absorption of water in a flame between 1000 and 3000 K and hence tabulated absorption coefficients for water from 1.1 to 10 μm, albeit with low resolution. In Fig. 4.3 a comparison between Ludwig's experimental data and the *ab initio* data is shown. The strength of the water absorption from 2.85 to 3.2 μm, obtained for this work, can be seen as intrinsically very strong. The *ab initio* water plot has been made from a subset of 6000 strong transitions and scaled to appear similar in amplitude to the laboratory data, though its much higher resolution means Fig. 4.3 is not a proper comparison of the band intensities. For a full intercomparison of the *ab initio*, Ludwig and HITRAN (Rothman et al. 1992) datasets we refer to Schryber, Miller & Tennyson (1995).

The Ludwig data have been widely used for the computation of cool star atmospheres, although other laboratory results, the *ab initio* line list used here and observations of cool stars themselves cast serious doubts on its accuracy. The Ludwig band strengths were derived by integrating the measured spectral emissivity of hot water vapour assuming that the fine structure of the spectrum is smeared out at high electron temperatures. Yamanouchi & Tanaka (1985) find that this assumption is not always valid and show large differences for the strengths of the 1.1 and 1.4 μm bands between the Ludwig data and their work (in agreement with Goldstein 1964 and Burch & Gryvnak 1966). Schryber et al. (1995) find a similar mismatch with their calculation of the 1.9 μm band

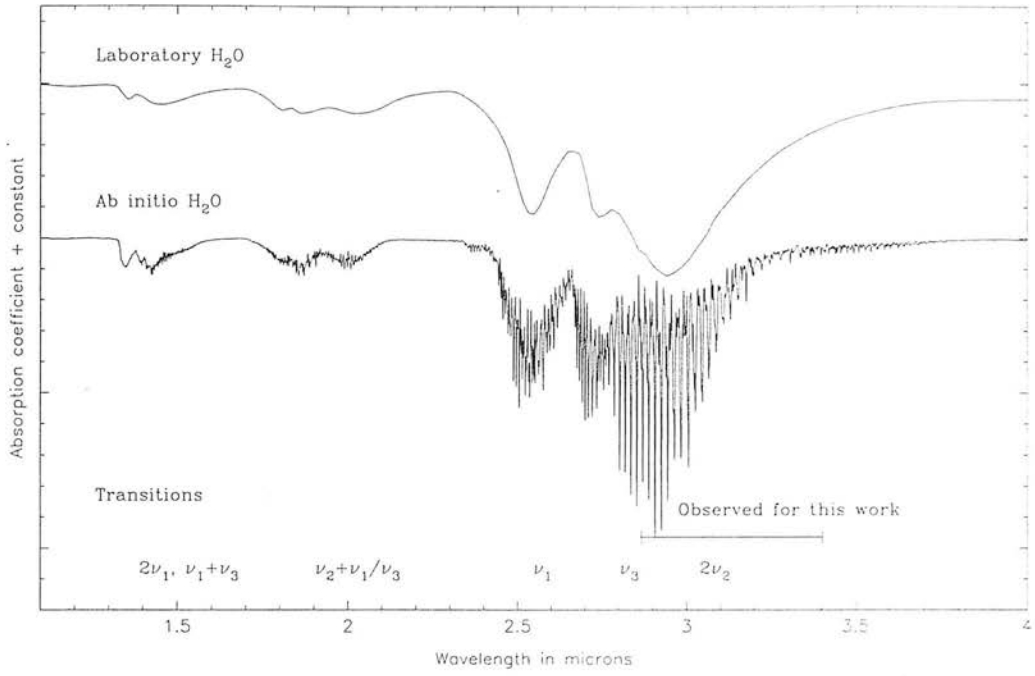

Figure 4.3: Comparison of Ludwig (1971) absorption coefficients for water vapour and those from the *ab initio* calculations at 3000 K. The band origins of the various features that make up the water vapour absorption coefficient are marked in the figure.

and suggest that Ludwig's results overestimate the absorption coefficient of water over the entire 1–2 μm region at higher electron temperatures.

Comparisons between synthetic and observed spectra for M dwarfs also indicate problems with the Ludwig dataset. The models of Mould (1976), Allard (1990), Ruan (1991), Tsuji (1994) and Brett (1995) which all use the Ludwig water opacities cannot simultaneously reproduce observed spectral energy distributions and absorption bands due to water vapour. For an effective temperature derived on the basis of spectral energy distribution the models all overestimate the importance of water vapour. This has prompted Brett (1995) to arbitrarily decrease the absorption coefficient for the Ludwig opacity data by a factor of three in a new set of cool dwarf models.

4.5 Model atmospheres

We use the model atmosphere code PHOENIX, version 4.9, to compute model atmospheres and synthetic spectra for cool dwarf stars. Its application to M dwarf atmospheres is described by Allard et al. (1994) and Allard & Hauschildt (1995). Here we draw attention

to the important assumptions relevant for this study.

•Since the gravities are high ($\log g \sim 5$), the atmospheres can be well approximated as plane-parallel.

•The velocities of the convection cells are too small to be detected in low-resolution spectra and will have a negligible influence on the transfer of radiation and so the effects of convective motion on line formation are neglected (Allard & Hauschildt 1995).

•A treatment for molecular line broadening due to collisional processes, for example with H_2 and H^- is not included. The line broadening for molecules is treated by altering ξ(molec), the isotropic micro-turbulent velocity for molecules caused by pressure and turbulent broadening, throughout the model structure. We investigate the effect of changing ξ(molec) in Section 4.6.1.

•Non-Local Thermodynamical Equilibrium (NLTE) effects are neglected. Although we are not aware of any research on their importance for water vapour transitions, complex molecules have many pathways for any given population to thermalise and so NLTE effects probably play only a small role.

The major difference between models presented here and those in Allard et al. and Allard & Hauschildt is the inclusion of new data for TiO which has allowed it to be treated using the opacity sampling technique rather than the less reliable Just Overlapping Line Approximation (JOLA) technique (Tsuji 1994). Jorgensen (1995) has calculated a line list for TiO comprising 12 million lines. The new treatment of TiO has the effect of reducing the effective temperatures derived by comparison of a previous generation of these model atmospheres (Kirkpatrick et al. 1993a) around 1 μm by around 150 K (Chapter 3). We thus consider the lack of molecular line lists for the other primary sources of opacity, VO and FeH, to be large uncertainties in the calculation of representative synthetic spectra for cool dwarf stars. However the inclusion of high quality line lists for the TiO and H_2O means that we expect that the dominant opacity over much of the peak of stellar energy distribution is well accounted for.

A small grid of synthetic spectra were calculated. We distinguish the different models using the notation, lteTT–G.G–Z.Z.I.D, where lte = local thermodynamic equilibrium

assuming ξ(LTE) = 2 km/s, TT = $T_{\rm eff}/100$, G.G = log g (surface gravity), Z.Z = [Z/H] (metallicity), where [Z] $\equiv$ log $Z_{\rm star}$ - log $Z_{\odot}$ for any abundance quantity Z, and I.D = batch number (ir3.7 for ξ(molec) = 2 km/s and ir3a.7 for ξ(molec) = 50 km/s). For ξ(molec) = 2 km/s, models were calculated for $T_{\rm eff}$ = 2000, 2500, 3000, 3500 K, log g = 5.0, [Z/H] = 0.0 and $T_{\rm eff}$ = 3000 K, log g = 4,0, [Z/H] = 0.0 and $T_{\rm eff}$ = 3000 K, log g = 5.0, [Z/H] = −1.0. Models were also calculated for ξ(molec) = 50 km/s for $T_{\rm eff}$ = 3000, 3500 K, log g = 5.0 and [Z/H] = 0.0. Fig. 4.6 shows comparisons with models of different effective temperature, metallicity and gravity over a similar wavelength range to the observations. These are discussed in Section 4.6.2.

4.6 Spectral Analysis

The models were calculated at a resolution of $5\text{x}10^{-5}$ μm and were transformed to the instrumental resolution by smoothing with a block function to mimic the effect of being detected by the square pixels used by the infrared detector of CGS4 and resampling to the same oversampling (x3) as employed for the observations. This was performed using routines within the KAPPA (Currie 1992) and SPECDRE (Meyerdierks 1993b) packages.

4.6.1 Line Broadening

Detailed line profiles can be modelled for atomic lines because their damping constants are known, but they they are not known for molecular transitions. Atomic lines computed with Voigt profiles and Van der Waals pressure broadening give an averaged full width half maximum of around 50 km/s. Initially this broadening was used to simulate the line broadening for water vapour transitions by setting ξ(molec) = 50 km/s. Although the 'true' microturbulence is expected to be close to 2 km/s (the speed of sound is 6–8 km/s) with this generation of models setting ξ(molec) = 50 km/s is the most practical way of allowing for the pressure broadening of water vapour transitions. Models with ξ(molec) = 2 km/s, no pressure broadening, were also calculated. In Fig. 4.4, GL411 and GL406 are compared with 3000 and 3500 K models for ξ(molec) = 2 and 50 km/s.

The ξ(molec) = 50 km/s models predict enhanced strengths of water absorption

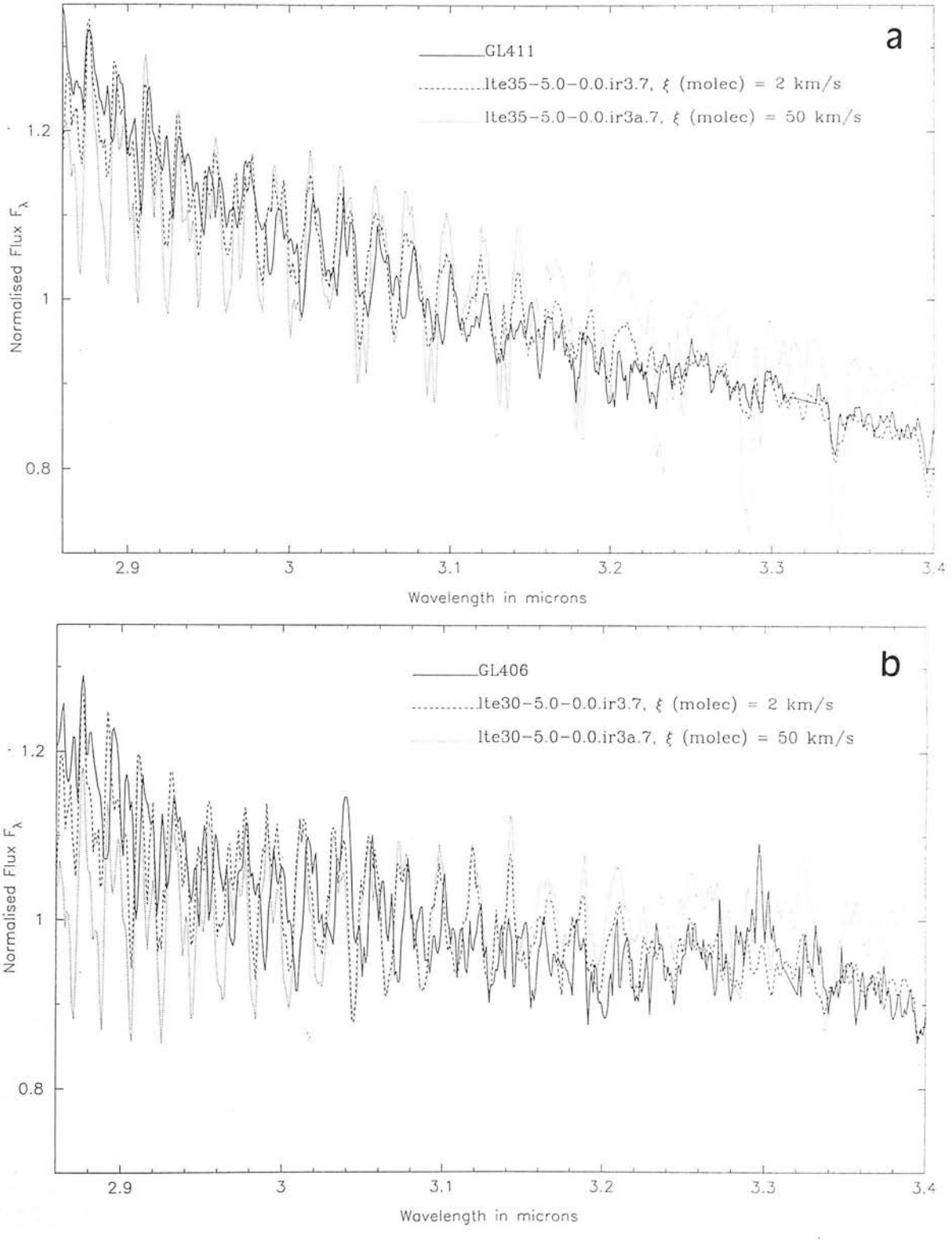

Figure 4.4: Comparison between observed and synthetic spectra from 2.86 to 3.4 μm using ξ(molec) = 2 and 50 km/s models: for (a) GL411 with 3500 K models and (b) GL406 with 3000 K models.

bands across the entire spectral region, particularly from 3.2 to 3.4 μm. To match the strengths of the water bands with the ξ(molec) = 50 km/s synthetic spectra it is necessary to increase the best fit effective temperatures by 200–800 K depending on the spectral region, effective temperature and adopted effective temperature scale. Doing so leads to a much poorer fit to the overall continua. The lack of agreement suggests that the damping constants of water (and therefore possibly all molecular lines), which are unknown, must be smaller than the damping constants of the average atomic lines. Alternatively water vapour lines form higher in the photosphere in regions of lower pressure. To test the latter hypothesis the model structure was investigated. For the 2500 K model it shows that the strongest water lines form in the outer parts of the atmospheres at gas pressures around 10^3 dyn/cm^2, the bulk of the water lines form around gas pressures of $5\text{x}10^4$ dyn/cm^2 whereas weak atomic lines form much deeper, around gas pressures of 10^6 dyn/cm^2. The formation of water lines at relatively low pressures explains why the broadening provided by the microturbulent velocity alone gives sufficient line broadening to match the observed spectra.

Previous models of M dwarfs have generally assumed that the high densities prevalent in their atmospheres mean that molecular lines are smeared together by their large pressure broadening (JOLA, e.g. Tsuji 1994). However the water band strengths in Fig. 4.4 and new examination of the model structures indicate low pressure broadening and suggest that flux is escaping between the water vapour line transitions, undermining the use of the JOLA approximation for water vapour transitions in cool dwarf atmospheres. The reduction in opacity caused by water vapour lines forming at lower pressures leads to weaker band strengths. This result is likely to explain much of the apparent overestimate of molecular band strengths in synthetic spectra for M dwarfs (e.g., Persson, Aaronson & Frogel 1977, Reid & Gilmore 1984, Ruan 1991, Tinney et al. 1993, Brett 1995). In Fig. 4.5 we show 2500 K models for ξ(molec) = 2 (solid line) and 50 (dotted line) km/s . The much weaker water bands seen around 1.4 and 1.9 μm in the ξ(molec) = 2 km/s model demonstrates how important this effect is for modelling the spectral energy distribution of M dwarfs across the peak of their energy distribution.

Low values for line broadening (modelled using the microturbulence parameter) are clearly most appropriate for water vapour lines. The following sections are based on

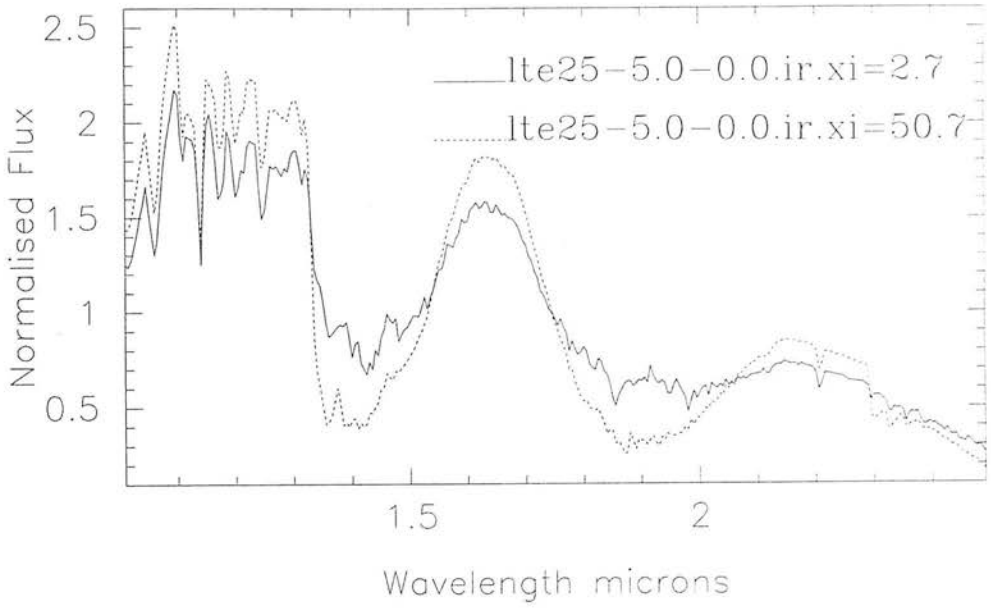

Figure 4.5: Comparison between synthetic spectra from 1.0 to 2.5 μm using ξ(molec) = 2 and 50 km/s models for 2500 K models.

models using ξ(molec) = 2 km/s, although this is not a proper physical approach to the damping problem and we do not yet know how the broadening varies between ξ(molec) = 2 and 50 km/s. The model atmosphere code is now being adapted so that the molecular broadening will be matched to the averaged atomic line broadening throughout the 50 layers between the "standard" optical depths of $\tau_{\rm std} = 10^{-10} - 10^{2}$ in the model atmosphere. A computationally efficient method for achieving this is planned for the next generation of water vapour transitions.

4.6.2 Sensitivity to model parameters

Water vapour is well known to be extremely sensitive to colour temperature in M dwarfs (Baldwin, Frogel & Persson 1973). However, its dependence on metallicity and gravity differences has not been investigated. In Fig. 4.6(a,b,c) the sensitivity of the synthetic spectra to changes in model parameters is examined. In each of (a), (b) and (c) one model parameter has been changed. In the lower part of each figure two models are normalised to have the same mean value and over plotted; in the upper part, the models have been divided by one another and the result offset by the addition of 0.25. The models were selected so that the differences in water band strength between them were similar. To

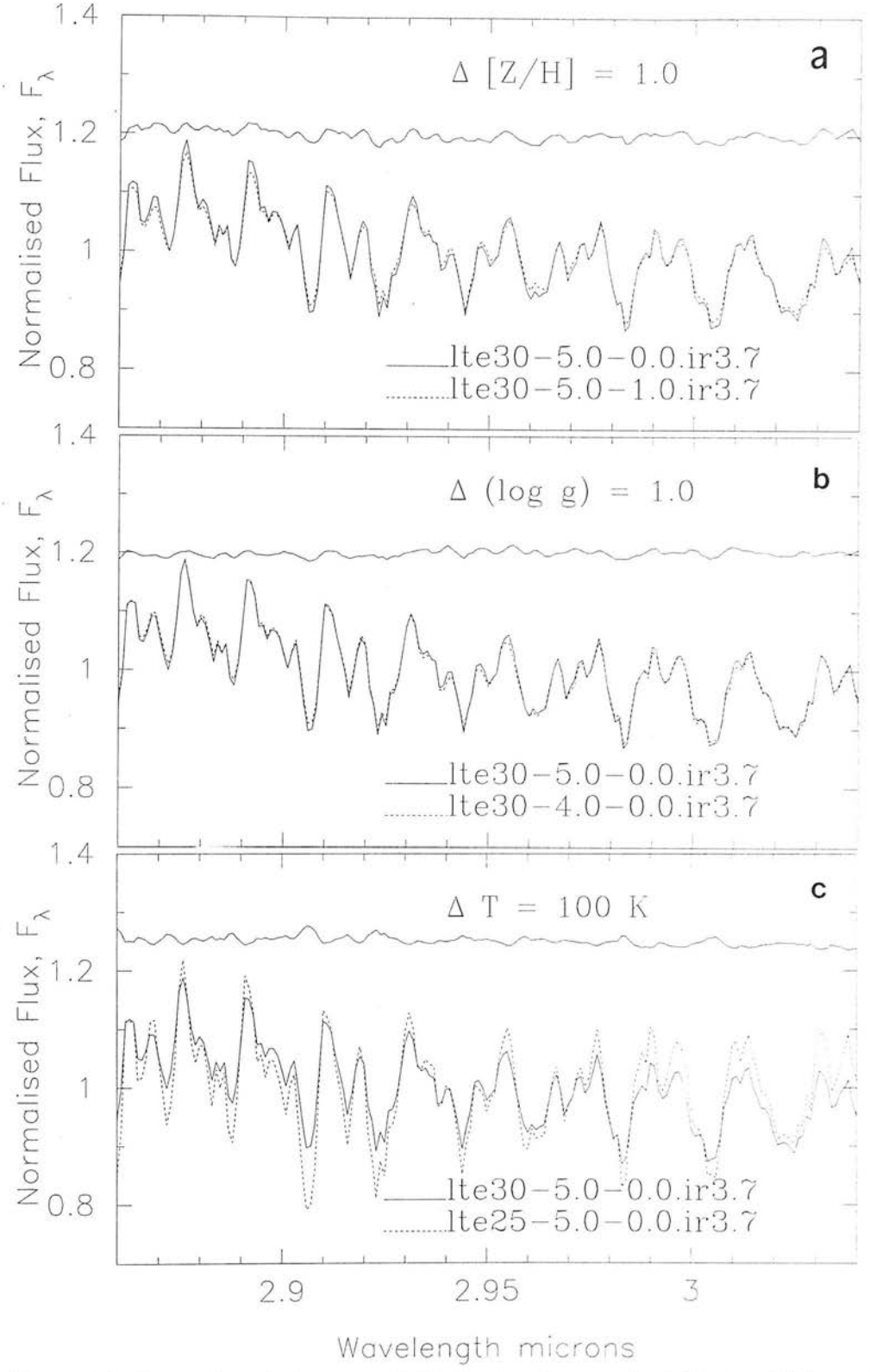

Figure 4.6: Comparisons between synthetic spectra showing the influence of (a) varying metallicity by a factor of ten from solar abundance ([Z/H] = 0.0) to that of a metal poor star ([Z/H] = −1.0), (b) varying surface gravity by a factor of 10 – the expected gravity difference between a young $\sim$ 5 Myr, 0.2 $M_{\odot}$ star and one on the main sequence (Burrows et al. 1993) (c) varying effective temperature by 100 K (equivalent to about half a spectral type, e.g. M5 to M5.5) on the synthetic spectra.

divided by one another and the result offset by the addition of 0.25. The models were selected so that the differences in water band strength between them were similar. To reproduce a variation in water band absorption from a change in temperature, equivalent to those in metallicity and gravity, it was necessary to interpolate the coarse model grid in temperature. To mimic the effect of a 100 K change in effective temperature, 2500 and 3000 K synthetic spectra were divided by one another multiplied by 0.2 and offset. A similar result was found when doing the same operation with the 3000 and 3500 K synthetic spectra.

In Fig. 4.6(a) a 3000 K, log g = 5.0 solar model (lte30-5.0-0.0.ir3.7) is compared to one with a tenth of solar metallicity. This comparison represents the probable extremes of metallicity of our sample objects (Chapter 3) and indicates a small sensitivity to metallicity. In Fig. 4.6(b) 3000 K solar models with gravities of log g = 4.0 and 5.0, within the expected gravity difference for these objects, are compared. The plots indicate that water vapour features are not very sensitive to gravity effects. In contrast to the insensitivity of the spectra to metallicity and gravity, comparison between Fig. 4.6(c) with (a) and (b) indicates that a small change in effective temperature ($\sim$ 100 K) has a similar effect to that produced by a change of a dex in gravity or in metallicity. The differences between the models presented in Fig. 4.6(a), (b) and (c) are smaller than the night-to-night differences between measurements across this spectral region, e.g. Fig. 4.1. With the observed sample, this study is not sensitive to differences in metallicity and gravity and so changes in water absorption strengths are treated as arising from differences of effective temperature between stars.

In Fig. 4.7 comparisons are made between the observed and synthetic spectra. From the small model grid we show the model whose water absorption bands best fit the observed spectra. We have interpolated between the models in the grid to give a finer resolution in effective temperature. The intensities of the calculated ro-vibrational bands accord well with the observed ones, though the positions of the bands do not match so well. From the comparisons made in Fernley, Miller & Tennyson (1992) band origins up to J = 20 are accurate to a standard deviation of $\sim$ 0.006 μm and those above J = 20 to better than 0.010 μm. These errors are considerably larger than the observational wavelength calibration error of $\sim$ 0.0006 μm (equivalent to a velocity of 180 km/s) or

The wavelength differences between the models and the observations might arise from a simple expansion or contraction of the wavelength scale due to a systematic error in the potential surface used to compute the water vapour transitions. To examine this the observed and synthetic spectra were cross correlated using the SCROSS routine within FIGARO (Meyerdierks 1993a). The spectra were cross correlated with one another in 0.1 μm intervals every 0.05 μm from 2.86 to 3.4 μm and the standard deviations computed. The observed spectra have standard deviations of typically 0.0005 μm for the hotter stars as expected from the wavelength calibration errors although the discrepancies with VB10 are much larger $\sim$ 0.005 μm due to its lower signal-to-noise ratio and markedly stronger water absorption bands. Comparison of the observations with their best fit synthetic spectra gives standard deviations around 0.015 μm and no evidence for a simple systematic wavelength shift between the models and observations. The wavelength discrepancies between synthetic and observed spectra are slightly larger than expected. We expect that this results from the lack of high order transitions included in the water line list. Although the errors on the water line list are well characterised they do not account for the lack of higher order transitions which means that there is an additional error term not included in the error estimate. As an example of the problems this can introduce Grevesse & Sauval (1994) find that for the accurate modelling of line shifts and asymmetries for the CO molecule in the Sun it is essential to include transitions up to very high J levels.

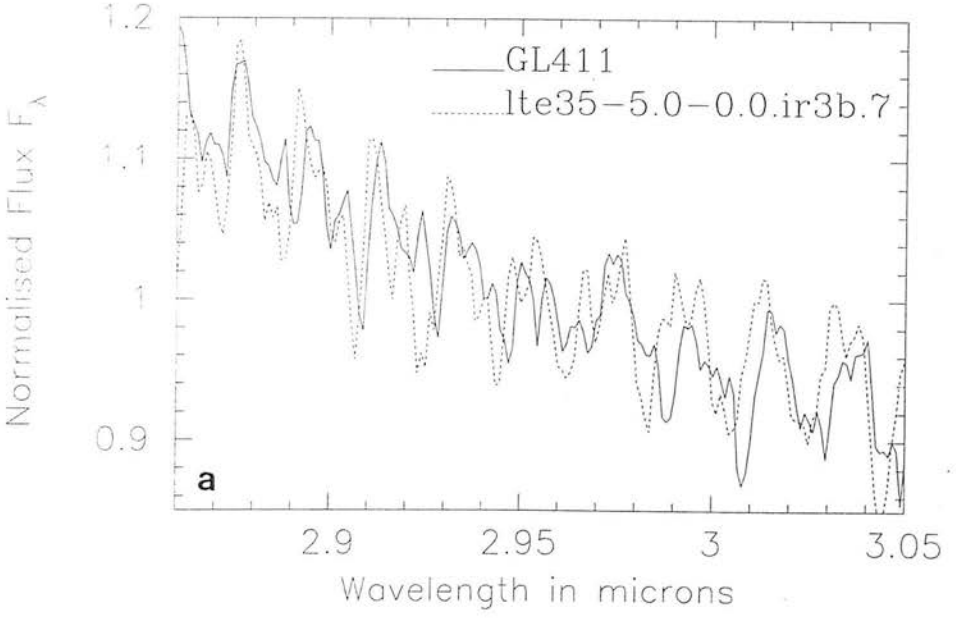

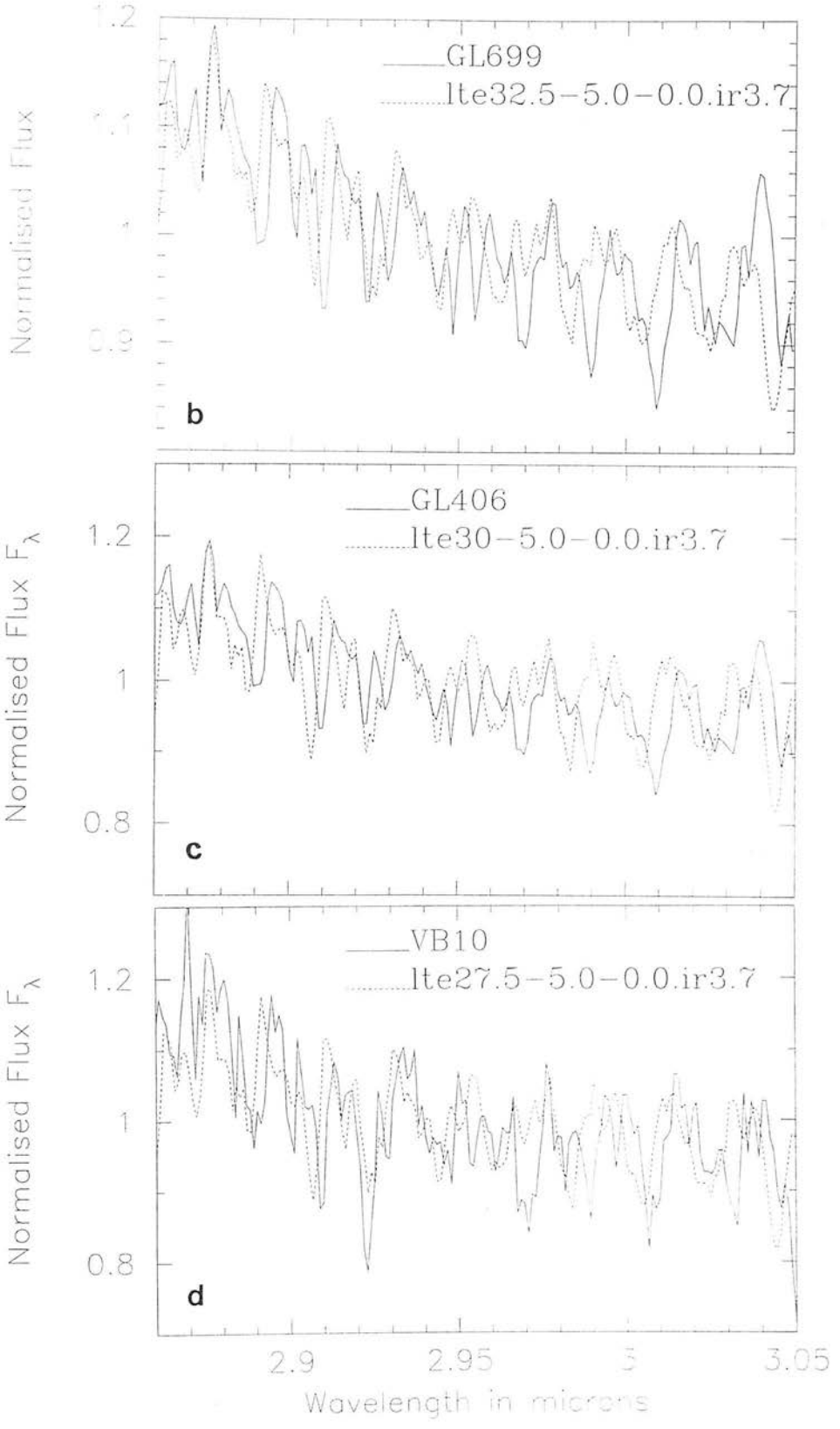

Figure 4.7: Comparisons of spectra with models: (a) GL411 and a 3500 K model, (b) GL699 and a 3250 K model, (c) GL406 and a 2800 K model, (d) VB10 and a 2500 K model. Models intermediate in effective temperature to those of the grid were created by linear interpolation

Table 4.2: Comparison of the effective temperatures indicated by this study with those found by recent investigations.

Object	This Work ±200 K	Bessell ±50 K	Kirkpatrick et al. ±125 K	Tinney et al. ±110 K	Chapter 2 ±160 K
GL411	3600	3500	>3500	3250	3471
GL699	3250	3250	-	3110	3095
GL406	3000	2800	3000	2580	2670
VB10	2750	2600	2875	2330	2506

4.6.3 Effective temperatures

Both models and observations indicate that water vapour transitions are not saturated but continue to increase with decreasing temperature as low as 2500 K. This is in agreement with Chapter 2 where it was shown that the depth of the 1.4, 1.9 and 2.6 μm water absorption features increase with decreasing effective temperature down to the coolest known dwarfs. Although the relatively short baseline of the observations presented here means that the underlying continuum are not very sensitive to temperature, the strengths of the water bands are sensitive, especially from 2.86 to 3.05 μm. In this region where the transitions are strongest we have interpolated over the model grid to estimate effective temperatures by overlaying a range of synthetic spectra on top of the observed spectra. The best fit by-eye values are given in Table 4.2 with values found by other recent studies of these objects. For GL411 and GL699 the effective temperatures are within the range found by previous investigators of whom Bessell (1991), Tinney et al. (1994) and Chapter 2 used methods independent of the model atmosphere calculation. The effective temperatures for VB10 and GL406 are closest to those by Kirkpatrick et al. (1993a) and Bessell, a poorer match for those by Chapter 2 and in disagreement with those of Tinney et al.

The comparisons in Fig. 4.7 indicate that the molecular opacity in the observed spectral region is reasonably well modelled. However the models used for these comparisons

do not have a complete inclusion of water opacity shortward of 2 μm (Allard et al. 1994) and so it seems unlikely that the model structure can be correct. Therefore we are not able to set a definitive effective temperature scale for M dwarfs. This must wait for the completion of the full water vapour calculation and a better understanding of molecular line broadening.

The observational spectra presented here show good agreement with the models both in terms of predicted line strengths and line positions. From these comparisons and recent improvements in the computation, we are confident that a complete *ab initio* calculation can produce an accurate description for the transitions of hot water vapour. A new calculation of the water line list is underway with completion expected by early 1996. This list will include all energies levels up to 30 000 cm^{-1} with the aim that it will give an accurate representation of hot water vapour for transitions longward of $\sim$0.2 μm with convergence to better than 0.1 cm^{-1}. We look forward to testing the match of this calculation included in PHOENIX to the spectra presented here and ISO measurements of the sample from 2.49 to 2.85 μm.

Chapter 5

A new brown dwarf candidate from a large area infrared survey

The discovery at infrared wavelengths of a very cool field brown dwarf candidate is reported. It has infrared colours $J - H = 0.90 \pm 0.19$, $H - K = 0.83 \pm 0.18$, compared with the previously-known coolest dwarf GD165B which has $J - H = 1.01 \pm 0.05$, $H - K = 0.64 \pm 0.05$.

• Its discovery within an infrared field survey places the first lower limit on the space density for objects fainter than $M_{\rm bol} = 14$ and suggests that the luminosity function does not fall dramatically into the brown dwarf regime.

• The new brown dwarf candidate is of intermediate age with a mass of 0.071–0.079 $M_{\odot}$, a temperature of 1825 ± 300 K and a bolometric magnitude of 14.56 ± 0.35. Comparisons with evolutionary models indicate that if it is younger than 1.5 Gyr it is a brown dwarf.

• Its colours are much redder than the expected colours $J - H = 0.70$, $H - K = 0.27$ for stars of intermediate age with masses of 0.08 $M_{\odot}$.

5.1 Introduction

Brown dwarfs are objects hypothesized to occupy the mass range between the lightest stars (~0.08 solar masses, $M_\odot$) and the heaviest planets (~0.001 $M_\odot$). They never become hot enough to sustain nuclear fusion and after their initial formation and heating by gravitational collapse, they develop a degenerate core and thereafter cool to low temperatures. Brown dwarfs might make a significant contribution to the dark matter in the Galactic disc, galactic haloes or even a background critical density (e.g. Kerins & Carr 1994). Large-area surveys have not identified any clear examples, and find the space density of stars has a maximum at a bolometric absolute magnitude $M_{\rm bol}$ ~10, corresponding to hydrogen-burning stars of about 0.2 $M_\odot$, and decreases to fainter luminosities (Tinney 1993). Searches in young clusters, where they are expected to be hotter and brighter, have discovered a number of candidates (Steele, Jameson & Hambly 1993 and Comeron et al. 1993) but their classification relies on the discrimination of cluster members from field objects and on reliable modelling of their rapid early cooling.

5.2 Observations

The new candidate brown dwarf was discovered during an infrared survey for faint red galaxies (Glazebrook et al. 1993). An area of 552 arcmin^2 was searched to a 5σ limit of $K \simeq 17.3$ and $R \simeq 23.8$ with incomplete coverage to $B \simeq 23.9$, $V \simeq 24.1$ and $I \simeq 23.6$. J- and H-band infrared photometry and optical spectra have been obtained for all objects redder than $R - K = 5$. The infrared data were taken using the IRCAM instrument with the UKIRT at the Mauna Kea Observatory on Hawaii. Optical imaging data were obtained at the Isaac Newton Telescope; optical spectroscopic data were obtained with the Low Dispersion Survey and Faint Object Spectrographs (FOS) at the William Herschel Telescope (WHT); both telescopes are at the Roque de los Muchachos Observatory on La Palma.

Follow-up imaging and spectroscopy revealed the object, JMG 0918–0023, to be an M5.5 dwarf (object A) separated from a fainter, extremely red, companion (object B) by 3″. Object B is below the survey limit and was only discovered during the follow-up

Table 5.1: UKIRT and INT photometry of the JMG 0918–0023 AB system. Based on the colours of GD165B and other extreme red dwarfs, B has $R-K>7$ and so R(B) > 25. This means that R(B) makes a negligible contribution to the R survey magnitude which is assumed to be R(A).

Object	R.A.	Decl. (1950)	Date	B	$R_{\rm CCD}$	$J_{\rm UKIRT}$	$H_{\rm UKIRT}$	$K_{\rm UKIRT}$
JMG 0918–0023 AB	09 18 25.37	–00 23 01.65	Oct 87 – Apr 89	>24.2	21.12±0.08			16.28±0.15
JMG 0918–0023 A			16-17 Oct 90			16.86±0.03	16.36±0.05	16.13±0.05
			2 May 93			16.97±0.04	16.31±0.06	16.01±0.07
JMG 0918–0023 B	offset 2.82″N	0.88″E	16-17 Oct 90			20.00±0.22	19.01±0.20	18.12±0.17
			2 May 93			19.96±0.17	19.00±0.16	18.16±0.20

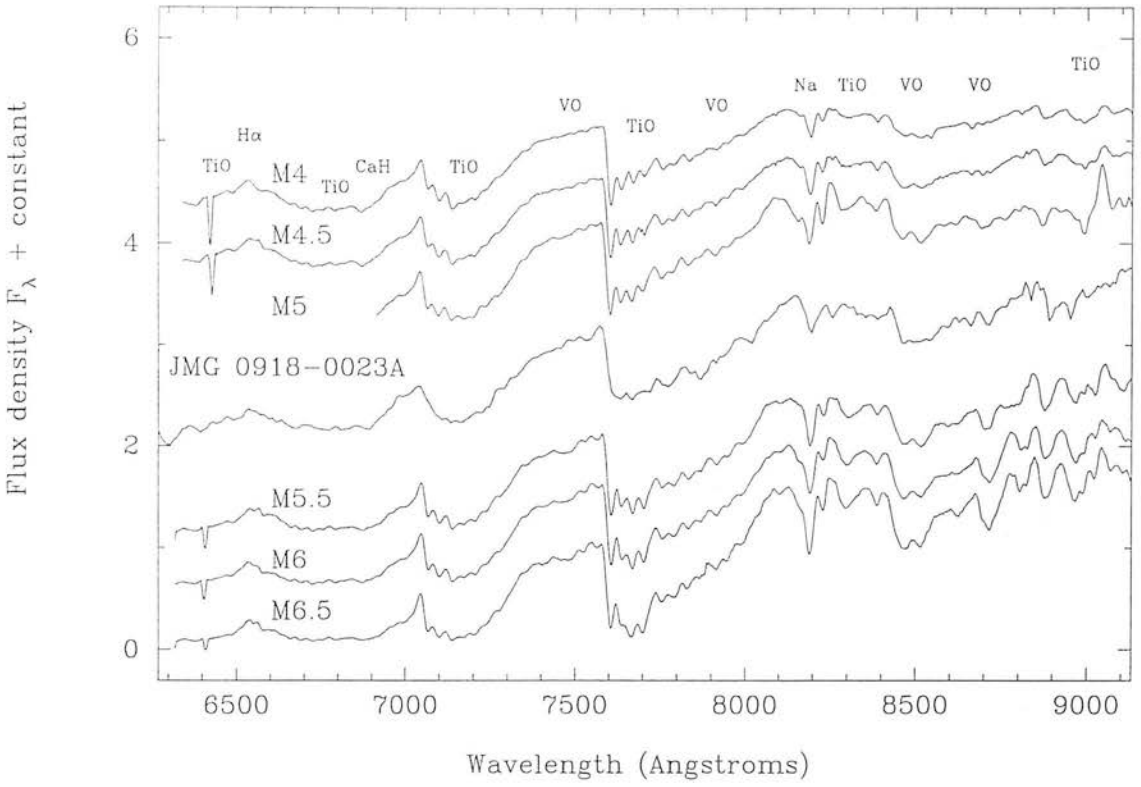

Figure 5.1: Spectrum for A corrected for telluric absorption compared to M5–M7 dwarfs from Kirkpatrick et al. (1991) which have not been corrected for telluric absorption. In spectral regions where there are telluric absorption bands this correction has the effect of increasing the flux. At the resolution and signal-to-noise presented here this correction is significant around 6900 and 7600 Å. The feature at 6415 Å is an artefact. The scale of flux density is arbitrary, and an offset has been added to separate the spectra.

observations. Table 5.1 lists the photometry of A and B. Each is discussed in turn.

5.3 Discussion

Fig. 5.1 shows a spectrum of A taken with the FOS on the WHT together with spectra of mid-type M dwarfs taken with the Multiple Mirror Telescope (MMT) on Kitt Peak in Arizona (Kirkpatrick, Henry & McCarthy 1991). Object B was too faint to be detected in the optical, as expected from its infrared colours. From its colours alone A could be classified as an M dwarf, a red galaxy or, implausibly, a giant star well beyond the galaxy. The presence of the strong sodium line at 8180 Å identifies A's spectrum as that of a dwarf rather than a giant (Kirkpatrick et al. 1991, Bessell 1991). It is unlikely to be young as it lacks the prominent Hα emission seen in young M-dwarf stars (Giampapa &

Liebert 1986), neither is it very old as it lacks the strong CaH absorption from 6750 to 7050 Å which is used to classify subdwarfs ([Z/H]$\leq$–1, Kirkpatrick et al. 1991). Based on Fig. 5.1, A resembles an M5.5±0.5 dwarf of intermediate metallicity and age.

The spectral type and colours of A indicate an absolute magnitude which can be used to obtain its distance. A strong constraint on its absolute magnitude comes from the longest-baseline colour. Interpolation of $R - K = 5.07 \pm 0.09$ within table 6 of Leggett (1992) gives a distance modulus of 7.09±0.23 if it is an M5.5V star from the old disk population (1.5–6 Gyr, Eggen 1989), or 7.30±0.27 if it is an M6V star from the young disk population (0.3–1.5 Gyr, Eggen & Iben 1988). The young disk has a scale height of ~100 pc whereas the old disk has a scale height of ~300 pc (Gilmore & Reid 1983). At a galactic latitude of +33° A is ~150 pc above the galactic plane, and can be classified A as a M5.5–6V star from the interface of the young and old disk populations.

If A and B are physically associated, then their angular separation of 2.96±0.15″ corresponds to a projected separation of 770±100 AU. Based on a visually selected sample (Gliese & Jahreiss 1979), of stars in M-dwarf multiple systems, Fischer & Marcy (1992) find that 3 out of 58 systems are binaries with separations between 770 and 10000 AU and note that the sample is incomplete in this range. The late-type M dwarf VB8 is one of these with a separation of 1730 AU. The colours and luminosity of B are as expected for a faint dwarf companion to an M5.5-6V star but it is much too faint to be a distant giant star. B is unlikely to be a background galaxy or an unrelated star as the density of galaxies and stars with $K < 18.3$ and $I - K > 3$ ($I - K > 3$ conservatively corresponds to $R - K > 5.5$) is 2.4×10^{-3} per 30 arcsec^2 (Hu et al. 1994). Its star-like profile and extreme infrared colours also make this hypothesis unlikely.

If B is physically associated with A, B's temperature and luminosity can be compared with those expected from evolutionary models to determine its mass. The determination of temperatures for late-type M dwarfs is problematic as their spectra are dominated by deep bands of water vapour absorption (Chapter 2), so that colours are not such reliable indicators of temperature as they are for hotter stars. A number of different approaches are possible (Kirkpatrick et al. 1993a; Tinney, Mould & Reid 1993; Chapter 2). Extrapolation of a 2nd order polynomial fit to the relation between $J - K$ colour and

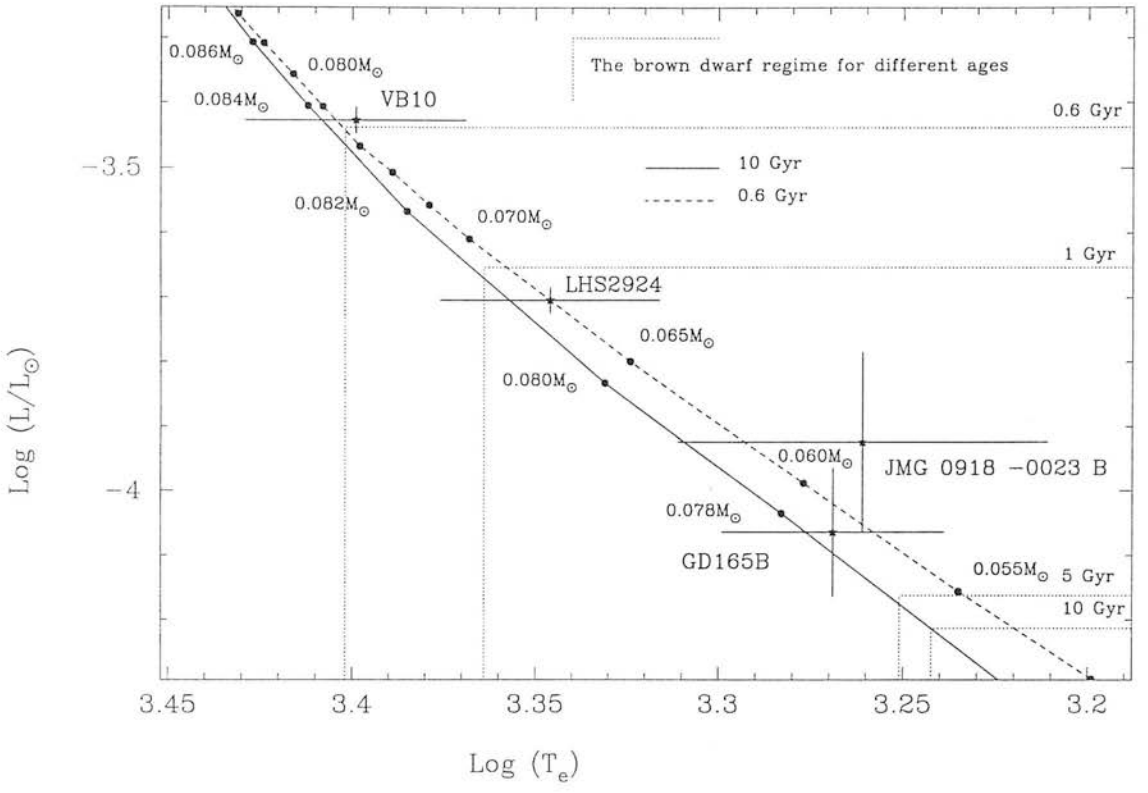

Figure 5.2: HR diagram for low-mass stars and brown dwarf candidates assuming $M_{\mathrm{bol}\odot} = 4.75$.

temperature gives 1855±300 K by Chapter 2, 1613±300 K by Tinney, Mould & Reid (1993) or 2262±300 K by Kirkpatrick et al. (1993b).

Model and observed bolometric magnitudes can be compared more directly than temperatures, radii or masses (except for short-period binaries). Although B has only be measured in the J, H and K passbands, the similar colours of GD165B, for which there is a wider range of photometry and spectroscopy (Chapter 2), enables a reasonable estimate for B's bolometric magnitude. We use bolometric corrections for GD165B at J, H and K to determine a bolometric magnitude in each passband and then took the average of them. Using this bolometric magnitude and the distance derived for A, B has $M_{\mathrm{bol}} = 14.56 \pm 0.35$. This compares with 14.91±0.26 for GD165B. Solar metallicity evolutionary models give 13.3, 13.9, 15.2 and 15.3 (Burrows et al. 1993) or 13.1, 13.5, 14.7 and 15.0 (Nelson, Rappaport & Joss 1993) for the end of the main sequence at ages

of 0.6, 1, 5 and 10 Gyr respectively.

Fig. 5.2 shows a HR diagram for late-type M dwarfs and brown dwarf candidates adopting the temperature scale from Chapter 2 and the standard solar metallicity model X from Burrows et al. (1993). The relation for an age of 10 Gyr is a solid line, for 0.6 Gyr a dashed line. Dotted lines are plotted for object ages of 0.6, 1, 5 and 10 Gyr to show the border between objects which burn hydrogen and those which do not (0.0767 $M_{\odot}$). Models from Nelson et al. (1993) produce a plot with masses increased by 0.0075 $M_{\odot}$ and luminosities increased by around 40 per cent at intermediate ages. Interpolating the temperature and bolometric luminosity for the young–old disc age range (1–3 Gyr, Eggen & Iben 1988; Eggen 1989) within model X, JMG 0918–0023 B has a mass of 0.071–0.079 $M_{\odot}$ and GD165B, which is older than 0.5 Gyr based on the cooling age for its white dwarf companion (Becklin & Zuckerman 1988), has a mass of 0.058–0.078 $M_{\odot}$. Whether they are brown dwarfs or very low-mass stars depends on the adopted evolutionary model and the age of the system. If they are younger than 1.5 Gyr they are brown dwarfs by either model; if they are 3–5 Gyr old they are (Nelson et al. 1993) or are not (Burrows et al. 1993) brown dwarfs; if they are older than 5 Gyr they are not brown dwarfs by either model. These conclusions are for solar metallicity models, however, if the objects are metal poor, the models predict higher temperatures, luminosities and masses for the star/brown dwarf interface, making the interpretation of these objects as brown dwarfs more probable.

The brown dwarf regime can also be shown by direct observational results. In Fig. 5.3 mass versus $J - K$ is plotted for a sample of M-dwarfs binaries, measured using the infrared speckle technique, with well determined orbits and intermediate ages (old and young disc). We also plot dotted lines to indicate the different hydrogen-burning limits derived by theoretical solar metallicity models (Burrows et al. 1993; Nelson et al. 1993). A weighted linear fit to the objects in Fig. 5.3 below 0.2 $M_{\odot}$ gives $J - K = 1.02 \pm 0.28$ for a mass of 0.0767 $M_{\odot}$. Although mass versus $J - K$ is not expected to be a linear relationship and although the ages and metallicities of these stars may differ from the candidates, the large difference > 0.6 between this $J - K$ value and those observed for JMG 0918–0023 B and GD165B is further evidence that they are brown dwarfs.

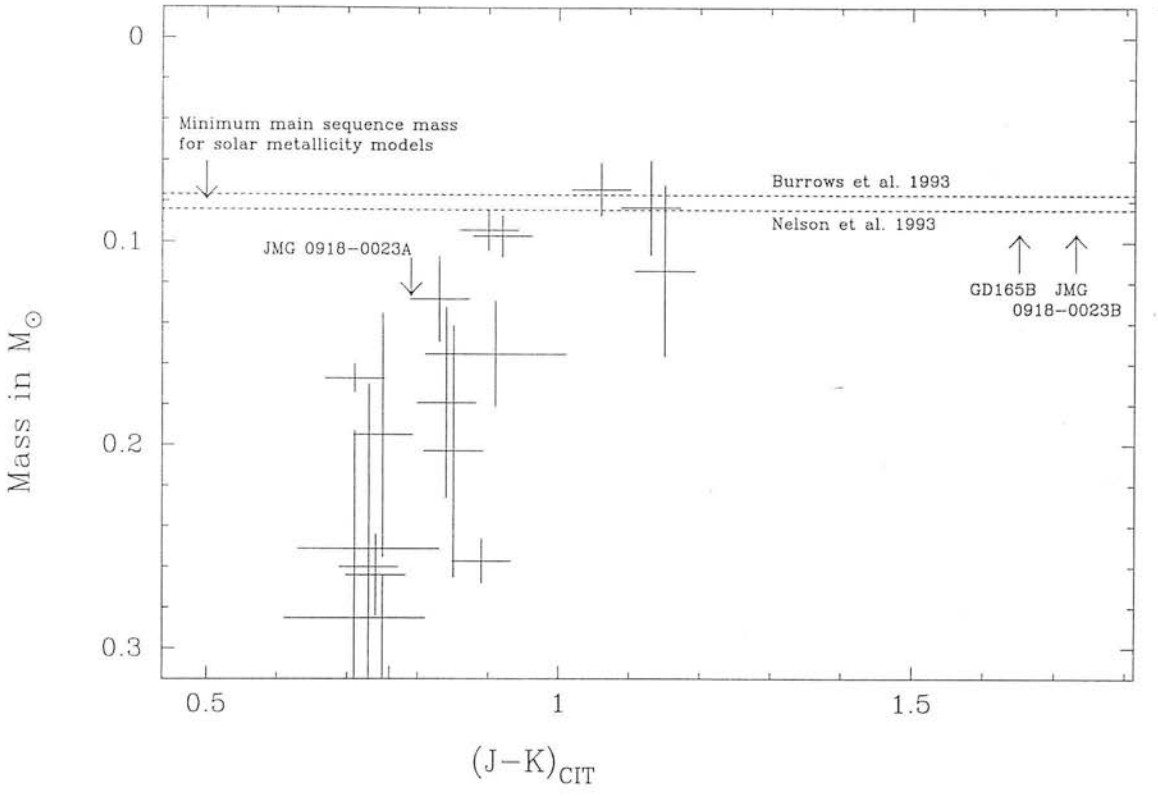

Figure 5.3: $J - K$ versus mass for the sample from Henry & McCarthy (1993), showing also the colours of JMG 0918–0023 B and GD165B. The photometric colours are on the CIT photometric system. The photometric conversion for B from the UKIRT to CIT system uses Casali & Hawarden (1992) although it is expected to be unreliable as the relations are only established for $J - K < 1$.

The previous faintest constraint on the luminosity function was based on an optical survey (Tinney 1993) with infrared follow-up which indicated a falling function towards the brown dwarf regime and measured the stellar density at its faintest limit, $M_{\rm bol}$ = 13.75, to be $3.6\pm^{5.6}_{2.2}\times10^{-3}$ pc^{-3}mag^{-1}. Although JMG 0918–0023 B is fainter than the limit of the survey, its discovery can be used to put a lower limit of $3.1\pm^{7.1}_{2.6}\times10^{-3}$ pc^{-3}mag^{-1} (68 percent confidence) on the luminosity function for low-mass objects at $M_{\rm bol}$ ~14.5. As the survey is incomplete for stars this faint, the true space density must be significantly greater which suggests that these objects are not as rare as would be expected from the extrapolation of previous work.

5.4 Latest Result

Becklin, Macintosh & Zuckerman of UCLA plan to submit a letter to the Astrophysical Journal discussing JMG 0918-0023B. They have resolved JMG 913-0023B into two components which they label 0918-0023B and 0918-0023C. They find that their images of 0918-0023B and 0918-0023C are extended and thus interpret them as interacting nuclear starburst galaxies at $z \sim 0.7$.

Whether they are actually galaxies or two very low-mass objects in our Galaxy (in addition to the A component), their infrared colours are redder than those of any published galaxy or brown dwarf candidate. Further observations discussed in Section 6.1.2 are imperative.

Chapter 6

Finale

6.1 Future Work

In this thesis I have presented four of my research projects. In addition to these I have been working with collaborators on a number of others. I divide these into three sections: projects for which data has been partially analysed, projects for which telescope time has been awarded and possible exciting new projects.

6.1.1 Data partially analysed

Is PC0025-0447 a 0.02 $M_{\odot}$, 10^8 yr old brown dwarf?

PC0025-0047 has Hα emission, a well known indicator of youth, a factor of 10 stronger than any known M dwarf (Schneider et al. 1991). One interpretation is that it is a 0.02 $M_{\odot}$, 10^8 yr old brown dwarf, however until its distance is known such a conclusion is very uncertain.

Distances for nearby stars are normally measured by the method of trigonometric parallaxes but PC0025-0447 ($V = 23$) is too faint for inclusion on existing parallax programs which are based on observations at optical wavelengths. We have used this as an opportunity to try parallax measurement in the infrared. In principle observing in

the infrared overcomes a major source of error in parallax measurements which is the differential refraction of reference objects. The third epoch of parallax measurements for PC0025-0047 and the second epoch for two M dwarfs of known parallax will soon be made.

50 brown dwarf candidates from digitally stacked Schmidt plates

A deep survey by Hawkins (1995) based on digitally stacking Schmidt photographic plates in the R and I bands from ESO/PPARC field 287 has produced 40 objects in an area of 25 deg^2 with R–$I > 3.0$ which is redder than any of the previous low-mass stars discovered from photographic plates. We have taken spectra from 0.6–0.95 μm of 25 of these which indicate that around 10 of them are redder than spectral type M9 (Jones & Hawkins 1995a). We are comparing these observed spectra with synthetic spectra from Allard & Hauschildt (1995, in preparation) to discern their temperatures and metallicities and to place these exciting new objects on a Hertzsprung-Russell diagram.

Possible identification of very young brown dwarf

Based on its infrared colours BRI2339-0014 has been classified as a probable giant (Tinney & Irwin, 1994, private communications) based on optical spectra and its infrared colours. Spectra obtained using CGS4 on UKIRT indicate that it has strong water vapour absorption. The strength of water vapour absorption in cool stars is a basic classifier to distinguish M giants from dwarfs. One plausible interpretation of the observations is that BRI2339-0014 is a very young cooling brown dwarf. This allows it to have a lower gravity and thus a spectral energy distribution different from that expected for older low-mass stars.

Brown dwarf candidate GD165B

GD165B is the best brown dwarf candidate which can be observed at a reasonable signal-to-noise ratio without a large investment of telescope time. We have recently obtained

0.6–0.95 μm spectroscopy and L' photometry of GD165B. Combining this with the 1–2.5 μm spectra presented in Chapter 2 and a recently improved parallax (Dahn 1995, private communication) it will be possible to derive a much more accurate bolometric luminosity. This together with inferences based on spectral analyses of its peculiar 0.6–0.95 μm spectrum (confirming the work of Kirkpatrick et al. 1993b) will enable a much improved mass estimate to be made allowing an improved determination of its status as a brown dwarf candidate.

LHS1070 + two low mass companions

LHS1070 was recently discovered to have two low mass companions (Leinert et al. 1994). A collaboration with a group based at Imperial College London who have expertise in infrared speckle observations should enable the masses of LHS1070 and its companions to be determined within the next four years. Based on the well determined parallax for the system the infrared absolute magnitudes indicate that the new objects are likely to have a mass substantially lower than any other brown dwarf candidate for which a direct mass determination has been made.

Synthetic line profiles for M dwarfs

Spectra at a resolution of 20 000 of the Na I features at 2.2062 and 2.2090 μm have been taken for a number of the objects presented in Chapter 2. This high resolution data will provide an important template to test the ability of synthetic line profiles to determine NLTE effects and rotational velocities for low-mass stars.

6.1.2 Telescope time has been awarded for the following projects

Brown dwarf candidates from digitally stacked Schmidt plates

In order to calculate reliable bolometric luminosities and effective temperatures for the new brown dwarf candidates, infrared photometry, I-band parallax measurements and infrared spectroscopy are scheduled.

Subdwarfs

There are a number of M dwarfs which from optical spectra and colours appear to have [Z/H] $\sim$ –2. Following Chapters 2 and 3 spectra of a sample of these will be taken from 1–2.5 μm to derive bolometric luminosities, effective temperatures, surface gravities and metallicities. The synthetic spectra predict that "metallic hydrogen" (Burrows & Liebert 1993) will be observed for the first time.

Brown dwarf candidate?

During a program of infrared imaging of a number of globular clusters, DRVB-M01, a star-like object with K'–K = 0.30±0.12 and V–K > 4 was discovered (Buckley 1993). Follow up J-, H- and K- band photometry is scheduled to check whether this could be a serendipitous foreground brown dwarf candidate.

Mass function of M4

Deep J, K imaging of M4 allows the chance to determine the luminosity function down to the hydrogen burning limit in one of the closest globular clusters.

JMG0918-0023B

The discovery of the reddest known brown dwarf candidate JMG0918-0023B is presented in Chapter 5. A number of follow-up observations in service-mode are scheduled to understand better this fascinating object.

(i) K-band spectra to check the possibility that it is a distant M giant and to enable its temperature to be derived from the strength of its CO (2.29 μm) and Na I (2.21 μm) absorption features.

(ii) Due it is faintness its infrared colours are not well determined (± 0.2), however, the advent of the IRCAM3 shift-and-add facility on the UKIRT and the proximity (30

arcsec) of a suitable nearby bright star mean that accurate infrared colours ($\pm$ 0.05) may now be easily determined.

(iii) WHT photometry in the R- and I-bands will give a longer wavelength baseline allowing improved estimates of its effective temperature and bolometric luminosity.

ISO Observations – Priority 1

(i) One of the major ISO open-time proposals is a survey of 25 deg^2 of sky at 6.7, 15 and 90 μm to much fainter magnitudes than the IRAS survey. This survey has 8 per cent of the available priority 1 time and encompasses many of the principal aims of the mission. One of the numerous scientific goals of the survey is to test whether the dark halo of our Galaxy is in the form of brown dwarfs.

(ii) High resolution spectra of the objects observed in Chapter 4 from 2.5—2.85 μm of the strongest water absorption band in late-type M dwarfs. These spectra, unobtainable using ground-based telescopes, will be compared to the latest generation of *ab initio* water vapour calculations (Viti, Tennyson & Miller 1995, in preparation) incorporated into PHOENIX (Allard & Hauschildt 1995).

(iii) Spectra of a sample of brown dwarf candidates from 2.5 to 45 μm (unobtainable with ground-based telescopes) to investigate methane and water absorption bands and other suspected molecular absorption bands. The strength (or absence) of such features will be a strong test of the model atmosphere calculations and the prevalence of dust formation in low-mass stars.

DENIS survey

A European consortium has the use of a 1-m ESO telescope to survey the Southern Sky. The result will be the first deep large-area near-infrared survey with a high probability of finding brown dwarfs and more generally deriving a high quality stellar mass function. DENIS will provide coverage simultaneously in two near-infrared bands to a sensitivity limit of $J = 16.0$ (3σ) and $K = 14.5$ (3σ) with a spatial resolution of 3 arcsec, and

one red band to a sensitivity limit of $I = 18.0$ (3σ) with a spatial resolution of 0.75 arcsec (Epchtein 1993). The infrared detectors are fully commissioned; the I-band CCD is currently being commissioned. The survey is expected to start in 1995 May and take five years to complete. A French team at Observatoire de Paris is responsible for the instrumentation and observing. Teams at Leiden and Institut d'Astrophysique de Paris are responsible for data processing. The Royal Observatories Wide Field Astronomy Unit are providing the British effort to measure U, B and R magnitudes for the objects using COSMOS scans of UK Schmidt plates.

6.1.3 Possible new projects

A globular cluster luminosity function beyond the main sequence

Deep K-band imaging of NGC 6397 (in conjunction with I-band Hubble Space Telescope data from Paresce, Marchi & Romaniello 1995) should enable the determination of the luminosity function to below the hydrogen burning limit in the closest globular cluster.

Fundamental parameters for cataclysmic variables

Measurement of the water band head at 1.35 μm in M dwarfs with cataclysmic variables companions. This will give a sensitive spectral classification leading to a mass estimate for the M dwarf and an improved determination of the system properties.

Are the faintest stars young brown dwarfs?

The deep wide area survey from the stacked Schmidt plates provides large numbers of very low-mass stars in a relatively small area. Radial velocities are only known for a few low-mass stars. The development of spectrographs allowing high resolution spectra to be taken of large numbers of nearby objects in the same field gives the opportunity to determine a large number of radial velocities and properly test the possibility (mentioned in Chapter 3.5.2) that the latest M dwarfs have a low scale-height of $\sim$ 100 pc, more characteristic of a 10^8 yr old population (B-type stars) than earlier type M dwarfs which

have a scale height of ~350 pc. If these radial velocity measurements are made from 0.65–0.70 μm it should also be possible to derive independent indicators of age for each star from (a) the equivalent width of Hα emission (e.g. Stauffer & Hartmann 1986), (b) the lithium abundance (e.g. Rebolo & Martin 1992) and (c) the CaH abundance (Kirkpatrick 1995).

Chemical evolution of the Galaxy and M dwarf ages

Using high resolution observations of the strength of the CO bands in M subdwarfs the isotopic ratios of C^{12}/C^{13} and $O^{16}/O^{17}/O^{18}$ can be determined. The ratios are a sensitive probe of the composition of the material from which the star was formed. Since M dwarfs are not expected to have evolved in chemical composition their isotopic ratios offer a sensitive probe of their age and an excellent record of the chemical evolution of the Galaxy.

Age of the Galaxy?

It has been realised for many years (e.g. Schwarzschild 1957) that for a given mass, the temperature and luminosity of a white dwarf can be used to derive its cooling time. This means that the coolest white dwarfs can be used to yield a minimum age for the Galaxy. The Schmidt plate stack (Section 6.1.1) has turned up a number of very cool white dwarfs. Follow-up observations are planned to determine their distances and temperatures and thus place a lower limit to the age of the Galaxy.

6.2 An Overview

The primary goal of this thesis is to examine the properties of M dwarfs and brown dwarfs candidates. This is essential to understand the bottom of main sequence and the brown dwarf regime. In the most basic way this is achieved by high quality observations of low-mass star energy distributions in the infrared where they emit the bulk of their flux. These observations enable accurate bolometric magnitudes to be derived and demonstrate large spectral differences between low-mass stars. The spectral identification of the variety of molecular and atomic features indicate the important sources of opacity for M dwarfs and have been an important feedback for model atmosphere calculations which have improved dramatically over the last three years.

The accurate spectral energy distributions determined for M dwarfs allow more reliable effective temperatures to be derived. Their hump-shaped energy distribution has in the past been a hindrance to the determination of M dwarf temperatures and led to large discrepancies between the temperatures derived by different investigators. A new method is presented which uses the shape of the humps to determine reliable temperatures. The method produces an observational HR diagram which compares well with the theoretical one. This gives confidence to state that objects with temperatures and luminosities similar to VB10 and LHS2924 are not brown dwarfs unless they are very young. Only objects with properties akin to JMG0918-0023B and GD165B are good candidates for field brown dwarfs. Further spectroscopic and photometric measurements will serve to improve the observational error bars on the HR diagram. However, in its conventional form the HR diagram becomes increasingly less useful for later type M dwarfs because objects with masses less than around 0.09 $M_{\odot}$ take many Gyr to reach the main sequence. This means that age becomes the vital third parameter for the interpretation of late-type M dwarfs and brown dwarf candidates.

Model calculations for synthetic spectra do not directly include age as a free parameter. It must be inferred from the metallicity and gravity appropriate to the spectrum under analysis. Although temperature is easily the most important parameter in determining the strengths of spectral features in M dwarfs there is nonetheless significant sensitivity to gravity and metallicity. This is investigated using the vast improvements in the sensitivity of infrared spectrometers and the atmospheric modelling of low-mass

stars. Although the complex behaviour of spectral features means that it has not been possible to disentangle absolute metallicities and gravities their effects on the observed spectra can be seen. From the sample investigated it is evident that an object's position on a Hertzsprung-Russell diagram is as useful an indicator of metallicity as its kinematic population type. To realise the potential of using metallicities and gravities to determine ages it will be necessary to calibrate the most sensitive spectral features for objects of known age. Such comparisons test the physical modelling of low-mass stars in a way not afforded by photometric measurements and lead to a critical examination of model assumptions.

The escape of flux from M dwarfs was generally expected to be modulated by low excitation energy atomic transitions, broadband continuum opacities and molecular transitions broadened by the high pressures prevalent in low-mass star atmospheres such that they could be treated at low resolution in a similar fashion to continuum opacity. However treatment of the dominant opacity, water vapour, as a line list indicates that this is not appropriate. It appears that water vapour lines are formed at pressures around an order of magnitude higher than atomic lines. This indicates they are subject to much lower pressure broadening and suggests that water vapour transitions cannot be treated as effectively smeared together in low-mass stars. Smaller line broadening allows more flux to escape decreasing water band strengths. This result is likely to explain why synthetic spectra of M dwarfs overpredict molecular band strengths in low-mass objects.

Although many new ideas have emerged for the nature of the dark matter (e.g. Carr 1994) the simple solution remains – much of the dark matter is made from very faint objects formed in the same manner as stars – brown dwarfs. This has led to more than 50 papers being published in the last ten years all with the overt aim of discovering brown dwarfs to derive the mass-luminosity function below the hydrogen burning limit and ascertain their contribution to the "dark matter". These searches have produced a plethora of new objects of which many have been claimed as brown dwarfs – the candidate presented in Chapter 5 being arguably the best of these. This was discovered during a survey using a 58x62 array while many large telescope facilities are now investing in 1024x1024 arrays. Infrared surveys have recently gained widespread credibility whereby large sums of European and American money is being invested in (i) 25 deg^2 ISO, (ii)

half-sky DENIS and (iii) all-sky 2MASS. One of the major scientific aims for these surveys is to find brown dwarfs of which they expect to find many at a variety of masses and ages. The large areas covered by these surveys are very promising for finding bright nearby brown dwarfs. Though in the shorter term the latest generation of infrared arrays promises the discovery of fainter candidates within several hundreds of parsecs.

Although my initial interest in this field was spurred by the quest for the solution to the dark matter question, my attitude has evolved. The understanding of the properties of these objects can be expected to have important consequences in a number of areas of astrophysics. For example, they may reveal the chemical evolution of the Galaxy – to these ends an extensions of the work presented in Chapter 3 are planned (Sections 6.1.2 and 6.1.3). To understand the brown dwarf regime requires proper accounting for molecules and dust, both in their formation rates in different conditions and their contribution to opacities. The widespread interest in the brown dwarf regime is bringing large scale effort to bear on these problems, e.g. the water vapour calculations made for Chapter 4. The accurate modelling of low-mass dwarfs can be expected to lead to the derivation of a reliable low-mass disk mass function and high quality molecular opacities. Both of these are likely to be essential inputs for a theory of star formation.

Like the several other people who have written PhD's concerned with low-mass stars I am disappointed that I am not able to report the discovery of a standout brown dwarf. Though I believe we now understand low-mass dwarfs a little better and now have more idea of the likely spectral characteristics of a brown dwarf. In 1994 August I attended a workshop entitled "The Bottom of the Main Sequence and Beyond". Many of the speakers expressed pessimism because the searches conducted so far have not discovered any standout brown dwarfs. I disagree with this point of view. None of the objects discovered prior to 1985 would be in most current top twenties of "Best Brown Dwarf Candidates". The new large telescopes together with larger and more sensitive infrared detectors lead me to believe it will soon be possible to identify and to determine the mass, composition and age for individual brown dwarfs. Much fundamental science should ensue, as their impact on cosmology, star formation, galactic structure, the interstellar medium and molecular physics is felt. Astronomers may then be able to tackle the age-old challenge of extra-solar planets and the search for extraterrestrial intelligence.

References

Alcock C. et al., 1993, Nature, 365, 621

Alexander D.R., Ferguson J.W., 1994, ApJ, 437, 879

Allard F.A., 1990, PhD thesis, University of Heidelberg

Allard F., Hauschildt P., 1995, ApJ, in press

Allard F., Hauschildt P., Miller S., Tennyson J., 1994, ApJL, 426, L39

Allen C.W., 1973, Astrophysical quantities, Athlone Press, London

Arnaud K.A., Gilmore G., Collier-Cameron A., 1989, MNRAS, 237,495

Aubourg E. et al., 1993, Nature, 365, 623

Baldwin J. R., Frogel J. A., Persson S. E., 1973, ApJ, 184, 427

Becklin E.E., Zuckerman B., 1988, Nature, 336, 656

Berriman G.B., Reid I.N., 1987, MNRAS, 227, 315

Berriman G.B., Reid I.N., Leggett S.K., 1992, ApJ, 392, L31

Bessell M. S., 1991, AJ., 101, 662

Bessell M. S., Stringfellow G.S., 1993, ARAA, 31, 433

Blackwell D.E., Smith G., Lynas-Gray A.E., 1995, A & A, in press

Boss A.P., 1986, ApJS, 62, 519

Boss A.P., 1989, PASP, 101, 767

Brett J., 1995, A & A, 295, 736

Buckley D.R.V., 1993, PhD thesis, University of Edinburgh

Burch D.E., Gryvnak D.A., 1966, Absorption by H_2O between 5045–14485 cm^{-1}, Aeronutronic Report No. U-3704, Contract No. 3560(00)

Burrows A., Liebert J., 1993, Rev. Mod. Phys., 65, 301

Burrows A., Hubbard W.B., Lunine J.I., 1989, ApJ, 345, 939

Burrows A., Hubbard W. B., Lunine J.I., 1994, ASP conf. ser., 64, 528

Burrows A., Hubbard W.B., Saumon D., Lunine J.I., 1993, ApJ, 406, 158

Carlsson M., Rutten R.J., Bruls J.H.M.J., Shchuckina N.G., 1995, A&A, 288, 860

Carr B., 1994, ARAA, 32, 531

Carter S., Handy N. C., 1987, J. Chem. Phys., 87, 4294

Casali M.M., Hawarden T.G., 1992, JCMT-UKIRT Newsletter, 4, 33

Chandrasekhar S., 1938, Stellar Evolution, University of Chicago Press

Chauville J., Querci F., Connes J., Connes P., 1970, A&AS, 2, 181

Clayton D.D., 1968, Principles of Stellar Evolution and Nucleosynthesis, McGraw-Hill

Comeron F., Rieke G. H., Burrows A., Rieke M.J., 1993, ApJ, 416, 185

Crawford D.L., Craine E.R., 1994, Instrumentation in Astronomy VIII, SPIE, 2198

Currie M.J., 1992, Starlink User Note 95.8, Rutherford Appleton Laboratory

D'Antona F., 1987, ApJ, 320, 653

D'Antona F., Mazzitelli I., 1985, ApJ, 296, 502

D'Antona F., Mazzitelli I., 1994, ApJS, 90, 467

Davidge T.J., Boeshaar P.C., 1991, AJ, 102, 267

Davidge T.J., Boeshaar P.C., 1993, ApJ, 403, L47

Eddington A.S., 1926, The Internal Constitution of Stars, Cambridge University Press

Eggen O.J., 1989, AJ, 100, 1159

Eggen O.J., Iben I. Jr., 1988, AJ, 96, 635

Elias J., Frogel J.A., Matthews K., Neugebauer G., 1982, AJ, 87, 1029

Epchtein N. 1993, DENIS Blue Book, http://www.strw.leidenuniv.nl/denis/Bluebook

Fabian A.C., 1994, ARAA

Fernley J.A., Miller S., Tennyson J., 1991, J. Mol. Spectrosc., 150, 597

Fischer D.A., Marcy G.W., 1992, ApJ, 396, 178

Fleming T.A., Giampapa M.S., Schmitt J.H.M.M., Bookbinder J.A., 1993, ApJ, 410, 387

Forrest W.J., Skrutskie M.F., Shure, M., 1988, ApJ, 330, L119

Fowler A., 1904, Proc. R. Soc., 73, 219

Giampapa M.S., Liebert J., 1986, ApJ, 305, 784

Gilmore G., Reid I.N., 1983, MNRAS, 202, 1025

Gilmore G., Wyse R.F.G., Kuijken K., 1989, ARAA, 27, 555

Glazebrook K., Peacock J.A., Collins C., Miller L., 1993, MNRAS, 266, 65

Gliese W., Jahreiss H., 1979, A&AS, 38, 423

Gliese W., Jahreiss H., 1991, Preliminary Version of the Third Catalogue of Nearby Stars, Astronisches Rechen-Institut Heidelberg, Germany

Goldstein R., 1964, JQSRT, 4, 343

Graham J.R., Matthews K., Greenstein J.L., Neugebauer G., Tinney C.G., Persson S. E., 1992, AJ, 104, 2016

Gray D.F., 1992, The observation and analysis of stellar photospheres, Cambridge University Press, Cambridge

Greenstein J.L., Neugebauer G., Becklin E.E., 1970, ApJ, 161, 519

Grevesse N., Sauval A.J., 1994, IAU Coll. No. 146, p.196, ed. Jorgensen U.G., Thejl P., Springer-Verlag, Berlin

Hall D., 1980, Atlas of infrared spectra of the solar photosphere and sunspot umbrae, Kitt Peak National Observatory

Hauschildt P.H., 1991, PhD thesis, University of Heidelberg

Hauschildt P.H., Starrfield S., Shore S. N., Allard F., Baron E.: 1995, ApJ, in press

Hauschildt P.H., Starrfield S., Shore S.N. Gonzales-Riestra R., Sonneborn G., Allard F., 1994, AJ, 108, 1008

Hawkins M.R.S. 1988, MNRAS, 234, 533

Hawkins M.R.S., 1993, Nature, 366, 242

Hawkins M.R.S., 1995, Nature, submitted

Hawkins M.R.S., Bessell M.S., 1988, MNRAS, 234, 177

Heintz W.D., 1994, AJ, 108, 233

Henkel C., Mauersberger R., 1993, å, 274, 730

Henry T.J., 1990, PhD thesis, University of Arizona

Henry T.J., Kirkpatrick, J.D., 1990, ApJ, 354, L29

Henry T.J., McCarthy D.W., 1993, AJ, 106, 773

Henry T.J., Kirkpatrick J.D., Simons D.A., AJ, 1994, 108, 1437

Hertzsprung E., 1911, Potsdam Pub., 3

Hoffleit D., Jaschek C., 1982, The Bright Star Catalogue, Yale University, New Haven

Hu E., Huang J.-S., Gilmore G., Cowie L.L., 1994, Nature, 371, 493

Jensen P., 1989, J. Mol. Spectrosc., 133, 438

Johnson H.L., 1966, ARAA, 4, 193

Jones H.R.A., Hawkins M.R.S, 1995a, AAT Newsletter, 72

Jones H.R.A., Hawkins M.R.S, 1995b, ESO Workshop "The bottom of the main sequence and beyond", ed. Tinney C., Springer-Verlag, p.68

Jorgensen, U., 1995, A&A, 284, 179

Kerins E.J., Carr B.J., 1994, MNRAS, 266, 775

Kessler M.F., Metcalfe L., Salama A., 1992, Space Science Reviews, 61, 45

Kirkpatrick J.D., 1995, ESO Workshop "The bottom of the main sequence and beyond", ed. Tinney C., Springer-Verlag, p.140

Kirkpatrick J.D., Henry T.J., Liebert J., 1993b, ApJ, 406, 701

Kirkpatrick J.D., Henry T.J., McCarthy D.W. Jr, 1991, ApJS, 77, 417

Kirkpatrick J.D., Henry T.J., Simons D.A., 1995, AJ, 109, 797

Kirkpatrick J.D., Kelly D,M., Rieke G.H., Liebert J., Allard F., Wehrse R., 1993a, ApJ, 402, 643

Kirkpatrick J.D., McGraw J.T., Hess T.R., Liebert J. McCarthy D.W. Jr, 1994, ApJS, 94, 749

Kleinmann S. G., Hall D. N. B., 1986, ApJS, 62, 501

Kleinmann S. G. et al. 1994, Astr. & Sp. Sci., 217, 3

Kumar S.S., 1963, ApJ, 137, 1121

Kurucz R.L., 1993, Atomic data for opacity calculations, CD Roms

Lacy C.H., 1977, ApJ, 218, 444

Leggett S.K., 1992, ApJS, 82, 351

Leggett S.K, Hawkins M.R.S, 1988, MNRAS, 234, 1065

Lenzini P., Chernogg, D., Salpeter, E.E., 1991, ApJS, 76, 759

Leung K-C., Schneider D.P., 1978, AJ, 83, 618

Liebert J., Boroson T.A., Giampapa M.S., 1984, ApJ, 282, 758

Lienert Ch., Weitzel, N., Richichi A., Eckart A., Tacconi-Garman, 1994, å, 291, L47

Ludwig C.B., 1971, Applied Optics, 10, 1057

Lynas Gray A.E., Miller S., Tennyson J., 1995, J. Mol. Spectrosc., in press

Magain P., 1987, A&A, 179, 176

Magain P., 1989, A&A, 209, 211

Merrill K.M., Ridgway S.T., 1979, ARAA, 17, 9

Meyerdierks H., 1993a, Starlink User Note 86.9, Rutherford Appleton Laboratory

Meyerdierks H., 1993b, Starlink User Note 140.3, Rutherford Appleton Laboratory

Mihalas D., Binney J., 1981, Galactic Astronomy Structure and Kinematics, W.H. Freeman, San Fransico

Miller S., Tennyson J., Jones H.R.A., Longmore, A.J., 1994, IAU Coll. No. 146, p.296, ed. Jorgensen U.G., Thejl P., Springer-Verlag

Monet D.G., Dahn C.C., Vrba F.J., Harris H.C., Pier J.R., Luginbuhl C.B., Ables H.D., 1992, AJ, 103, 638

Mould J.R., 1976, A & A, 48, 443

Mould J.R., 1978, ApJ, 226, 923

Mountain C.M., Robertson D.J., Lee T.J., Wade R., 1991, SPIE, 1235, 35

Naftilan S.A., Sandmann W.S., Pettersen B.R., 1992, PASP, 104, 1045

Nelson L.A., Rappaport S., Joss P.C., 1993, ApJ, 404, 723

Paresce F., Marchi G.D, Romaniello M., 1995, ApJ, 440, 216

Persson S.E., Aaronson M., Frogel J.A., 1977, AJ, 82, 729

Peterson B.R., 1980, A&A, 82, 53

Popper, D.M., 1980, ARAA, 18, 115

Probst R.G., Liebert J., 1983, ApJ, 274, 245

Puxley P.J., Ramsay S.K., Beard S.M., 1992, Proc of 4th ESO/ST-ECF data analysis workshop, ed. Grosbol, P.

Ramsay S.K., Mountain C.M., Geballe T.R., 1992, MNRAS, 259, 751

Rebolo R., Martin E.L., 1992, ApJ, 389, L83

Reid I.N., Gilmore G., 1984, MNRAS, 206, 19

Reid M., Tinney C.G., Mould J., 1994, AJ, 108, 1456

Robertson J.G., 1986, PASP, 98, 1220

Rogers F.J., Iglesias C.A., 1992, ApJS, 79, 501

Rothman L.S., Gamache R.R., Tipping R.H., Rinsland C.P., Smith M.A.H., Benner D.C., Malathy Devi V., Flaud J.-M., Camy-Peyret C., Perrin A., Goldman A., Massie S.T., Brown L.R., Toth R.A., 1992, JSQRT, 48, 469

Ruan K.,1991, PhD thesis, National University of Australia

Russell H.N., 1913, Pro. Am. Phil. Soc., 51, 569

Sandage A., 1986, ARAA, 24, 421

Saumon D., Bergeron P., Lunine J.I., Hubbard W.B., Burrows A., 1994, ApJ, 424, 333

Schlosser W., Schmidt-Kaler T., Milone E.F., 1991, Challenges of astronomy: hands-on experiments for the sky and laboratory, Springer, New York

Schneider D.P., Greenstein J.L., Schmidt M., Gunn J.E., 1991, AJ, 102, 1180

Schryber J.H, Miller S. , Tennyson J., 1995, JSQRT, in press

Schwarzchild M., 1958, Structure and evolution of the stars, Princeton University Press

Seaton M.J., Yu Yan, Mihalas D., Pradhan A.K., 1994, MNRAS, 266, 605

Spirko V., Jensen P., Bunder P.R., Cejchan A., 1985, J. Mol. Spectrosc., 112, 183

Spinrad H., Wing R.J., 1969, ARAA, 7, 149

Stauffer J.R., Hartmann L.W., 1986, ApJS, 61, 531

Steele I.A., Jameson R.F., 1995, MNRAS, 272, 630

Steele I.A., Jameson R.F., Hambly N.C., 1993, MNRAS, 263, 647

Sutcliffe B. T. Tennyson J., 1986, J. Mol. Phys., 53, 1053

Tarter J.C., 1986, Astrophysics of Brown Dwarfs, p. 121, ed. Kafatos M.C., harrington R.S., Maran S.P., Cambridge University Press

Tennyson J., 1986, Comp. Phys. Reports, 4, 1

Tennyson J., Henderson J.R., Fulton N.G., 1995, Computer Phys. Comms, submitted

Tennyson J., Miller S., Henderson J.R., 1993, In: Methods in Computational Chemistry, 4, 91, Plenum, New York

Tennyson J., Miller S., Le Sueur C.R., 1993, In: Methods in Computer Phys. Comms., 75, 339

Tinney C.G., 1993, ApJ, 414, 279

Tinney C.G., Mould J. R., Reid I. N., 1993, AJ, 105, 1045

Tokunga A.T., 1986, IRTF Photomerty Manual., University of Hawaii, Honolulu

Tsuji T., 1966, Publ. Astron. Soc. Japan, 18, 127

Tsuji T, 1967, Coll. on Late-Type Stars, ed. Hack M., p. 260, Astron. Obs. Trieste

Tsuji T, 1994, IAU Coll. No. 146, p.79, ed. Jorgensen U.G., Thejl P., Springer-Verlag

van Altena W.F., Lee T., Hoffleit E.D., 1994, The General Catalogue of Trigonometric Parallaxes, Yale University Observatory, New Haven

Veeder G.J., 1974, AJ, 79, 1056

Vieira T., 1985, Uppsala Astronomical Observatory, Report No. 32

Wade R.A. Horne K., 1988, ApJ, 324, 41

Wattson R.B., Rothman L.S., 1992, JQSRT, 48, 763

Wheeler J.C., Sneden C., Truran J.W. Jr, 1989, ARAA, 27, 279

Wing R.F., 1979, in IAU Coll. 47, Spectral Classification of the Future, p.347, ed. McCarthy M.F., Philip A.G.D, Coyne G.V., Springer-Verlag

Yamanouchi T., Tanaka M., 1985, JQSRT, 34, 463

Young A., Skumanich A., Stauffer J.R., Harlan E., Bopp B.W., 1989, ApJ, 344, 427

Zuckerman B., Becklin E.E. 1992, ApJ, 386, 260

Mon. Not. R. Astron. Soc. **267**, 413–423 (1994)

An infrared spectral sequence for M dwarfs

H. R. A. Jones,[1] A. J. Longmore,[2] R. F. Jameson[3] and C. M. Mountain[4]

[1]*Institute for Astronomy, University of Edinburgh, Blackford Hill, Edinburgh EH9 3HJ*
[2]*Royal Observatory, Blackford Hill, Edinburgh EH9 3HJ*
[3]*Astronomy Group, Department of Physics & Astronomy, University of Leicester, University Road, Leicester LE1 7RH*
[4]*Gemini Project, 950 N. Cherry Avenue, PO Box 26732, Tucson, AZ 85726-6732, USA*

Accepted 1993 October 26. Received 1993 October 25; in original form 1993 June 11

ABSTRACT

We present a spectral sequence from 1 to 2.5 μm of M dwarfs, from GL411 (M2V) to the best brown dwarf candidate GD165B which is classified as cooler than M9V. This sequence shows the progressive importance of water absorption in the atmospheres of M dwarfs. We take the strength of the water absorption bands as the basis of a new method to derive a temperature from which we calculate effective temperatures and radii. We also identify many of the stronger atomic and molecular features and correlate their strengths with our derived temperature scale. For a given luminosity, this method yields temperatures close to those predicted by evolutionary models for low-mass stars, but not always close to those found by previous investigators. We find that GD165B has a temperature of 1860 ± 160 K and that it is the only star in the sample that might be classified as a brown dwarf, but to decide its true nature a more accurate parallax and a representative model atmosphere will be necessary.

Key words: stars: late-type – stars: low-mass, brown dwarfs – infrared: stars.

1 INTRODUCTION

M dwarfs are the most common stars in our stellar neighbourhood, yet are also amongst the least understood, largely due to their intrinsic faintness. Over the last decade, numerous surveys have been made in an attempt to derive the space density of stars at the bottom of the main sequence. Such studies have been motivated by the desire to find substellar objects (brown dwarfs) and to understand the space density of such objects by extrapolating the mass function for objects above the hydrogen-burning limit to masses below. While the numbers of known faint M dwarfs and candidate brown dwarfs have increased dramatically, our understanding of their fundamental properties has not. In particular, the scales used to convert the optical or infrared colours into bolometric luminosities and effective temperature (and, by extension, into estimates of mass) are poorly defined. The interpretation has relied on (i) the assumption that the observed colours are monotonic in their effective temperature, and (ii) a bolometric luminosity determined from spectrophotometry and from extrapolation of a blackbody curve into unmeasured parts of the star's energy distribution. Between 1 and 5 μm, however, where a 2500-K star emits 80 per cent of its flux, there are four strong water absorption bands, and thus spectra of cool dwarf stars do not resemble the blackbody curves which are shown by hotter stars across the infrared.

This deviation from a blackbody curve has implications for the measurement both of colour and of bolometric luminosity. The early temperature determinations (e.g. Veeder 1974) were achieved by fitting a blackbody to the observed broad-band colours of each star, assuming short wavelengths to have a certain amount of blocking and requiring the total flux under the blackbody curve and the bolometric luminosity to be equal. This technique was extended in later determinations where it was assumed that no significant backwarming occurs at 2.2 μm, and so the flux at that wavelength was adopted as a measure of the continuum emission from a blackbody with a temperature the same as the star's effective temperature (e.g. Berriman & Reid 1987). Hence the temperature for each star was determined from the blackbody curve having (i) flux equal to the observed flux at 2.2 μm, and (ii) the same bolometric luminosity. Such methods (Greenstein, Neugebauer & Becklin 1970; Veeder 1974; Peterson 1980; Reid & Gilmore 1984; Berriman & Reid 1987; Tinney, Mould & Reid 1993) indicate a Hertzsprung–Russell (HR) diagram offset by some 400 K from theoretical predictions. This is accepted to be an offset in temperature rather than in luminosity, in that many of the stars in the above studies have parallaxes measured to better

than 1 per cent and so the errors associated with the measurement of luminosity tend to be considerably smaller than those of temperature. This is supported by the large scatter in determinations of temperature but not in the determinations of luminosity found by the various investigators.

In order to construct accurate luminosity and mass functions for these stars, it will be necessary to understand how their spectra behave with temperature, metallicity and gravity. We have taken 1–2.5 μm spectra of a sample of M dwarfs and brown dwarf candidates with similar metallicity but a range of temperature. The observations and data reduction are presented in Sections 2 and 3, a derivation of effective temperatures of low-mass stars in Section 4, an HR diagram in Section 5 and a discussion of trends shown by the strong atomic and molecular features in Section 6. The conclusions are highlighted in Section 7.

2 OBSERVATIONS

We observed the brown dwarf candidate GD165B and a range of M dwarfs: LHS2924, VB10, GL406, GL699 and GL411. GD165B, discovered by Becklin & Zuckerman (1988), was chosen because its photometric colours make it the best brown dwarf candidate yet discovered by the numerous surveys for low-mass stars conducted over the last 40 years. The others were chosen because they have been the subject of previous studies of M dwarfs (Veeder 1974; Mould 1978; Berriman & Reid 1987; Bessell 1991; Berriman, Reid & Leggett 1992; Leggett 1992; Kirkpatrick et al. 1993a; Tinney et al. 1993), and because they form a sample whose space motions and colours indicate approximately the same age and metallicity (Table 1).

Observations were made with the Cooled Grating Spectrometer 4 (CGS4, Mountain et al. 1990) on the UK Infrared Telescope on Mauna Kea, Hawaii. Our observations were made with a 58×62 InSb array, which was moved in the focal plane in order to over-sample the spectrum. Sky subtraction was performed by nodding the telescope approximately 30 arcsec up and down the slit, ensuring that during alternate 'object' and 'sky' observations the star remained on the detector. There were two observing runs, on 1991 June 20 and 1992 May 6–8.

The 75 line mm^{-1} grating was used in six different configurations in order to cover the wavelength range of 1–2.5 μm with some overlap between each spectral segment. The coverage and resolution of the grating positions used are shown in Table 2. The combined spectra from 1 to 2.5 μm for all the objects are shown in Fig. 1, and their photometric colours in Table 1. For the fainter objects, GD165B, LHS2924 and VB10, integration times at each grating position were 20–35 min; for the brighter objects, GL411, GL699 and GL406, they were about 5 min. In this paper we have also made use of far-red spectra for all of the stars other than GD165B. These spectra were taken on the Multiple Mirror Telescope (MMT), Kitt Peak, Arizona, and kindly made available to us by Douglas Kelly and Davy Kirkpatrick. The full data set and reduction procedures are described by Kirkpatrick, Henry & McCarthy (1991) and Kirkpatrick et al. (1993a).

2.1 Standards

Stars in the spectral type ranges F6–G0 and A0–5 were used to remove from the observations the effects of atmospheric

Table 1. Photometry and distances of observed objects. The data for GL411, GL699, GL406, VB10 and LHS2924 are taken from Leggett's (1992) compilation of photometry for low-mass stars; for GD165B the data are from Zuckerman & Becklin (1992) and Tinney et al. (1993). The errors are quoted as ±0.03, except for GD165B for which the errors are ±0.05. *U*, *B* and *V* photometry is on the Johnson system; *R*- and *I*-band photometry is on the Cousins system; *J*, *H* and *K* photometry is on the California Institute of Technology (CIT) system; *L* and *L'* photometry is on the Mauna Kea Observatories system (MKO). Distances, *d*, are derived from the absolute trigonometric parallaxes from the Yale General Catalogue of Trigonometric Stellar Parallaxes (van Altena, Lee & Hoffleit, in preparation), except for GD165B (from Zuckerman & Becklin 1992) and GL411 (from Gliese & Jahreiss 1979). Population types are taken from Leggett (1992), where KIN signifies kinematic and COL colour, OD means old disc and O/H means old disc–halo type. Old disc represents $[M/H] \sim -0.5$, and an old disc–halo type corresponds to $[M/H] \sim -1.0$.

Object	d (pc)	Population		U_J	B_J	V_J	R_J	I_C	J_{CIT}	H_{CIT}	K_{CIT}	L_{CIT}	L'_{MKO}	M_{UKIRT}	$IRAS_{12}$	$IRAS_{25}$
		KIN	COL													
GL411	2.535	OD	O/H	10.12	8.98	7.47	6.46	5.32	4.10	3.56	3.36	3.20	3.08	-	2.7	2.43
GL699	1.83	O/H	O/H	12.54	11.28	9.55	8.34	6.77	5.27	4.77	4.51	4.20	4.17	4.2	4.0	3.9
GL406	2.39	OD	-	17.03	15.44	13.45	11.57	9.39	7.06	6.44	6.08	5.73	5.69	-	-	-
VB10	5.79	OD	-	-	19.63	17.50	15.10	12.80	9.90	9.24	8.80	8.35	8.15	-	-	-
LHS2924	10.7	OD	-	-	-	19.58	-	15.21	11.84	11.17	10.67	-	10.02	-	-	-
GD165B	36.0	-	-	-	-	-	-	19.25	15.78	14.77	14.13	13.30	-	-	-	-

Table 2. Grating positions used to obtain spectra in Fig. 1.

λ_{cen} μm	λ range μm	$\lambda/\Delta\lambda$ at λ_{cen} μm	Date	Object
1.04	0.95 – 1.14	349	5–7/5/92	All
1.22	1.12 – 1.33	374	"	All except VB10
1.40	1.29 – 1.51	429	"	"
1.67	1.46 – 1.88	255	"	"
2.03	1.82 – 2.24	310	"	"
2.31	2.19 – 2.61	367	"	"
1.10	1.00 – 1.20	305	20/6/91	VB10
1.30	1.20 – 1.40	398	"	"
1.50	1.40 – 1.60	460	"	"
1.75	1.56 – 1.95	268	"	"
2.04	1.84 – 2.24	312	"	"
2.20	2.00 – 2.40	337	"	"

absorption. Except for Paschen and Brackett series hydrogen lines and very weak CO bands in the G dwarfs, these standards are thought to be featureless at the spectral resolution we used and to be well described by a Rayleigh–Jeans tail. All observations were made in excellent conditions (typically around 1-arcsec seeing), and the airmass difference between object and standard never exceeded 0.05. Thus we believe that the spectra have excellent cancellation of atmospheric features.

2.2 Wavelength calibration

The 1992 May observations were calibrated using a combination of arc lines from krypton and argon. The 1991 June observations (VB10) were taken without arc lines, and so use was made of the OH lines in the *J* and *H* windows (as

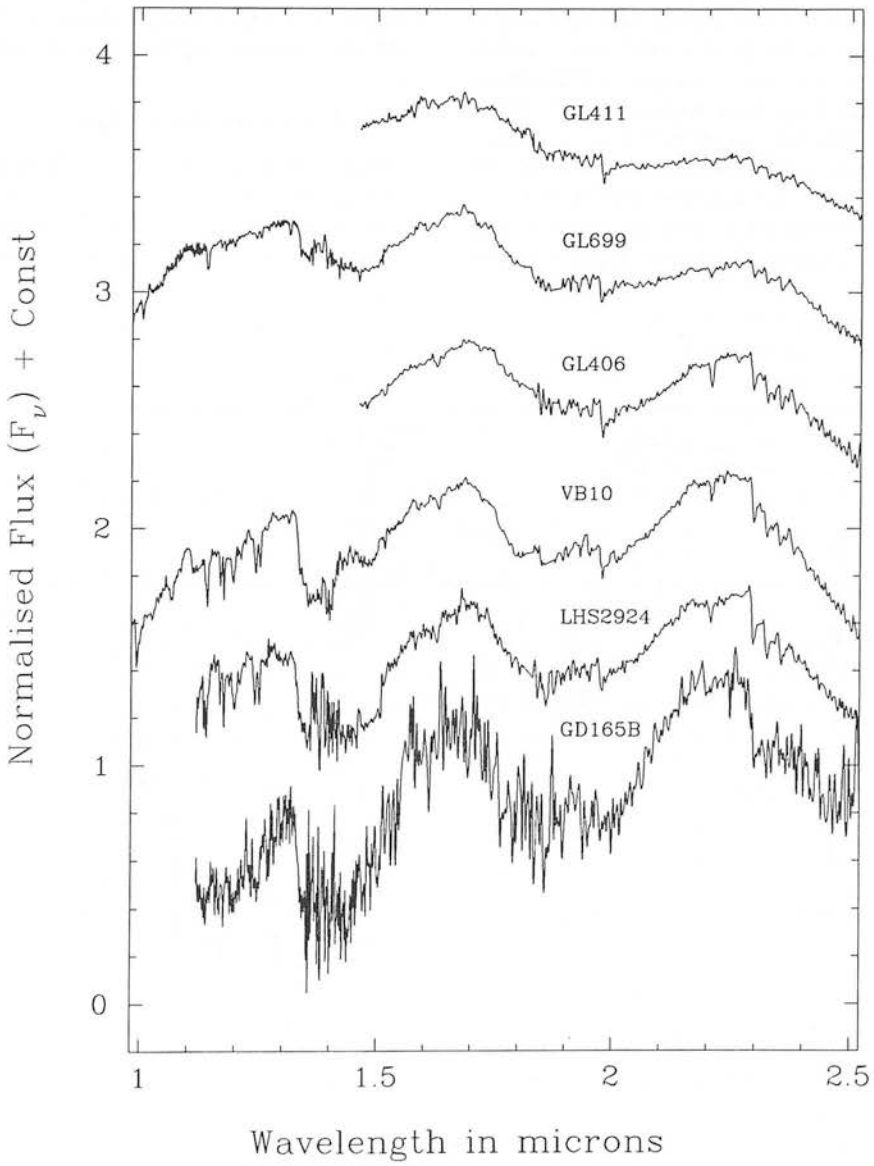

Figure 1. A spectral sequence for M dwarfs. The various spectra have been normalized and then shifted vertically in steps of 0.5 for the purpose of display. The increasingly humped appearance of the spectra with decreasing spectral type (down the page) results from the increasing importance of water absorption.

described by Ramsay, Mountain & Geballe 1992) and the hydrogen recombination lines in the standards. VB10 was calibrated using OH lines and is accurate to $0.3\Delta\lambda$ μm, where $\Delta\lambda$ is the instrumental resolution; the other spectra were calibrated with arc lines and are typically accurate to $0.1\Delta\lambda$ μm.

3 DATA REDUCTION

In the reduction of CGS4 data, we have used the off-line CGS4 data reduction system (described in detail by Puxley, Ramsay & Beard 1992) together with the library of routines contained in the software packages FIGARO and SPECDRE supplied by Starlink. Identifiable Paschen and Brackett series absorption lines were interpolated across, before using the spectra of our standard stars to correct for the effects of terrestrial absorption in our target objects. The target object spectra were then divided by the standard star spectra and multiplied by a blackbody spectrum for the temperature (from Popper 1980) appropriate to the spectral type of that standard star. In addition to the deep, broad water absorption bands, the resolution of each spectrum is sufficient to show a number of other prominent molecular and atomic features. Such features are vital in determining the metallicities of cool dwarf stars, which have so far only been estimated by using space motions and colours (Leggett 1992).

Once reduced, the overlapping spectral regions were joined together into *J*, *H* and *K* spectral regions. In the regions of overlap, the spectral features and continuum shape are well reproduced but the flux levels between different spectral regions differ by 5–20 per cent. Such differences probably arise from wind shake, which causes the target to move out of the narrow slit (3 arcsec) during an observation. The overlapping spectral regions were combined by adjusting the flux levels of each of the spectral *J*, *H* and *K* bands so that the combined spectra reproduced the observed photometric colours. We used California Institute of Technology (CIT) filter profiles and atmospheric transmission profiles (for 1.5 mm of precipitable water vapour at 5000 m) to ensure that the photometric $J-H$ and $H-K$ colours derived from the spectra agreed with the values given in Table 1.

4 A TEMPERATURE SCALE FOR M DWARFS

In order for the methods of temperature determination discussed in the Introduction to be successful, it is necessary to appeal to a representative model atmosphere, which for M dwarfs has frequently been that of a blackbody.

4.1 Use of model atmospheres

Allard (1990) and Kui (1991) have computed model atmospheres for M dwarfs. As yet, however, the models are not in good agreement with infrared observations (e.g. Graham et al. 1992; Kirkpatrick et al. 1993a; Tinney et al.

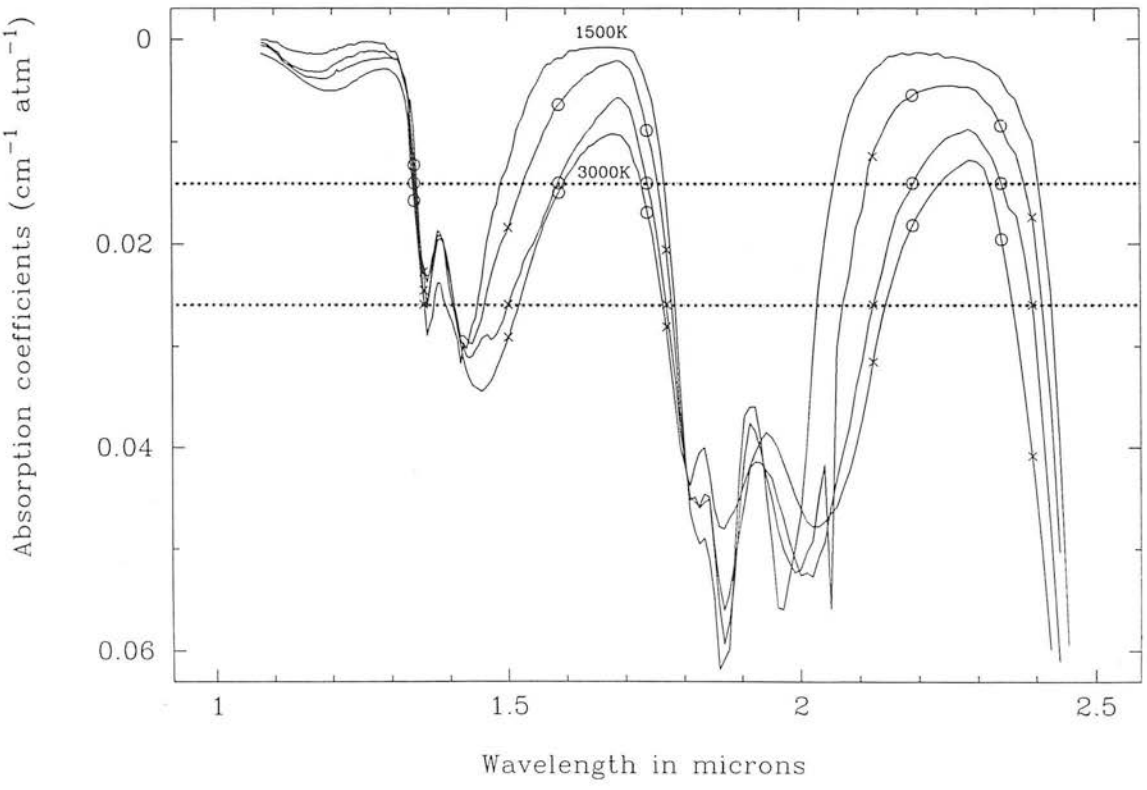

Figure 2. Absorption coefficient versus wavelength for water vapour at 1500, 2000, 2500 and 3000 K from Ludwig (1971). Wavelengths that are chosen have exactly equal opacity at 2500 K, but have slightly different values at 2000 and 3000 K. Crosses denote high-opacity points; circles denote low-opacity points.

1993). In particular, there are considerable problems in modelling the 0.65–1.1 μm regions of the spectra and in the treatment of the dominant absorber in the infrared – water. In the 0.65–1.1 μm region, the models used by Kirkpatrick et al. (1993a) did not include FeH which produces a deep band at 0.99 μm, and were unable properly to include bands due to TiO ε and VO (C–X) for which laboratory oscillator strengths have not been measured. While there are gross discrepancies in the 0.6–1.1 μm region, which is near the blackbody peak for many of these spectra, it is problematic to make useful comparisons with the models in the infrared. In their papers, Graham et al. and Tinney et al. illustrated the problems and discussed the drawbacks of the models, in particular the use of the 'just overlapping line approximation' for water vapour absorption, which gives a mean absorption coefficient for 72 spectral meshes between 0.27 and 30 μm. New derivations of the molecular band strengths (Allard et al., in preparation), together with a detailed theoretical treatment of the water band (Miller et al., in preparation), should allow models and observations to be more reasonably compared. In the meantime, since the laboratory data for water absorption coefficient versus wavelength (Fig. 2, from Ludwig 1971) have a very similar shape to our M dwarf spectra, we use these absorption coefficients to derive effective temperatures for our sample.

4.2 Derivation of effective temperature

At wavelengths longer than 1.34 μm, water vapour is the dominant opacity. Allard's models confirm that it dominates over its nearest rival, H^-, between 1 and 2.5 μm. The oscillatory nature of the water vapour opacity allows us to choose a number of wavelengths at which the optical depths will be equal at a given temperature, say 2500 K. It can be seen from Fig. 2 that at 2000 and 3000 K the opacities at these wavelengths are different from but still close to those at 2500 K. Stellar atmosphere theory tells us that we should be able to fit a blackbody through points of constant optical depth; such a fit generates a temperature T. Having found T we can select slightly better wavelengths that have exactly equal opacities at this temperature. This can be done by interpolation between the water absorption coefficients. This procedure can be iterated until a convergence is found. In order to get the most reliable fits, for GD165B and LHS2924 it was necessary to smooth the spectra through the water bands to the same resolution as the laboratory data. In regions where water opacity is clearly not the dominant opacity at a chosen wavelength point, in particular for the CO bands at 2.29–2.51 μm, it was necessary to interpolate across the feature. The final value of T is not the effective temperature, T_e. However, T does allow us to calculate $(R/d)^2$ from the equation

$$f_\lambda = R^2 F_\lambda(T)/d^2,$$

where f_λ is the measured flux at one of the wavelengths, R the effective radius, d the distance of the object and $F_\lambda(T)$ the Planck function. The effective temperature T_e can now be found from the bolometric flux, F_{bol}, using

$$\sigma T_e^4 = (d/R)^2 F_{bol},$$

where σ is the Stefan–Boltzmann constant. The radius can be assumed to be constant, as the photospheres of these high-gravity dwarf stars are extremely thin (e.g. Allard 1990). We find no evidence for a difference in the radii derived from blackbody fits for levels of different opacity, and so consider this to be a valid assumption.

Except for GD165B, the bolometric flux was determined by combining the photometry presented in Table 1, the 0.65–1.45 μm spectra from Kirkpatrick et al. (1991, 1993a) and the infrared spectra presented in Fig. 1 and beyond 2.5 μm with spectra from Berriman & Reid (1987) and synthetic spectra from Allard (in preparation). For GD165B, Allard's models were also used for wavelengths shortward of 1.1 μm.

Hence we derived effective temperatures for our sample by determining f_λ, $F_\lambda(T)$ and F_{bol}. We checked the validity of the method by repeating the fitting sequence for different levels of opacity. Use of wavelength points corresponding to lower water opacity led to slightly higher values for T and a larger f_λ. For example, for the star GL406 shown in Fig. 3, using high-opacity points (0.0262 cm^{-1} atm^{-1}) a constant opacity temperature of 2660 K is found, which gives an effective temperature of 2671 K; using a set of low-opacity points (0.01405 cm^{-1} atm^{-1}) the constant-opacity temperature is 2756 K and the effective temperature is 2667 K. Higher temperatures for all the objects were derived using the points of lower opacity, because the blackbody is then fitted to a region slightly deeper (and hotter) in the photosphere. The quality of such blackbody fits tended to be poorer than that obtained when using high-opacity points. The derived effective temperatures were in all cases within 160 K of one another. Our final adopted values for effective temperature were found by weighting the T_e values derived from the high opacity by 2/3 and those derived from the low opacity by 1/3. The high-opacity points were favoured because (i) they gave the lower fitting errors, (ii) we expect them to be the least affected by other sources of opacity, and (iii) they allow a longer wavelength baseline.

Our derived values for T_e, M_{bol} and R are given in Table 3. In Fig. 4 we compare our values of effective temperature and bolometric luminosity with those derived by previous authors. Our bolometric luminosities are similar to those found by other investigators. Our effective temperatures, however, are considerably hotter than those obtained by Veeder (1974), Berriman & Reid (1987) and Tinney et al. (1993), but cooler than those derived by Kirkpatrick et al. (1993a). In Fig. 3 the blackbody corresponding to T_e lies virtually on top of the high-opacity curve which passes about mid-way between the spectral peaks and troughs. The method of Berriman & Reid (1987) is to solve the equation

$$C f_{2.2}/f_{bol} = F_2(T_e)/\sigma T_e^4,$$

where $f_{2.2}$ and f_{bol} are the measured quantities, with the assumption that the constant $C = 1$. However, we find in Fig. 3 that $C < 1$ and so 2.2 μm is not a point of continuum for such cool stars. This possibility was discussed by Berriman & Reid (and by Tinney et al., who chose a reference wavelength of 3.82 μm). The lower values of T_e found by Berriman & Reid can be explained in terms of C as follows. 2 μm is close to the wavelength of maximum intensity of the Planck curve at 2000 K, so that $F_\lambda(T_e) \propto T_e^3$. Therefore, for an observed value of $f_{2.2}/f_{bol}$, $T_e \propto C^{-1}$ and so our finding that $C < 1$ leads us to derive systematically higher temperatures than did these investigators. We expect that the stars' rank order in temperature will be unaffected by the value of C.

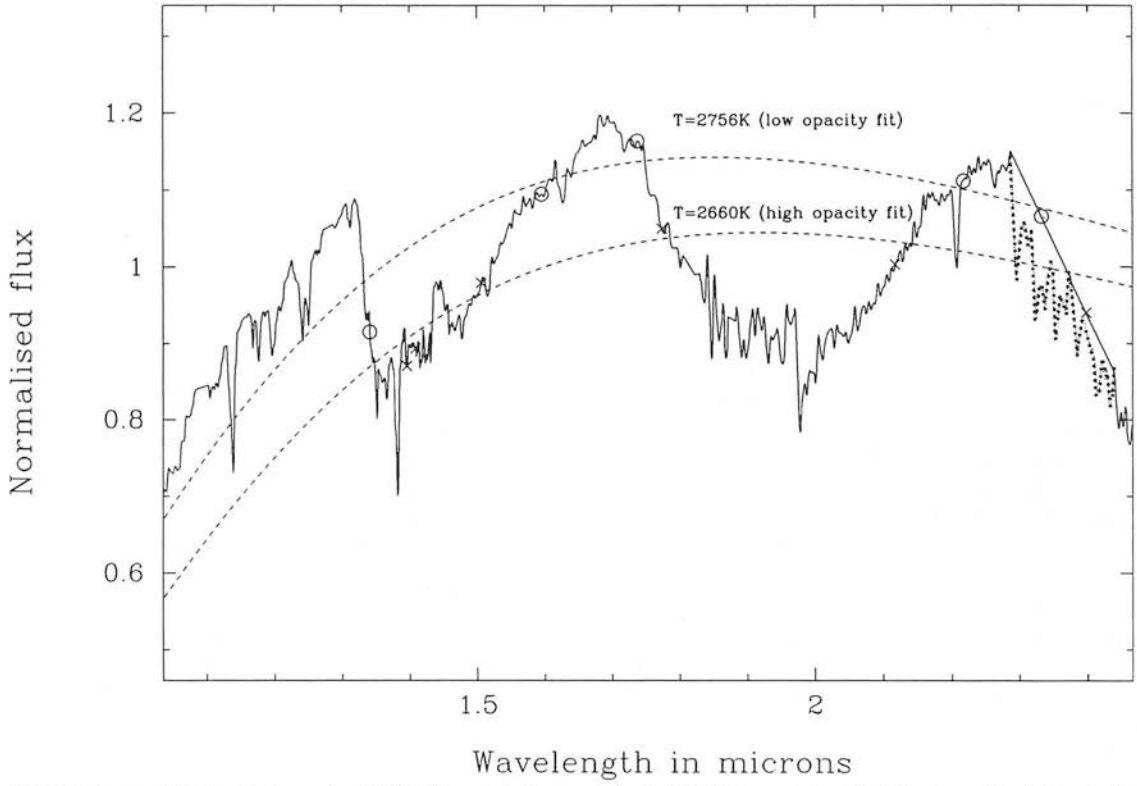

Figure 3. GL406 shown with the high-opacity (2660 K) and the low-opacity (2756 K) best-fitting blackbodies. The derived effective temperature would lie virtually on top of the high-opacity fit. The worst-fitting point for GL406 and the other objects is the longest wavelength one, which falls in a regime where CO absorption dominates over water vapour absorption. We corrected for this by linear interpolation over the CO absorption bands.

Table 3. Fundamental parameters derived for observed stars. In our derivation of bolometric luminosity, we assume effective wavelengths and flux densities for a zero-magnitude star as given by Berriman et al. (1992) for the *U*, *B* and *R* bands, by Tokunaga (1986) for *V*, *I*, *J*, *H*, *K*, *L* and *L'*, and by Berriman & Reid (1987) for the *M* and *IRAS* bands. The values of *g* and *R* are calculated assuming $M_{bol} = 4.75$ and $T_e = 5770$ K for the Sun (Allen 1973).

Object	R ($R_\odot$)	Mass ($M_\odot$)	g ($g_\odot$)	M_{bol}	T_{eff} (K)
GL411	0.430	0.43	2.33	8.79	3471
GL699	0.208	0.17	3.91	10.86	3095
GL406	0.149	0.10	4.50	12.23	2670
VB10	0.103	0.085	7.96	13.30	2506
LHS2924	0.095	0.081	8.97	14.01	2219
GD165B	0.089	0.078	9.68	14.91	1856

Kirkpatrick et al. determined temperatures by comparisons with Allard's (1990) model atmospheres, which show reasonable agreement with observations from 1.1 to 1.35 μm. However, it is difficult to trust these higher temperatures whilst the fit through the 0.65–1.1 μm and 1.35–2.5 μm regions has been shown to be poor. If water vapour is indeed the dominant source of opacity then our method should be reliable. Nevertheless, we note that the major problem with the models has been with the strength of the water vapour bands (e.g. Kui 1991, ch. 3.4).

5 LOCATION ON THEORETICAL HR DIAGRAM

In Fig. 4 we also plot (i) the evolutionary model from D'Antona & Mazzitelli (1985), which has become the benchmark for evolutionary models of low-mass stars, (ii) the extremal models from the study by Burrows, Hubbard & Lunine (1989), and (iii) the standard model X adopted by Burrows et al. (1993). Using these models, we have derived masses for the objects in our sample (Table 3).

Leggett (1992) classifies all the stars in our sample, apart from GD165B, as old disc stars. In Fig. 4 we notice that for masses above $0.09\,M_\odot$ the evolutionary tracks for stars between 0.6 and 10 Gyr are almost indistinguishable. This means that for all of our sample, apart from LHS2924 and GD165B, masses can be derived with some confidence. Below $0.09\,M_\odot$, however, the mass of an object with a given temperature and luminosity cannot be determined reliably without first assigning an age. For example, the standard model from Burrows et al. (1993) predicts that an object at about 2090 K and $L/L_\odot \approx 1.5 \times 10^{-4}$ will have a mass of $0.065\,M_\odot$ if it is 0.6 Gyr old, whereas if it is 10 Gyr old then its mass will be $0.080\,M_\odot$. Since LHS2924 is classified as an old disc star and its equivalent widths do not indicate it to be

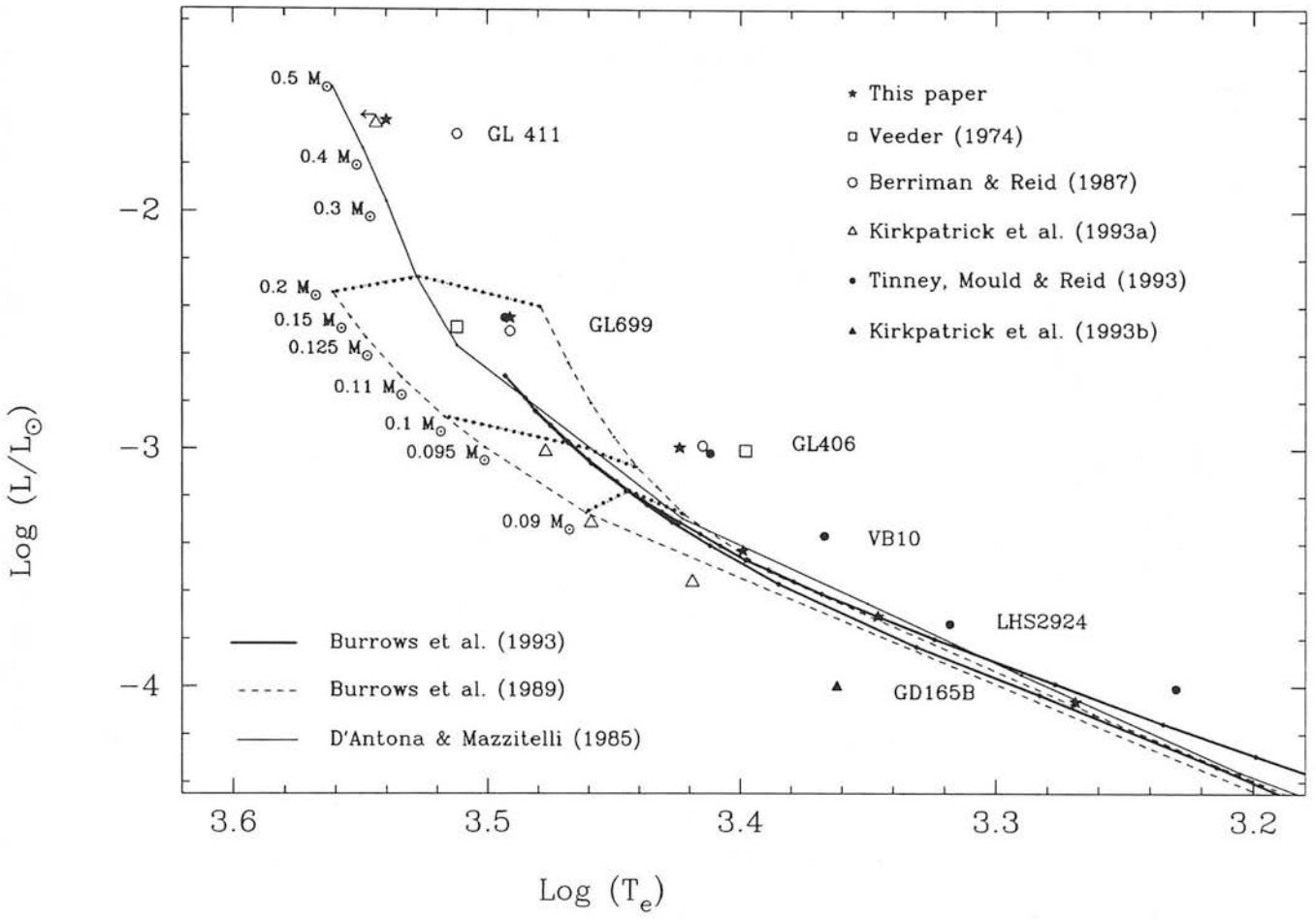

Figure 4. Derivation of mass using theoretical temperature versus luminosity for different models. The dashed lines represent the two extremes of the models presented by Burrows et al. (1989) at 10 Gyr. Each of the model points is marked with a small solid dot, and some equal-mass lines are shown as dotted lines connecting the corresponding points from models D (high opacity, low helium abundance) and E (low opacity, high helium abundance). The value of the mass is given to the left of the model E isochrone. The thick solid lines are the standard models at 0.6 and 10 Gyr (the younger one is the slightly higher of the two) due to Burrows et al. (1993); below $0.09\,M_{\odot}$ these models are incremented in steps of $0.02\,M_{\odot}$. The thin solid line is due to D'Antona & Mazzitelli (1985), and is for 1 Gyr. All models are for solar abundances. Previous determinations of the temperature and bolometric luminosity for our sample of low-mass stars are plotted as open squares (Veeder 1974), open circles (Berriman & Reid 1987), open triangles (Kirkpatrick et al. 1993a), filled circles (Tinney et al. 1993), filled triangles (Kirkpatrick et al. 1993b) and stars (this paper).

younger (Section 6), we adopted the 10-Gyr model track to derive its mass. For GD165B the situation is slightly more ambiguous. Leggett's (1992) assignments of age/metallicity were based on space motions which have not yet been measured for GD165B. However, it does have a well-studied companion, the cool ZZ Ceti white dwarf GD165A which had a progenitor in the mass range 1.5–$6\,M_{\odot}$. This places only a loose constraint on evolution, plus cooling time-scales of greater than 0.5 Gyr. We can put conservative limits on the mass of GD165B by using models at 0.6 and 10 Gyr, that is, between 0.067 and $0.078\,M_{\odot}$. Burrows et al. (1993) find that the main sequence ends at $0.0767\,M_{\odot}$ for solar-metallicity objects and at $0.094\,M_{\odot}$ for zero-metallicity objects, so GD165B is a good brown dwarf candidate. To decide its true nature, a more accurate parallax (better than the current 12 per cent) and an accurate model atmosphere will probably be necessary.

6 SPECTRAL FEATURES

The spectra are dominated by deep broad absorption bands of H_2O, but have many other strong features, both molecular and atomic. The spectral identifications shown for VB10 in Fig. 5 come from M giants (Chauville et al. 1970), α Orionis (Vieira 1985) and an infrared solar line list by Hall (1980). Other important sources were Kirkpatrick et al. (1993a), Allard (1990), Kui (1991), Davidge & Boeshaar (1991, 1993), Allen (1973), Spinrad & Wing (1969), Merrill & Ridgway (1979) and Kleinmann & Hall (1986). In Table 4, the absorption lines for which we have firm identifications and which are observable in all the objects are given with the equivalent widths measured using ABLINE (Robertson 1986). For each feature we assign a quality index to indicate the estimated errors of our measurement: x (±15 per cent), y (±25 per cent) and z (±50 per cent) for the brighter stars in

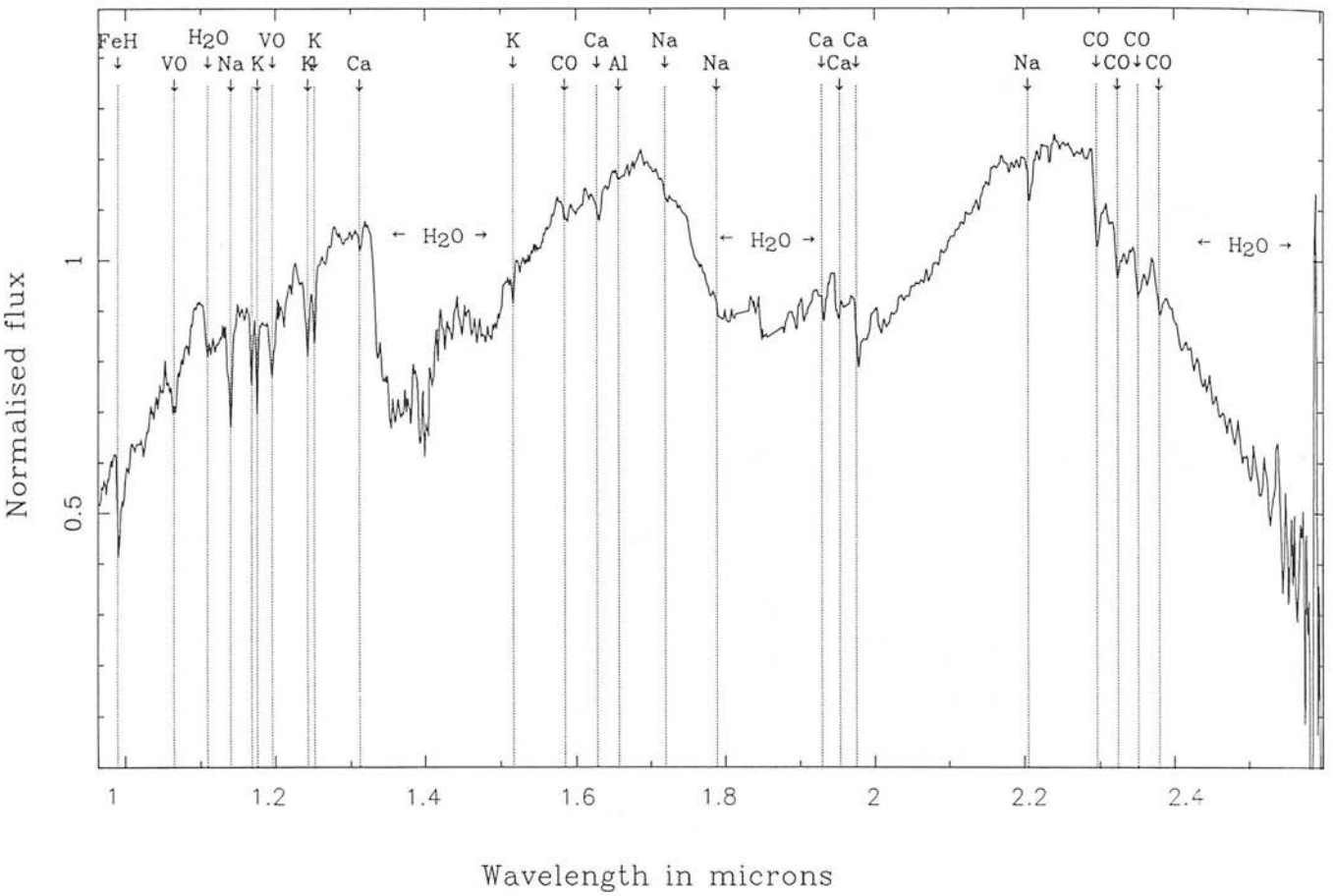

Figure 5. Spectral identifications for VB10.

the sample, and 40, 60 and 80 per cent respectively for GD165B because of its considerably poorer signal-to-noise ratio. It should be noted that in absolute terms these widths are very tricky to determine, since all of the features measured are superposed at some level on molecular bands and in many cases also blended with other atomic lines. By using the same procedure for each line in different objects, we trust that these widths should at least be internally consistent. All continuum fits were based on fitting a low-order polynomial to the level immediately adjacent to the feature rather than trying to measure the equivalent widths of features by estimating an overall continuum level. Overlapping atomic doublets and triplets were in a number of cases measured as single equivalent widths, rather than attempting to measure a number of blended lines. In Fig. 6 the equivalent widths are plotted against our values for effective temperature. A number of prominent spectral features have equivalent widths that are apparently very strongly correlated with temperature.

Within the uncertainties of poorly defined metallicity, the $I-K$ colour is a reliable temperature indicator. This result should be useful, as it allows good temperature estimates to be made from $I-K$ colour alone without the need for higher spectral resolution. Within the same caveat for metallicity, a number of features at higher resolution scale with temperature: at low spectral resolution, the water bandhead at 1.34 μm, the 2.05–2.15 μm gradient and the CO bandhead at 2.29 μm; at higher spectral resolution, potassium with two strong doublets in the J window, FeH at 0.99 μm and VO at 1.2 μm. Particular care is needed when using features that occur in between the atmospheric windows. For example, there are a number of strong Ca lines around 1.95 μm for which it is especially difficult to deduce a reliable continuum. In addition, there are a number of features that we think are strongly blended with other species – in particular, the VO band at 1.20 μm is probably blended with Fe and Ti.

The interpretation of atomic equivalent widths in cool stars is considerably more complex than in hotter stars because, below 4000 K, hydrogen is neutral and easily ionized metal elements, such as Na, Ca and K, are the major contributors of free electrons. Because the metallic elements are partly ionized, the number densities of the atomic metallic species are determined not only by the elemental abundance but also by the ionization state of the stellar atmosphere, so that, even for an accurate $[M/H]$, the uncertainty in ionic abundances will be significant. Moreover, some metallic elements are involved in the formation of molecules, and the number densities of the atomic species

Table 4. Equivalent widths for the major infrared absorption features observed in M stars.

Species	λ (μm)	Equivalent widths in nm						Quality
		GL411*	GL699	GL406*	VB10	LHS2924	GD165B	
FeH	0.99	*0.305*	0.714	*1.66*	2.51	-	-	x
NaI	1.1404,1.1381	*0.299*	0.468	*1.37*	1.49	2.26	2.40	y
KI	1.1690	*0.0299*	0.102	*0.153*	0.575	0.556	1.36	x
KI	1.1777, 1.1773	*0.0559*	0.157	*0.321*	0.664	0.902	1.33	x
VO	1.20	*0.0714*	0.139	*0.449*	0.808	1.37	2.46	y
KI	1.2432	*0.0468*	0.179	*0.574*	0.995	1.22	2.35	x
KI	1.2522	*0.111*	0.133	*0.353*	0.656	0.790	1.81	x
CaI	1.3135	*0.149*	0.205	*0.146*	0.176	0.149	0.325	y
KI	1.5167, 1.5172	0.151	0.0896	0.211	0.261	0.459	1.28	z
AlI	1.6755, 1.6768	0.139	0.0932	0.00153	0.0784	0.176	0.829	z
CaI	1.9272	0.284	0.320	0.192	0.403	0.141	1.46	y
CaI	1.95	0.340	0.281	0.514	0.504	0.505	1.62	y
CaI	1.987,1.992	0.741	0.771	1.01	0.919	0.850	0.992	z
NaI	2.2062, 2.2090	0.187	0.229	0.697	0.471	0.427	0.910	x
Spectral indices								
H_2O bandhead at 1.34 (1.286–1.303)/(1.338–1.356)		*1.12*	1.13	*1.21*	1.39	1.47	1.85	x
CO bandhead at 2.294 (2.22–2.28)/(2.30–2.36)		1.07	1.06	1.12	1.20	1.18	1.27	x
2.05-2.15 gradient		1.02	1.05	1.19	1.23	1.33	1.75	x

*Data in italics are equivalent widths measured from the Kirkpatrick et al. (1993) data set.
The Quality measure in the final column assigns an error bar to the measurement of each feature, x < 15 per cent, y < 25 per cent and z < 50 per cent.

are not therefore directly proportional to the abundances of the elements. Whereas in hotter stars the equivalent widths of 'weak' (< 0.6 nm) metallic lines are insensitive to small changes in number density, in cooler stars such changes will affect the atmospheric structure and with it the measured equivalent width. Kui (1991) shows that the separation between curves of growth calculated with slightly different values of $[M/H]$ dramatically increases as the temperature falls. Furthermore, it can be seen from Table 3 that our sample of stars covers a range of $g/g_{\odot}$, where g is surface gravity, which increases with decreasing temperature. It is expected that many of the spectral features will also have some gravity dependence. Until we have investigated the detailed dependences of temperature, elemental abundance and gravity on the derived equivalent width using accurate synthetic spectra, our interpretation of the trends apparent from Fig. 6 in terms of temperature only must be treated with caution.

7 CONCLUSIONS

We have derived a new set of temperatures for M dwarf stars by using the dominance of water opacity. These temperatures correlate well with $I-K$ colour and agree with the theoretical main-sequence predictions for the coolest M stars, but not with those found by previous investigators. We show that most atomic and molecular infrared spectral features in M dwarf stars are sensitive to temperature, and find the depth of the water band at 1.34 μm, the strongest spectral feature, to be a direct indicator of temperature. It does, however, have the disadvantage that it is measurable in faint objects only from a high, dry site. On the other hand, the 2.05–2.15 μm gradient and the CO bandhead at 2.29 μm, although not quite as prominent, are free of such problems.

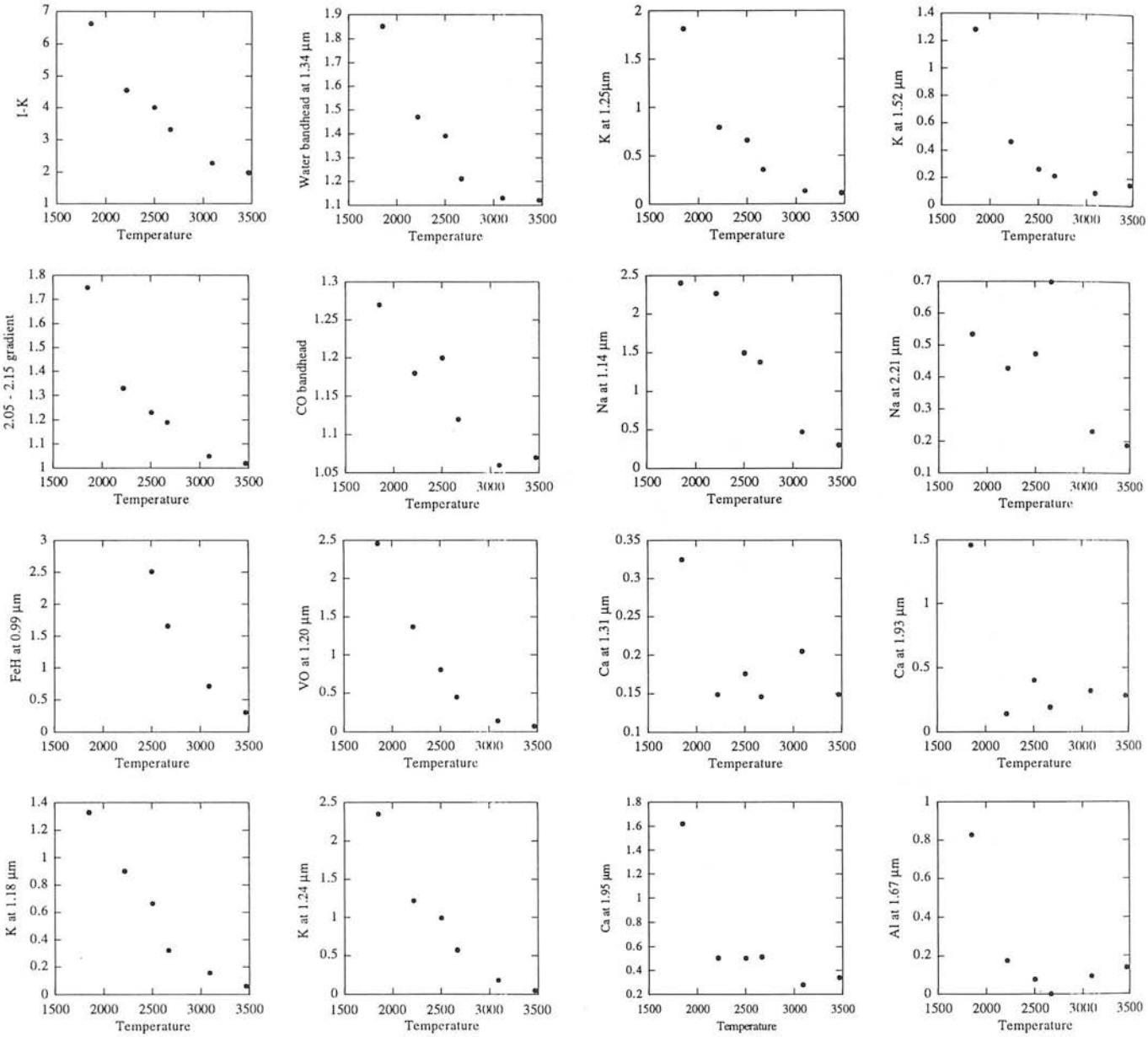

Figure 6. Equivalent width (in nm) versus temperature (in K) for infrared features that appear in each of our sample of M dwarfs.

ACKNOWLEDGMENTS

We are indebted to Davy Kirkpatrick and Douglas Kelly for their spectra, to France Allard for use of her models and to Eric Persson for CIT filter profiles. We thank Horst Meyerdierks and Dave Buckley for computing assistance and Suzanne Ramsay and Phil Puxley for help with CGS4 data reduction. We acknowledge the SERC for UKIRT time, for travel and subsistence funds, for providing computing resources through Starlink and for HRAJ's research studentship.

REFERENCES

Allard F. A., 1990, PhD thesis, University of Heidelberg
Allen 1973, Astrophysical quantities. Athlone Press, London
Baldwin J. R., Frogel J. A., Persson S. E., 1973, ApJ, 184, 427
Becklin E. E., Zuckerman B., 1988, Nat, 336, 656
Berriman G. B., Reid I. N., 1987, MNRAS, 227, 315
Berriman G. B., Reid I. N., Leggett S. K., 1992, ApJ, 392, L31
Bessell M. S., 1991, AJ, 101, 662
Burrows A., Hubbard W. B., Lunine J. I., 1989, ApJ, 345, 939
Burrows A., Hubbard W. B., Saumon D., Lunine J. I., 1993, ApJ, 406, 158
Chauville J., Querci F., Connes J., Connes P., 1970, A&AS, 2, 181
D'Antona F., Mazzitelli I., 1985, ApJ, 296, 502
Davidge T. J., Boeshaar P. C., 1991, AJ, 102, 267
Davidge T. J., Boeshaar P. C., 1993, ApJ, 403, L47
Gliese W., Jahreiss H., 1979, A&AS, 38, 423
Graham J. R., Matthews K., Greenstein J. L., Neugebauer G., Tinney C. G., Persson S. E., 1992, AJ, 104, 2016
Greenstein J. L., Neugebauer G., Becklin E. E., 1970, ApJ, 161, 519

Hall D., 1980, Atlas of infrared spectra of the solar photosphere and sunspot umbrae. Kitt Peak National Observatory
Kirkpatrick J. D., Henry T. J., McCarthy D. W. Jr, 1991, ApJS, 77, 417
Kirkpatrick J. D., Kelly D. M., Rieke G. H., Liebert J., Allard F., Wehrse R., 1993a, ApJ, 402, 643
Kirkpatrick J. D., Henry T. J., Liebert J., 1993b, ApJ, 406, 701
Kleinmann S. G., Hall D. N. B., 1986, ApJS, 62, 501
Kui R., 1991, PhD thesis, National University of Australia
Leggett S. K., 1992, ApJS, 82, 351
Ludwig C. B., 1971, Appl. Opt., 10, 1057
Merrill K. M., Ridgway S. T., 1979, ARA&A, 17, 9
Mould J. R., 1978, ApJ, 226, 923
Mountain C. M., Robertson D. J., Lee T. J., Wade R., 1990, Proc. SPIE, 1235, 35
Peterson B. R., 1980, A&A, 82, 53
Popper D. M., 1980, ARA&A, 18, 115
Puxley P. J., Ramsay S. K., Beard S. M., 1992, in Grosbol P., ed., Proc. 4th ESO/ST-ECF data analysis workshop
Ramsay S. K., Mountain C. M., Geballe T. R., 1992, MNRAS, 259, 751
Reid I. N., Gilmore G., 1984, MNRAS, 206, 19
Robertson J. G., 1986, PASP, 98, 1220
Spinrad H., Wing R. J., 1969, ARA&A, 7, 149
Tinney C. G., Mould J. R., Reid I. N., 1993, AJ, 105, 1045
Tokunaga A. T., 1986, IRTF Photometry Manual. Univesity of Hawaii, Honolulu
Veeder G. J., 1974, AJ, 79, 1056
Vieira T., 1985, Upps. Astron. Obs., Rep. No. 32
Zuckerman B., Becklin E. E., 1992, ApJ, 386, 260

Mon. Not. R. Astron. Soc. **270**, L47–L51 (1994)

A new candidate brown dwarf from an infrared survey

Hugh R. A. Jones,[1] Lance Miller[2] and Karl Glazebrook[3]

[1]*Institute for Astronomy, University of Edinburgh, Blackford Hill, Edinburgh EH9 3HJ*
[2]*Royal Observatory, Blackford Hill, Edinburgh EH9 3HJ*
[3]*Institute of Astronomy, University of Cambridge, Madingley Road, Cambridge CB3 0HA*

Accepted 1994 August 1. Received 1994 July 14; in original form 1994 June 21

ABSTRACT

We report the discovery at infrared wavelengths of a very cool field brown dwarf candidate. It has infrared colours $J-H=0.90\pm0.19$ and $H-K=0.83\pm0.18$, compared with the previously known coolest dwarf GD165B which has $J-H=1.01\pm0.05$ and $H-K=0.64\pm0.05$. Both are much redder than the expected colours $J-H=0.70$ and $H-K=0.27$ for stars of intermediate age with masses of 0.08 $M_\odot$. Based on the colours and spectra of a probable companion star and by comparison with evolutionary models, we infer that the new brown dwarf candidate is of intermediate age with a mass of 0.071–0.079 $M_\odot$, a temperature of 1825 ± 300 K and a bolometric magnitude of 14.56 ± 0.35. Classification as a star or a brown dwarf depends on the adopted age and the evolutionary model used. The discovery of this object within an infrared field survey places the first lower limit on the space density for objects fainter than $M_{bol}=14$, and suggests that the luminosity function does not fall dramatically into the brown dwarf regime.

Key words: stars: fundamental parameters – stars: late-type – stars: low-mass, brown dwarfs – stars: luminosity function, mass function – infrared stars.

1 INTRODUCTION

Brown dwarfs are objects hypothesized to occupy the mass range between the lightest stars (~0.08 solar masses, $M_\odot$) and the heaviest planets (~0.001 $M_\odot$). They never become hot enough to sustain nuclear fusion and, after their initial formation and heating by gravitational collapse, they develop a degenerate core and thereafter cool to low temperatures. Brown dwarfs might make a significant contribution to the dark matter in the Galactic disc, galactic haloes or even a background critical density (e.g. Kerins & Carr 1994). Large-area surveys have not identified any clear examples, and find that the space density of stars has a maximum at a bolometric absolute magnitude $M_{bol}\sim10$, corresponding to hydrogen-burning stars of about 0.2 $M_\odot$, and decreases to fainter luminosities (Tinney 1993). Searches in young clusters, where brown dwarfs are expected to be hotter and brighter, have discovered a number of candidates (Steele, Jameson & Hambly 1993; Comeron et al. 1993), but their classification relies on the discrimination of cluster members from field objects and on reliable modelling of their rapid early cooling.

2 OBSERVATIONS

The new candidate brown dwarf was discovered during an infrared survey for faint red galaxies (Glazebrook et al. 1993). An area of 552 arcmin^2 was searched to a 5σ limit of $K\simeq17.3$ and $R\simeq23.8$ with incomplete coverage to $B\simeq23.9$, $V\simeq24.1$ and $I\simeq23.6$. J- and H-band infrared photometry and optical spectra have been obtained for all objects redder than $R-K=5$. The infrared data were taken using the IRCAM instrument with the United Kingdom InfraRed Telescope (UKIRT) at the Mauna Kea Observatory on Hawaii. Optical imaging data were obtained at the Isaac Newton Telescope (INT); optical spectroscopic data were obtained with the Low Dispersion Survey and Faint Object Spectrographs (FOS) at the William Herschel Telescope (WHT); both telescopes are at the Roque de los Muchachos Observatory on La Palma.

Follow-up imaging and spectroscopy revealed the object, JMG 0918 – 0023, to be an M5.5 dwarf (object A) separated from a fainter, extremely red, companion (object B) by 3 arcsec. Object B is below the survey limit and was only discovered during the follow-up observations. Table 1 lists the photometry of A and B. We discuss each in turn.

3 DISCUSSION

Fig. 1 shows a spectrum of A taken with the FOS on the WHT, together with spectra of mid-type M dwarfs taken with the Multiple Mirror Telescope (MMT) on Kitt Peak in Arizona (Kirkpatrick, Henry & McCarthy 1991). Object B

Table 1. UKIRT and INT photometry of the JMG 0918−0023 AB system. Based on the colours of GD165B and other extreme red dwarfs, we expect B to have $R-K>7$ and so $R(B)>25$. This means that $R(B)$ makes a negligible contribution to the R survey magnitude which is assumed to be $R(A)$.

Object	R.A.	Decl. (1950)	Date	B	R_{CCD}	J_{UKIRT}	H_{UKIRT}	K_{UKIRT}
JMG 0918−0023 AB	09 18 25.37	−00 23 01.65	Oct 87 – Apr 89	>24.2	21.12±0.08			16.28±0.15
JMG 0918−0023 A			16-17 Oct 90			16.86±0.03	16.36±0.05	16.13±0.05
			2 May 93			16.97±0.04	16.31±0.06	16.01±0.07
JMG 0918−0023 B	offset 2.82″N	0.88″E	16-17 Oct 90			20.00±0.22	19.01±0.20	18.12±0.17
			2 May 93			19.96±0.17	19.00±0.16	18.16±0.20

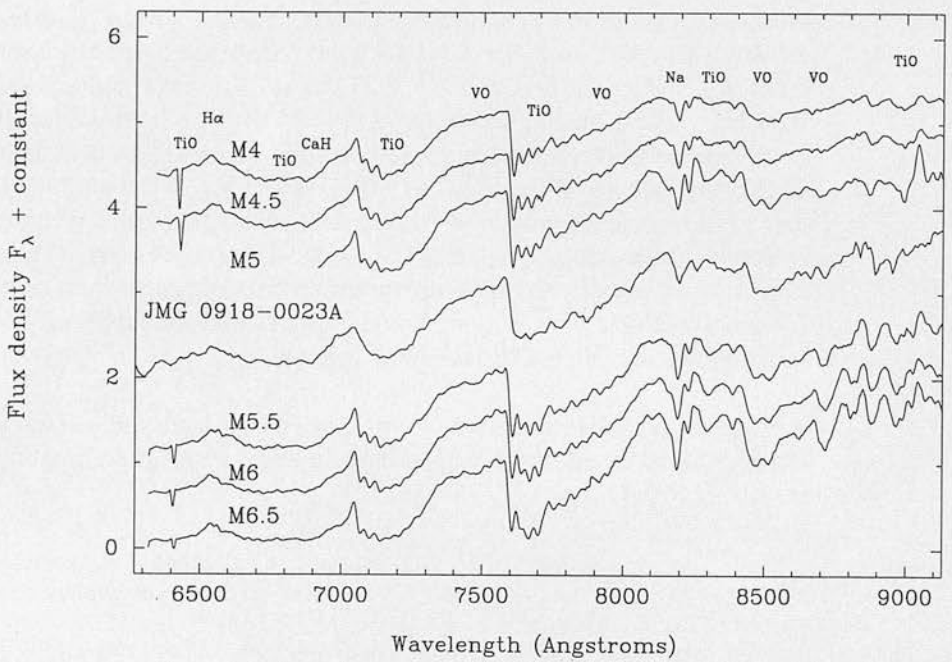

Figure 1. Spectrum for A, corrected for telluric absorption, compared to those of other M5–M7 dwarfs from Kirkpatrick et al. (1991), which have not been corrected for telluric absorption. In spectral regions where there are telluric absorption bands, this correction has the effect of increasing the flux. At the resolution and signal-to-noise ratio presented here, this correction is significant around 6900 and 7600 Å. The feature at 6415 Å is an artefact. The scale of flux density is arbitrary, and an offset has been added to separate the spectra.

was too faint to be detected in the optical, as expected from its infrared colours. From its colours alone, A could be classified as an M dwarf, a red galaxy or, implausibly, a giant star well beyond the Galaxy. The presence of a strong sodium line at 8180 Å identifies A's spectrum as that of a dwarf rather than a giant (Bessell 1991; Kirkpatrick et al. 1991). It is unlikely to be young, as it lacks the prominent Hα emission seen in young M-dwarf stars (Giampapa & Liebert 1986); neither is it very old, as it lacks the strong Ca H absorption at 6750–7050 Å which is used to classify subdwarfs ([M/H]≤ -1: Kirkpatrick et al. 1991). Based on Fig. 1, A resembles an M5.5±0.5 dwarf of intermediate metallicity and age.

The spectral type and colours of A indicate an absolute magnitude which can be used to obtain its distance. A strong constraint on its absolute magnitude comes from the longest-baseline colour. Interpolation of $R-K=5.07\pm0.09$ within table 6 of Leggett (1992) gives a distance modulus of 7.09 ± 0.23 if it is an M5.5V star from the old disc population (1.5–6 Gyr: Eggen 1989), or 7.30 ± 0.27 if it is an M6V star from the young disc population (0.3–1.5 Gyr: Eggen & Iben 1988). The young disc has a scaleheight of ~100 pc, whereas the old disc has a scaleheight of ~300 pc (Gilmore & Reid 1983). At a Galactic latitude of +33°, A is ~150 pc above the Galactic plane, and we classify A as an M5.5–6V star from the interface of the young and old disc populations.

If A and B are physically associated, then their angular separation of 2.96±0.15 arcsec corresponds to a projected separation of 770±100 au. Based on a visually selected sample (Gliese & Jahreiss 1979) of stars in M-dwarf multiple systems, Fischer & Marcy (1992) find that three out of 58 systems are binaries with separations between 770 and 10 000 au, and note that the sample is incomplete in this range. The late-type M dwarf VB8 is one of these, with a

separation of 1730 au. The colours and luminosity of B are as expected for a faint dwarf companion to an M5.5–6V star, but it is much too faint to be a distant giant star. B is unlikely to be a background galaxy or an unrelated star, as the density of galaxies and stars with $K<18.3$ and $I-K>3$ ($I-K>3$ conservatively corresponds to $R-K>5.5$) is 2.4×10^{-3} per 30 arcsec^2 (Hu et al. 1994). Its star-like profile and extreme infrared colours also make this hypothesis unlikely.

If B is physically associated with A, B's temperature and luminosity can be compared with those expected from evolutionary models to determine its mass. The determination of temperatures for late-type M dwarfs is problematic, as their spectra are dominated by deep bands of water vapour absorption (Jones et al. 1994), so that colours are not such reliable indicators of temperature as they are for hotter stars. A number of different approaches are possible (Kirkpatrick et al. 1993; Tinney, Mould & Reid 1993; Jones et al. 1994). Extrapolation of a second-order polynomial fit to the relation between $J-K$ colour and temperature gives 1855 ± 300 K by Jones et al. (1994), 1613 ± 300 K by Tinney et al. (1993) or 2262 ± 300 K by Kirkpatrick et al. (1993).

Model and observed bolometric magnitudes can be compared more directly than temperatures, radii or masses (except for short-period binaries). Although we have only measured B in the J, H and K passbands, the similar colours of GD165B, for which there is a wider range of photometry and spectroscopy (Jones et al. 1994), enable us to make a reasonable estimate for B's bolometric magnitude. We use bolometric corrections for GD165B at J, H and K to determine a bolometric magnitude in each passband, and then take the average of them. Using this bolometric magnitude and the distance derived for A, B has $M_{bol}=14.56\pm0.35$. This compares with 14.91 ± 0.26 for GD165B. Solar-metallicity evolutionary models give 13.3, 13.9, 15.2 and 15.3 (Burrows et al. 1993) or 13.1, 13.5, 14.7 and 15.0 (Nelson, Rappaport & Joss 1993) for the end of the main sequence at ages of 0.6, 1, 5 and 10 Gyr respectively.

Fig. 2 shows a Hertzsprung–Russell diagram for late-type M dwarfs and brown dwarf candidates, adopting the temperature scale from Jones et al. (1994) and the standard solar-metallicity model X from Burrows et al. (1993). The relation for an age of 10 Gyr is shown by a solid line, and that for 0.6 Gyr by a dashed line. Dotted lines are plotted for object ages of 0.6, 1, 5 and 10 Gyr to show the border between objects that burn hydrogen and those that do not ($0.0767\ M_\odot$). Models from Nelson et al. (1993) produce a plot with masses increased by $0.0075\ M_\odot$ and luminosities increased by 20–60 per cent. Interpolating the temperature and bolometric luminosity for the young-old disc age range (1–3 Gyr: Eggen & Iben 1988; Eggen 1989) within model X, we find JMG 0918 − 0023 B to have a mass of 0.071–0.079 $M_\odot$ and GD165B, which is older than 0.5 Gyr based on the cooling age for its white dwarf companion (Becklin &

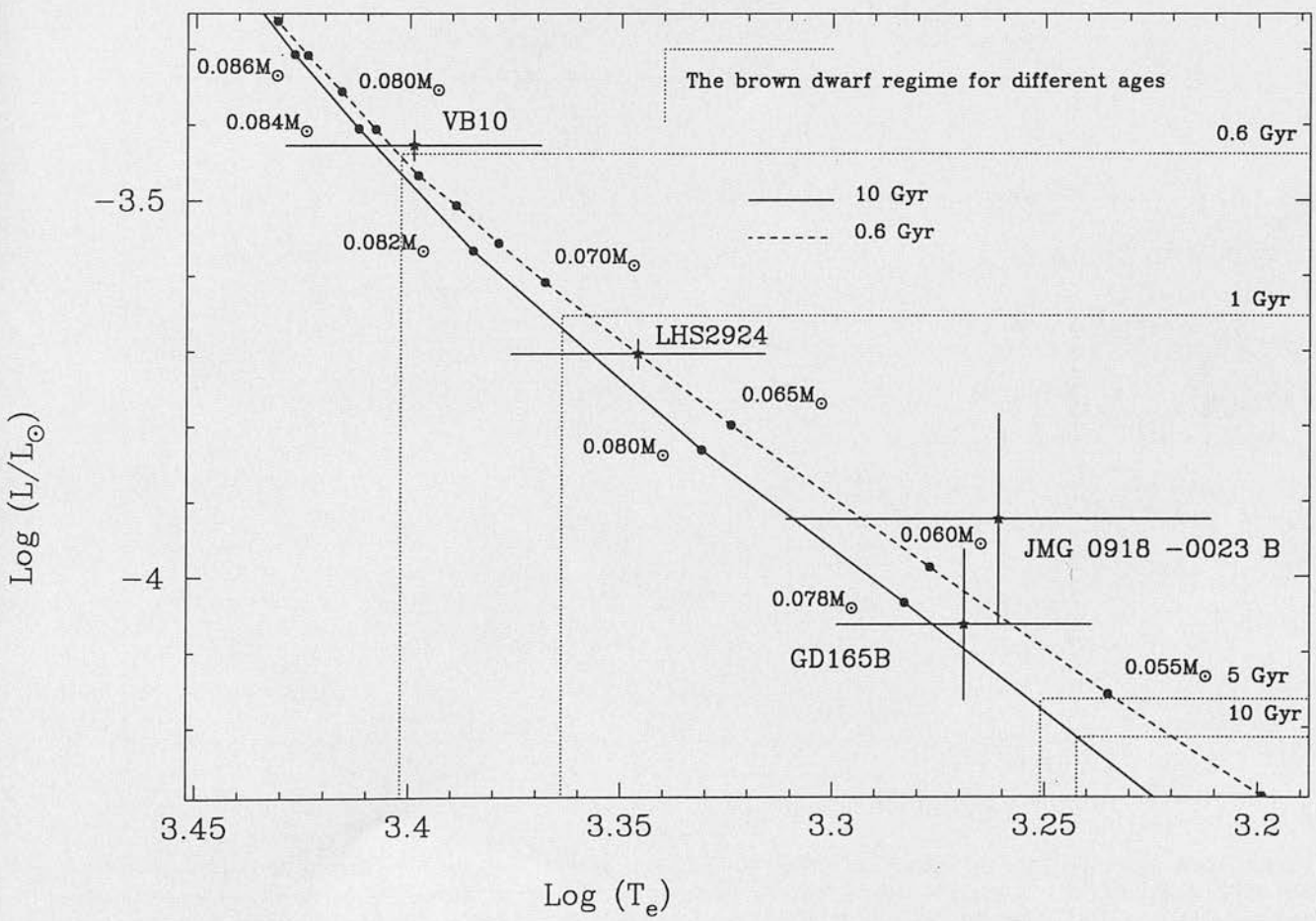

Figure 2. Hertzsprung–Russell diagram for low-mass stars and brown dwarf candidates assuming $M_{bol\odot}=4.75$.

Zuckerman 1988), to have a mass of 0.058–0.078 $M_\odot$. Whether they are brown dwarfs or very low-mass stars depends on the adopted evolutionary model and the age of the system. If they are younger than 1.5 Gyr, they are brown dwarfs by either model; if they are 3–5 Gyr old, they are (Nelson et al. 1993) or are not (Burrows et al. 1993) brown dwarfs; if they are older than 5 Gyr, they are not brown dwarfs by either model. These conclusions are for solar-metallicity models; however, if the objects are metal-poor, the models predict higher temperatures, luminosities and masses for the star/brown dwarf interface, making the interpretation of these objects as brown dwarfs more probable.

The brown dwarf regime can also be shown by direct observational results. In Fig. 3 we plot mass versus $J-K$ for a sample of M-dwarf binaries, measured by using the infrared speckle technique, with well-determined orbits and intermediate ages (old and young disc). We also plot dashed lines to indicate the different hydrogen-burning limits derived by theoretical solar-metallicity models (Burrows et al. 1993; Nelson et al. 1993). A weighted linear fit to the objects in Fig. 3 below 0.2 $M_\odot$ gives $J-K=1.02\pm0.28$ for a mass of 0.0767 $M_\odot$. Although we do not expect mass versus $J-K$ to be a linear relationship, and although the ages and metallicities of these stars may differ from those of the candidates, the large difference of >0.6 between this $J-K$ value and those observed for JMG 0918−0023 B and GD165B is further evidence that they are brown dwarfs.

The previous faintest constraint on the luminosity function was based on an optical survey (Tinney 1993) with infrared follow-up, which indicated a falling function towards the brown dwarf regime and measured the stellar density at its faintest limit, $M_{bol}=13.75$, to be $3.6^{+5.6}_{-2.2}\times10^{-3}$ pc^{-3} mag^{-1}. Although JMG 0918−0023 B is fainter than the limit of our survey, its discovery can be used to put a lower limit of $3.1^{+7.1}_{-2.6}\times10^{-3}$ pc^{-3} mag^{-1} (68 per cent confidence) on the luminosity function for low-mass objects at $M_{bol}\sim14.5$. As the survey is incomplete for stars this faint, the true space density must be significantly greater, which suggests that these objects are not as rare as would be expected from the extrapolation of previous work.

ACKNOWLEDGMENTS

HRAJ and KGB acknowledge SERC/PPARC studentships. We also acknowledge considerable allocations of telescope time at the UKIRT, the INT and the WHT, and the service programme of the UKIRT and the WHT. The INT and the WHT are operated by the Royal Greenwich Observatory in the Spanish Observatorio del Roque de los Muchachos of the Instituto de Astrofísica de Canarias. UKIRT is operated by the Royal Observatory Edinburgh. We thank D. Kirkpatrick for allowing us to reproduce the MMT spectra and P. Hauschildt, F. Allard, D. Saumon and L. Nelson for providing model calculations for low-mass objects.

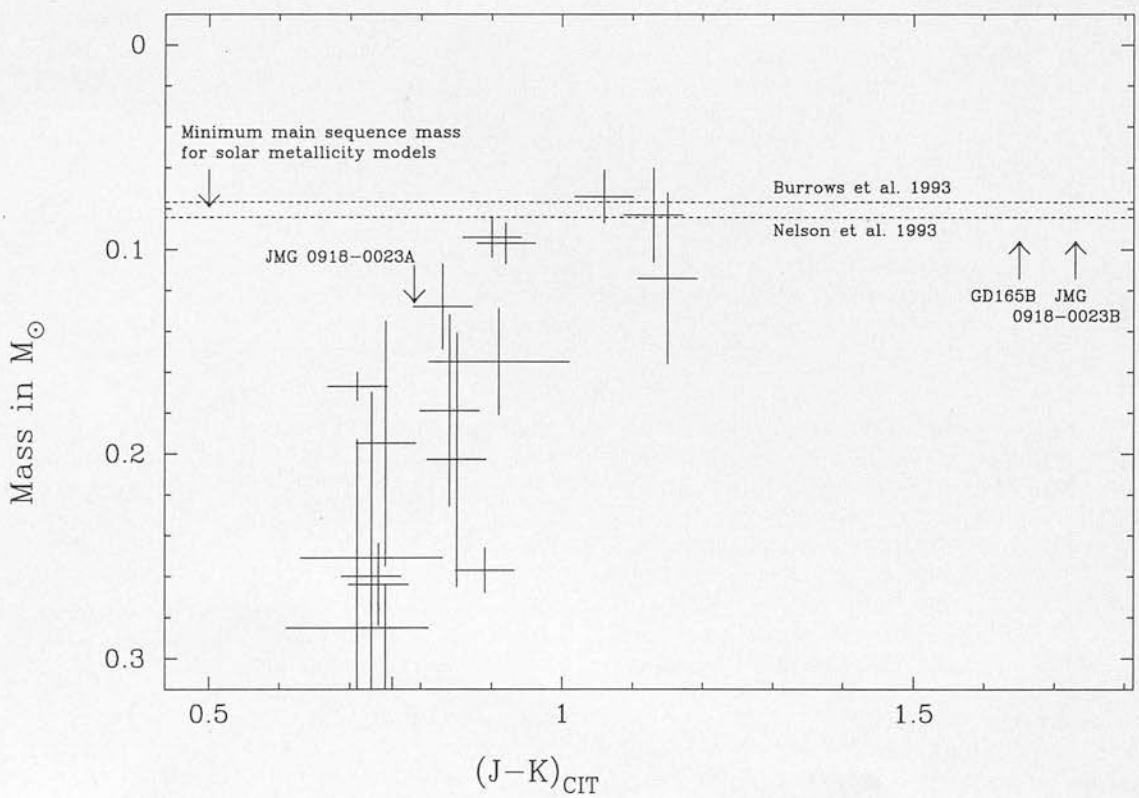

Figure 3. Mass versus $J-K$ for the sample from Henry & McCarthy (1993), showing also the colours of JMG 0918−0023 A, JMG 0918−0023 B and GD165B. The photometric colours, in this figure and throughout the text, are on the CIT photometric system. The photometric conversion for B from the UKIRT to the CIT system uses the results of Casali & Hawarden (1992), although it is expected to be unreliable as the relations are only established for $J-K<1$.

REFERENCES

Becklin E. E., Zuckerman B., 1988, Nat, 336, 656
Bessell M., 1991, AJ, 101, 662
Burrows A., Hubbard W. B., Saumon D., Lunine J. I., 1993, ApJ, 406, 158
Casali M. M., Hawarden T. G., 1992, JCMT-UKIRT Newsletter, 4, 33
Comeron F., Rieke G. H., Burrows A., Rieke M. J., 1993, ApJ, 416, 185
Eggen O. J., 1989, AJ, 100, 1159
Eggen O. J., Iben I., Jr, 1988, AJ, 96, 635
Fischer D. A., Marcy G. W., 1992, ApJ, 396, 178
Giampapa M. S., Liebert J., 1986, ApJ, 305, 784
Gilmore G., Reid I. N., 1983, MNRAS, 202, 1025
Glazebrook K., Peacock J. A., Collins C., Miller L., 1993, MNRAS, 266, 65
Gliese W., Jahreiss H., 1979, A&AS, 38, 423
Henry T. J., McCarthy D. W., 1993, AJ, 106, 773
Hu E., Huang J.-S., Gilmore G., Cowie L. L., 1994, Nat, in press
Jones H. R. A., Longmore A. J., Jameson R. F., Mountain C. M., 1994, MNRAS, 267, 413
Kerins E. J., Carr B. J., 1994, MNRAS, 266, 775
Kirkpatrick J. D., Henry T. J., McCarthy D. W., Jr, 1991, ApJS, 77, 417
Kirkpatrick J. D., Kelly D. M., Rieke G. H., Liebert J., Allard F., Wehrse R., 1993, ApJ, 402, 643
Leggett S. K., 1992, ApJS, 82, 351
Nelson L. A., Rappaport S., Joss P. C., 1993, ApJ, 404, 723
Steele I. A., Jameson R. F., Hambly N. C., 1993, MNRAS, 263, 647
Tinney C. G., 1993, ApJ, 414, 279
Tinney C. G., Mould J. R., Reid I. N., 1993, AJ, 105, 1045